NTNU

Norwegian University of
Science and Technology

Modelling and Analysis of Autonomous Inflow Control Devices

Stian Håland

Petroleum Geoscience and Engineering
Submission date: June 2017
Supervisor: Curtis Hays Whitson, IGP
Co-supervisor: Milan Stanko, IGP

Norwegian University of Science and Technology
Department of Geoscience and Petroleum

Preface

The work in this thesis was motivated by challenges brought up by Igor Orlov of Statoil ASA related to field development planning. He contacted my supervisor, Professor Curtis H Whitson, who suggested this topic to me. Early in the semester, Associate Professor Milan Stanko also became involved in the process. Together, the four of us worked towards problems related to Igor's work. However, mainly due to lack of data, the thesis took a turn to a more general problem.

I hope that the work in Thesis may still be of use for Igor in his work.

I would like to express gratitude towards the supervisors and associates. Igor did a good job in directing his needs towards something that could be used as a thesis. He has been proactive, and provided me with data to work with, to the best of his abilities. Even when the Thesis deviated from his specific work, he provided me with valuable input and help.

Curtis and Milan have both been of great help with this thesis. Their interest and involvement in the project has been above all expectations. They have provided great input, discussions and ideas on how to solve the problems. Milan has spent a great amount of time personally teaching me about specific topics related to the thesis. Curtis has given me invaluable lessons in 'real life' problem solving, and engineering skills. I am confident that this will help me in my future career.

Abstract

Gas and water coning is a significant problem in many oil fields. Inflow control technology is used to limit the negative effects of coning, and newer technology is regularly introduced.

This thesis investigates Autonomous Inflow Control Devices (AICD) and Autonomous Inflow Control Valves (AICV). Laboratory test data has been found for two types of AICDs: (1) Statoil's RCP-valve and (2) Halliburton's Fluidic Diode Valve.

Four models has been tested for both datasets: Statoil's AICD-model, the Bernoulli model, Sachdevas model and Asheims model. The latter three models are originally intended for flow through chokes and simple valves. The Statoil model was found to fit the datasets better than all the other models, with an average of 21.8% and 11.3% absolute relative error for datasets 1 and 2, respectively.

A new method was suggested to improve the modelling of AICDs in reservoir simulators. The method consist of splitting the Statoil model up in 4 datasets each representing oil, gas, water and multiphase flow and merging the models in a VFP-table. A tool to do this was made in Excel, and Eclipse VFP-tables for AICDs specific for Troll conditions was made and attached. The use of the tables has not been tested or confirmed in Eclipse.

A one-dimensional steady state well performance analysis was performed. A horizontal producing well typical of the Troll field was created, and a representative inflow and GOR-Model was made to represent a coning well. The analysis was done for three different reservoirs, for three different gas-coning models with three different completions.

Open hole, AICD and AICV completions were analyzed. AICVs were assumed to behave identical to AICD; but capable of shutting off above a certain gas or water volume fraction. The results suggested that wells completed with AICD and AICV significantly increased oil recovery, while AICDs were slightly better than AICVs.

Sammendrag

Gass- og vannkoning er et betydelig problem i mange oljefelt. Innstrømningskontroll - teknologi brukes til å begrense de negative effektene av koning, og nyere teknologi er regelmessig introdusert.

Denne oppgaven undersøker Autonome Innstrømningskontroll-enheter (AICD) og Autonome Innstrømningskontroll-ventiler (AICV). Laboratorie-testdata er funnet for to typer AICD: (1) Statoils RCP-ventil og (2) Halliburtons Fluidic Diode-ventil.

Fire modeller har blitt testet for begge datasettene: Statoils AICD-modell, Bernoulli-modellen, Sachdeva-modellen og Asheims modell. De sistnevnte tre modellene er opprinnelig beregnet for strømning gjennom strupeventiler. Statoil-modellen ble funnet å modellere datasettene bedre enn alle andre modeller, med et gjennomsnitt på 21,8% og 11,3% absolutt relativ feil for datasett 1 og 2.

En ny metode ble foreslått for å forbedre modelleringen av AICD i reservoar-simulatorer. Den metoden består av å splitte Statoil-modellen i 4 modeller, hvor hver modell er individuelt tilpasset for olje, gass, vann og flerfasestrøm. Disse modellene er så sammenføyet i et Eclipse VFP-tabellformat. Et verktøy for å gjøre dette ble laget i Excel. VFP-tabeller for AICDer, spesifikke for Troll-forhold ble laget og vedlagt. Anvendelsen av tabellene er ikke testet eller bekreftet i Eclipse.

En endimensjonal stasjonær brønnanalyse ble utført. En horisontal produksjonsbrønn typisk for Troll-feltet ble opprettet, og en representativ innstrømnings og gas-koning modell ble laget. Analysen ble utført for tre forskjellige reservoarer, for tre forskjellige gas-koning modeller for tre typer komplettering.

Åpent hull, AICD og AICV kompletteringer ble analysert. AICV ble antatt å oppføre seg identisk som AICD, men med mulighet for å stenge igjen over en viss gass- eller vannvolumfraksjon. Brønnene komplettert med AICD og AICV viste betydelig økt oljeutvinning, mens AICD viste seg noe bedre enn AICV.

Table of contents

Preface 1
Abstract 2
Sammendrag 3
Table of contents 4
List of Tables 7
List of Figures 8
Chapter 1: Introduction 12
1.1: Multiphase flow theory: 13
1.1.1: Single phase pressure drop for fluids 13
1.1.2: Multiphase properties 16
1.2: Introduction to Horizontal wells 21
1.3: Inflow Control Technology 22
1.3.1: Traditional Inflow Control Devices 22
1.3.2: Inflow Control Valves 24
1.3.3: Autonomous Inflow Control Devices 24
1.3.4: Autonomous Inflow control Valve 26
Chapter 2: AICD modelling 28
2.1: AICD Laboratory test data 29
2.1.1: Dataset 1 - Statoil RCP Valve 30
2.1.2: Dataset 2 - Haliburton fluidic diode valve 32
2.2: AICD Models 34
2.2.1: Statoil model 34
2.2.2: Bernoulli model 35
2.2.3: Asheim's model 37
2.2.4: Sachdeva et al. model 39
2.3: Results 41
2.3.1: Evaluating the model 41
2.3.2: Model matching 43
2.3.3: Results overview 44
2.4: Discussion 46
2.4.1: Model performance 46
2.4.2: Comparing the models 47

2.4.3: Sources of error 48
Chapter 3: VFP tables method for modelling AICDs 50
3.1: Vertical Flow Performance tables 51
3.2: The Black Oil model 53
3.3: Statoil Hybrid model in VFP format 58
3.4: Results and discussion about the method 63
Chapter 4: AICD in well performance 66
4.1: Well Performance Theory 67
4.1.1: Inflow Performance Relationship (IPR) 68
4.1.2: Pressure drop through outer completion 69
4.1.3: Horizontal Pipe flow: 70
4.1.4: Vertical pipeflow 70
4.2: Modelling a typical Troll well 72
4.2.1: Well geometry 72
4.2.2: Production 73
4.2.3: Fluid properties 74
4.2.4: Reservoir and Inflow Performance 74
4.2.5: AICD modelling 80
4.3: Production Network 81
4.4: Well performance analysis 84
4.5: Results 86
4.6 Discussion 90
Chapter 5: Recommendations for future work 92
Chapter 6: Conclusions 93
Nomenclature 94
References 96
Appendix A: Overview of Attachments 98
A.1: (Excel sheet “AICD_model_StatoilRCP.xlsm”) 98
A.2: (Excel sheet “AICD_model_Haliburton.xlsm”) 98
A.3: (Excel sheet “VFP_table_generation.xlsm”) 98
A.4: (Excel sheet “Network_Analysis.xlsm”) 99
A.5: (Eclipse VFP-file “VFPtable_primary.ECL”) 99
A.6: (Eclipse VFP-file “VFPtable_multiphase.ECL”) 99
A.7: (ZIP-file “BOPVT-Troll.ZIP”) 99

Appendix B: AICD test datasets 101
B.1: Dataset 1: Statoil RCP Valve 101
B.2: Dataset 2: Haliburton Fluidic Diode Valve 106
Appendix C: AICD Model results 107
C.1: Dataset 1: Statoil RCP Valve 107
C.2: Dataset 2: Haliburtin Fluidic Diode Valve 110
Appendix D: Extracted GOR-Model data 113
Appendix E: Network Analysis Results 114
E.1: Optimized drawdown for all sections 114
E.2: Inflow distribution for all sections 118
E.3: Pressure distribution for all sections 128
Appendix F: VBA-code Overview 138
F.1: AICD modelling spreadsheets 139
F.1.1: Multiphase properties 139
F.1.2: Multiphase models 140
F.1.3: Spreadsheet procedures 142
F.2: VFP-table generation spreadsheet 143
F.3: Network Analysis spreadsheet 147

List of Tables

Table 1: Fluid properties at test conditions for Dataset 1 30
Table 2: Multiphase compositions used Dataset 1 30
Table 3: Fluid properties for Dataset 2 32
Table 4: Multiphase compositions used for Dataset 2 32
Table 5: Model performance results for Dataset 1 44
Table 6: Model performance results for Dataset 2 45
Table 7: Tuning parameters for optimized solution, Statoil model 45
Table 8: Tuning parameters for optimized solution, Bernoulli, Asheim and Sachdeva model 45
Table 9: Limit volume fractions chosen for the Hybrid model to use single-phase parameters 59
Table 10: Fluid properties from the Black Oil Table. 59
Table 11: Optimized tuning parameters for the Statoiul Hybrid model 60
Table 12: Error results for the different phases in the optimized Hybrid Model 60
Table 13: VFP-table parameter distribution used. Linear distribution between the upper and lower bound 61
Table 14: Well geometry for a typical Troll well 72
Table 15: Production data and properties for a typical Troll well 73
Table 16: Reservoir conditions 74
Table 17: Tuning parameters for replicdating the GOR-Model 77
Table 18: Productivity Index distribution for the suggested reservoirs 79
Table 19: Overview of analysis cases. All three reservfoirs are analyzed for three completions, and each for three GOR-Models. 84
Table 20: Results from analysis on Reservoir 1 86
Table 21: Results from analysis from Reservoir 2 87
Table 22: Result from analysis from reservoir 3 87
Table 23: Results from analysis from reservoir 3 with varying GOR-Model per section 87
Table 24: complete dataset for Statoil RCP Valve, converted to volumetric flow 105
Table 25: Complete dataset for the Haliburton Fluidic Diode Valve, converted to volumetric flow 106
Table 26: Extracted data from Statoil's GOR-Model 113
Table 27: Solved drawdown pressures [bar] for cases 1-9 (Reservoir 1) 114
Table 28: Solved drawdown pressures [bar] for cases 10-18 (Reservoir 2) 115
Table 29: Solved drawdown pressures [bar] for cases 19-27 (Reservoir 3) 116
Table 30: Solved drawdown pressures for cases 28-30 117

List of Figures

Figure 1: Visual representation of laminar and turbulent flow regime. From [2]. 14
Figure 2: Visual representation of the critical flow behavior, Pressure ratio (y) plotted against flow rate (Q). Pressure ratios below critical pressure ratio (y_c) does not increase flow rate. 19
Figure 3: Sketch of a horizontal well experiencing gas and water coning. From [16] 21
Figure 4: Channel (top), Nozzle (middle) and Orifice (bottom) type ICDs. Adapted from [5] 23
Figure 5: Scetch of the Statoil RCP Valve, with flow path indicators. From [10] 25
Figure 6: Sketch of the AICV. The large and medium arrows indicate the main flow path. The smallest arrow indicate the pilot flow. The piston marked as yellow. From [19] 26
Figure 7: Simplified sketch of the flow paths in the AICV. From [19] 26
Figure 8: Sketch of typical pressure drop over the laminar flow element (left) and turbulent flow element (right). From [16] 27
Figure 9: Single-phase test data for Dataset 1. 31
Figure 10: Multiphase test data for Dataset 1 31
Figure 11: Single-phase test data for Dataset 2 33
Figure 12: Multiphase data for Dataset 2 33
Figure 13: Sketch of a function with several local minimums and one global minimum 43
Figure 14: Pseudocode of the VFP-table format in Eclipse (.ECL). Producing well in metric units. Adapted from Eclipse Manual [23] 52
Figure 15: Sketch of a surface process for obtaining surface phases from reservoir phases. From [27] 53
Figure 16: Black-Oil parameter behaviour with relation to pressure, with consant temperature From [24] 55
Figure 17: Black-Oil parameter variation with different compositions (GORs). From [24] 56
Figure 18: Statoil Hybrid Model performance to test data, split into the four different phases. 61
Figure 19: Screenshot from the spreadsheet used for creating and writing VFP tables 62
Figure 20: Graph relating test data and datapoint from the VFP table. 63
Figure 21: Sketch of a horizontal producing well system 67
Figure 22:Single-phase linear inflow performance relationship. From [25] 68
Figure 23: Multi-phase inflow performance relationship. From [21] 69
Figure 24: Sketch of tipcal AICD completion. Arrows inducate flow through sandscreen, annulus, AICD and tubing. From [9] 69
Figure 25: Flow chart showing the iteration process of finding the Tubinghead pressure 71

Figure 26: A typical Troll well. From [8] 72
Figure 27: Production data for a typical Troll well. From [13] 73
Figure 28: Gas Oil Ratio model for a typical Troll well. Modelled at different points in time. From [13]. 75
Figure 29: Optimized expressions for replicating the Troll GOR-Model 77
Figure 30: Geological cross sectio for a typical Troll well. From [7] 78
Figure 31: Productivity Index distribution for the suggested reservoirs. Section 1 is the toe, and section 30 is the heel of the well. 80
Figure 32: Nodal production network sketch 81
Figure 33: Convergence on Network node sketch. Pressure calculations from both inflow directions must give the same result. 82
Figure 34: Results from analysis on reservoir 1 88
Figure 35: Results from analysis on reservoir 2 88
Figure 36: Results from analysis on reservoir 3 89
Figure 37: Results from analysis on reservoir 3 with varying GOR-Model per section 89
Figure 38: Screenshot of the production Network Analysis spreadsheet. Cells of interest in selecting reservoir and completion type are highlighted. 100
Figure 39: Screenshot of the production Network Analysis spreadsheet. Cells of interest in solving the system higthlighted. 100
Figure 40: Error distribution plots for all models, Dataset 1 107
Figure 41: Error vs gas fraction for all models, dataset 1 108
Figure 42: Error vs deltaP plots for all models, dataset 1 109
Figure 43: Error distribution plot for all models, dataset 2 110
Figure 44: Error gas fraction plot for all models, dataset 2 111
Figure 45: Error vs DeltaP for all models, dataset 2 112
Figure 46: Inflow distribution for cases 1-3. Reservoir 1, Open Hole, GORM 1-3. 118
Figure 47: Inflow distribution for cases 4-6. Reservoir 1, AICD, GORM 1-3. 119
Figure 48: Inflow distribution for cases 7-9. Reservoir 1, AICV, GORM 1-3. 120
Figure 49: Inflow distribution for cases 10-12. Reservoir 2, Open Hole, GORM 1-3. 121
Figure 50: Inflow distribution for cases 13-15. Reservoir 2, AICD, GORM 1-3. 122
Figure 51: Inflow distribution for cases 16-18. Reservoir 2, AICV, GORM 1-3. 123
Figure 52: Inflow distribution for cases 19-21. Reservoir 3, Open Hole, GORM 1-3. 124
Figure 53: Inflow distribution for cases 22-24. Reservoir 3, AICD, GORM 1-3. 125
Figure 54: Inflow distribution for cases 10-12. Reservoir 3, AICV, GORM 1-3. 126

Figure 55: Inflow distribution for cases 28-30. Reservoir 3 with varying GORM. Open Hole, AICD and AICV. 127
Figure 56: Pressure distribution for cases 1-3. Reservoir 1, Open Hole, GORM 1-3. 128
Figure 57: Pressure distribution for cases 4-6. Reservoir 1, AICD, GORM 1-3. 129
Figure 58: Pressure distribution for cases 7-9. Reservoir 1, AICV, GORM 1-3. 130
Figure 59: Pressure distribution for cases 10-12. Reservoir 2, Open Hole, GORM 1-3. 131
Figure 60: Pressure distribution for cases 13-15. Reservoir 2, AICD , GORM 1-3 132
Figure 61: Pressure distribution for cases 16-18. Reservoir 2, AICV, GORM 1-3. 133
Figure 62: Pressure distribution for cases 19-21. Reservoir 3, Open Hole, GORM 1-3. 134
Figure 63: Pressure distribution for cases 22-24. Reservoir 3, AICD, GORM 1-3. 135
Figure 64: Pressure distribution for cases 25-27. Reservoir 3, AICV, GORM 1-3. 136
Figure 65: Pressure distribution for cases 28-30. Reservoir 3, GORM 1 for low PI sections. GORM 3 for high PI sections. Open Hole, AICD and AICV completion. 137

Chapter 1: Introduction

Excessive gas and water production is a big challenge in production from oil reservoirs. There are many technical and procedural solutions to limit gas and water production, while maintaining oil production at an economic rate. This paper will investigate advanced technology for inflow control, primarily Autonomous Inflow Control Devices (AICD) and Autonomous Inflow Control Valves (AICV).

The thesis can be divided into three major parts:

- Investigate and analyze models used to characterize AICDs
- Propose a new method of modelling AICDs
- Analyze well performance in wells completed with AICDs and AICVs.

Theoretical framework for this thesis is primarily based on *multiphase flow theory, phase behavior and well performance theory.*

This chapter will introduce relevant theory and background information for the following chapters.

1.1: Multiphase flow theory:

1.1.1: Single phase pressure drop for fluids

The total pressure for flowing along a streamline can be described as a sum of three individual pressure drops: pressure drop due to gravitation, acceleration (or momentum) and friction.

$$dP_{total} = dP_{gravitation} + dP_{acceleration} + dP_{friction} \quad (1)$$

$$dP_{gravitation} = \rho g \, dh \quad (2)$$

$$dP_{acceleration} = \rho u \, du \quad (3)$$

$$dP_{friction} = f \frac{\rho u^2}{2D} dL \quad (4)$$

Where:

- ρ is the fluid density
- g is the gravitational contstant
- h is the height difference
- u is the fluid velocity
- P is the pressure

And Equation (4) is the Darcy-Weisbach equation, where:

- f is the Darcy friction factor
- L is the travelling length of the fluid
- D is the diameter of the flow area

Assuming incompressible flow, and integrating Equation (3) gives

$$\Delta P_{acceleration} = \frac{\rho u_2^2}{2} - \frac{\rho u_1^2}{2} \quad (5)$$

Combining equations (1) to (5), and rearranging gives the Bernoulli Equation for steady state incompressible flow:

$$P_1 + \frac{\rho u_1^2}{2} + \rho g h_1 = P_2 + \frac{\rho u_2^2}{2} + \rho g h_2 + \Delta P_{friction} \tag{6}$$

Depending on the situation, some of the terms may be neglected. For pressure drops across flow restrictions, like chokes or valves, acceleration is usually the dominant term. Most choke models neglect gravitation and friction, and base their derivation on the acceleration term. For pipe flow, gravitation and friction are usually the most important terms.

Flow regime:

There are generally two types of flow regimes: *Laminar* and *Turbulent* flow. Laminar flow is steady and smooth, while turbulent flow is randomly fluctuating and chaotic (Figure 1). Because of this, the two flow regimes have vastly different characteristics. Laminar flow is well understood, and have accurate solutions to most problems. Turbulent flow cannot be accurately described by analytical models, and most turbulent flow theory is therefore semi-empirical.

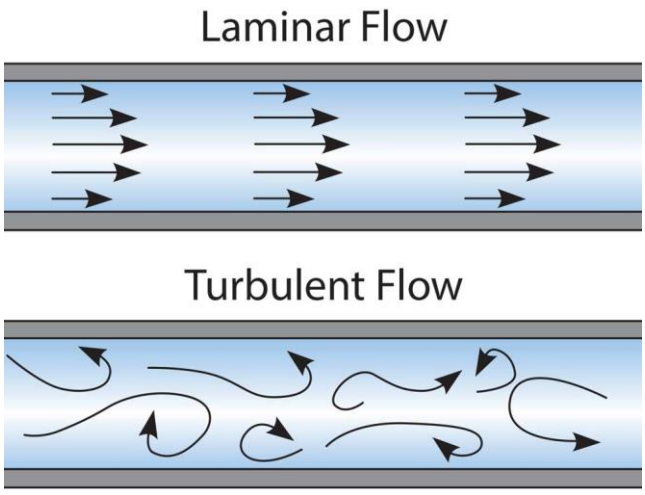

Figure 1: Visual representation of laminar and turbulent flow regime. From [2].

In order to distinguish between the two flow regimes, the Reynolds number is introduced. The Reynolds number is a dimensionless value that describes the ratio of inertial and viscous forces of the fluid. At low Reynolds numbers, the flow is dominated by viscous forces, and is laminar.

$$Re = \frac{\rho V D}{\mu} \tag{7}$$

As the Reynolds number increases, the flow will eventually start to experience turbulence. Depending on geometry, fluid will usually enter a transition from laminar turbulent flow around Re =1000. The transitional flow eventually reaches fully developed turbulent flow. For commercial pipes, the accepted design value for full turbulent flow is above a Reynolds number of 2300 [26] . For practical applications, this paper will neglect transitional flow, and use a Reynolds number of 2300 as the discrete limit between flow regimes.

$$Re < 2300 \quad Laminar\ flow$$
$$Re > 2300 \ \ Turbulent\ flow$$

Friction

For a fully developed laminar flow regime, the friction factor can be expressed as:

$$ƒ = \frac{64}{Re} \tag{8}$$

Combining this with Equation (4) and rearranging, the frictional pressure drop for laminar flow in pipes becomes:

$$\Delta P_{laminar} = \frac{32 \mu v L}{D^2} \tag{9}$$

Turbulent friction factors are empirically described based on experimental data. Colebrook proposed an implicit formula to represent the friction factor:

$$\frac{1}{\sqrt{f}} = -2\,log\left[\frac{\varepsilon/_D}{3.7} + \frac{2.51}{Re\sqrt{f}}\right] \tag{10}$$

Where ε is the pipe roughness. Haaland [26] suggested an explicit formula as an approximation for the Colebrook equation. The equation deviates around 2% from equation (10), and is generally easier to use for engineering purposes.

$$\frac{1}{\sqrt{f}} = -1.8\,log\left[\left(\frac{\varepsilon/_D}{3.7}\right)^{1.11} + \frac{6.9}{Re}\right] \tag{11}$$

Equations (9) to (11) shows that laminar frictional pressure drop is mostly dependent on the viscosity of the fluid, while the main contributor in turbulent flow is the fluid velocity and density.

1.1.2: Multiphase properties

Multiphase flow is defined as fluid of different states or phases flowing simultaneously in a system. In petroleum engineering practice, this usually means a mixture of oil, gas and/or water. Multiphase flow adds to the complexity of modelling due to compressional, mixing and emulsion effects.

This type of flow can be modelled by defining average fluid properties (velocity, viscosity, density) for the mixture, and solving problems with single-phase theory. In this way, the multiphase flow is modeled as one fluid. To derive multiphase properties, the following terms need to be defined:

$$\alpha_i = \frac{q_i}{q_{tot}} \tag{12}$$

Where:

- α_i is the volume fraction of fluid *i*
- q_i is the volumetric flow rate of fluid *i*
- $q_{tot}$is the total volumetric flow rate of the mixture

$$x_i = \frac{\dot{m}_i}{\dot{m}_{tot}} \tag{13}$$

Where:

- x_i is the mass fraction of fluid *i*
- $\dot{m}_i$ is the mass flow rate of fluid *i*
- $\dot{m}_{tot}$ is the total mass flow rate of the mixture

For a perfectly mixed mixture, the density and viscosity can be estimated as Homogenous volumetric average:

$$\rho_H = \alpha_{gas}\rho_{gas} + \alpha_{liquid}\rho_{liquid} \tag{14}$$

$$\mu_H = \alpha_{gas}\mu_{gas} + \alpha_{liquid}\mu_{liquid} \tag{15}$$

Where:

$$\rho_{liquid} = \alpha_{oil}\rho_{oil} + \alpha_{water}\rho_{water} \tag{16}$$

$$\mu_{liquid} = \alpha_{oil}\mu_{oil} + \alpha_{water}\mu_{water} \tag{17}$$

For further sections, the homogenous density is useful to define in terms of mass fractions:

$$\frac{1}{\rho_H} = \frac{x_{gas}}{\rho_{gas}} + \frac{x_{liq}}{\rho_{liq}} \tag{18}$$

Slip ratio

When the multiphase fluid is non-homogeneous (not perfectly mixed), the gas will have the tendency to have a higher velocity than the liquid phase. This phenomenon is called slip, and is defined by:

$$k = \frac{u_{gas}}{u_{liq}} \tag{19}$$

Where u_{gas} and u_{liq} are the phase velocities of gas and liquid. When considering slip, Equation (18) can be derived into the Two Phase (TP) density, in Equation (20). This will

always be higher than the Homogenous density, as the gas velocity is higher and thus takes up less space in the flowing geometry.

$$\frac{1}{\rho_{TP}} = \frac{x_{gas}}{\rho_{gas}} + k\frac{x_{liq}}{\rho_{liq}} \tag{20}$$

When the fluid velocities are equal, the slip ratio will be equal to unity, and Equation (20) collapses into Equation (18).

There are several models for finding the slip factor, and this paper will look at two of these:

1. Chisholm's model [12]:

$$k_{Ch} = \begin{cases} \left(\frac{\rho_{liq}}{\rho_H}\right)^{\frac{1}{2}} = \sqrt{1 + x_{gas}\left(\frac{\rho_{liq}}{\rho_{gas}} - 1\right)} & \chi > 1 \\ \left(\frac{\rho_{liq}}{\rho_H}\right)^{\frac{1}{4}} & \chi \leq 1 \end{cases} \tag{21}$$

Where k_{Ch} is Chisholm's slip factor, and:

$$\chi = \frac{x_{liq}}{x_{gas}}\sqrt{\frac{\rho_{gas}}{\rho_{liq}}} \tag{22}$$

2. Simpson's model [12]:

$$k_{Si} = \left(\frac{\rho_{liq}}{\rho_{gas}}\right)^{a} \tag{23}$$

Where k_{Ch} is Simpsons slip factor, and $a = \frac{1}{6}$, and can be adjusted if needed. Both models account for fluid densities, but only Chisholm's model accounts for fluid volume fractions. Therefore, the differences between the models can be large with a large spread in gas fraction.

Critical Flow:

If the pressure ratio over a flow restriction is low enough, the flow will enter a critical flow regime. At this pressure ratio, the fluid reaches its sonic velocity. Any further reduction of the

downstream pressure does not increase the flow rate. This is sketched in *Figure 2*. Theoretically, both liquid and vapor can experience critical flow, as all fluids have a defined sonic velocity. For fluids, this is mathematically extremely unlikely, due to low compressibility. However, in the case of a fluid reaching its bubble point though a valve; it can start flashing out vapor and inducing critical flow.

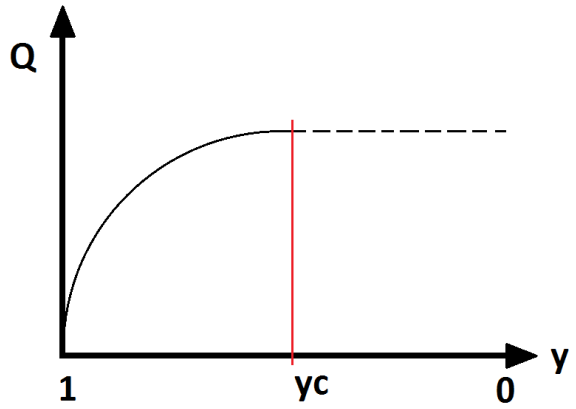

Figure 2: Visual representation of the critical flow behavior, Pressure ratio (y) plotted against flow rate (Q). Pressure ratios below critical pressure ratio (y_c) does not increase flow rate.

Gas compressibility

Gas expansion behavior can be modelled using the real gas law:

$$PV = Z\,nRT \tag{24}$$

Where Z is the gas compressibility factor, n is the gas amount in moles, R is the universal gas constant and P, V, T are pressure, volume and temperature. The Z-factor can be modelled using Sutton's correlations for pseudocritical pressure and temperature and Hall-Yarboroughs correlation for the Z-factor.

Sutton correlations:

$$P_{pc} = 756.8 - 131y - 3.6y^2 \tag{25}$$

$$T_{pc} = 169.2 + 349.5y - 74y^2 \tag{26}$$

Where y is the specific gravity of the gas:

$$y = \frac{M_{gas}}{M_{air}} = \frac{M_{gas}}{28.97} \tag{27}$$

Hall Yarborough Z-factor correlation:

First, the definition of pseudo reduced pressure and temperature:

$$T_{pr} = \frac{T}{T_{pc}} \tag{28}$$

$$P_{pr} = \frac{P}{P_{pc}} \tag{29}$$

Hall and Yarborough developed a correlation for determining the Z-factor. The correlation was made to fit the Standing-Katz chart, and is accurate enough for most engineering applications [27]. The correlation is a series of equations with pseudo reduced pressure and temperature as the variables.

$$Z = \frac{A\,P_{pr}}{Y} \tag{30}$$

Where:

$$t_r = \frac{1}{T_{pr}} \tag{30) (a}$$

$$f(Y) = \frac{Y + Y^2 + Y^3 - Y^4}{(1-Y)^3} - Ap_{pr} - BY^2 + CY^D = 0 \tag{30) (b}$$

$$A = 0.06125\; t_r\; e^{-1.2(1-t_r)^2} \tag{30) (c}$$

$$B = t_r(14.76 - 9.67t_r + 4.58t_r^2) \tag{30) (d}$$

$$C = t_r(90.7 - 242.2t_r + 42.4t_r^2) \tag{30) (e}$$

$$D = 2.18 + 2.82t_r \tag{30) (f}$$

Equation (30) (b) has to be solved by an iterative process. Whitson [27] recommends a Newton Raphson procedure with a starting value of 0.001. A convergence should be found from 3-10 iterations in most cases.

1.2: Introduction to Horizontal wells

Many reservoirs are composed of a thin oil column, sandwiched between an underlying aquifer and an overlying gas gap. These kinds of reservoirs are often subject to oil or water coning, occurring as gas or water moves towards the wellbore in a cone shape fashion, and eventually entering the wellbore. This is referred to as gas of water breakthrough, and is sketched in Figure 3. Increased mobility of the lower viscosity fluids can give progressively higher rates of water and gas, thus severely limit oil recovery [11].

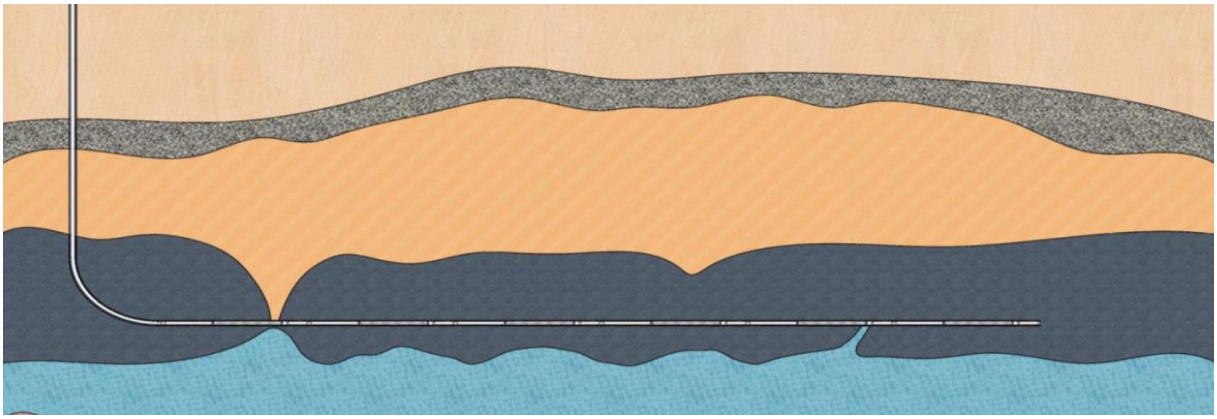

Figure 3: Sketch of a horizontal well experiencing gas and water coning. From [16]

For the last couple of decades, horizontal wells have been used to maximize contact with the reservoir pay zone. A lower pressure drawdown is therefore required to produce the same oil rate as for a vertical well [18]. For this reason, horizontal wells generally have a higher oil recovery, and are more profitable [15].

Together with the benefits of horizontal wells, they also pose some new challenges. In high productivity wells, frictional pressure drop in the tubing cause an increasing pressure drawdown from toe to heel, which can in turn lead to coning effects near the heel of the well.

If the reservoir is heterogeneous, some sections of the well might have a far higher productivity than the rest, due to variations in permeability or fractures in the reservoir. In this case, the higher productivity sections of the well might experience coning effects early in the life of the well.

This kind of reservoir and well type is typical for Troll field, located of the West coast of Norway [20]. It is operated by Statoil ASA, and can be divided into two main structures. Troll East is the main gas-producing segment, while Troll West is the main oil producer. Troll West has similar properties as described above, with a thin oil layer sandwiched between gas and water. Models and technology from the Troll field will be revisited throughout this paper.

1.3: Inflow Control Technology

1.3.1: Traditional Inflow Control Devices

In order to delay gas or water breakthrough, the inflow to the horizontal well needs to be closer to uniform. Historically this could be done by varying the perforation intervals along the wellbore [4]. Today, this is popularly obtained by using Inflow Control Devices (ICD). ICDs are flow restrictions distributed along the horizontal well, with the purpose of provide an extra pressure drop to create a more uniform inflow profile along the well. This can delay the gas and water breakthrough, and significantly increase oil recovery compared to wells without ICDs [5], [14].

Traditional ICD technology are passive devices, meaning they do not move or have any other functions than to provide an added pressure drop. Devices are designed with different sizes and geometries for the specific pressure drop required. The types of ICD most used are Nozzle, Orifice of Annular types (Figure 4).

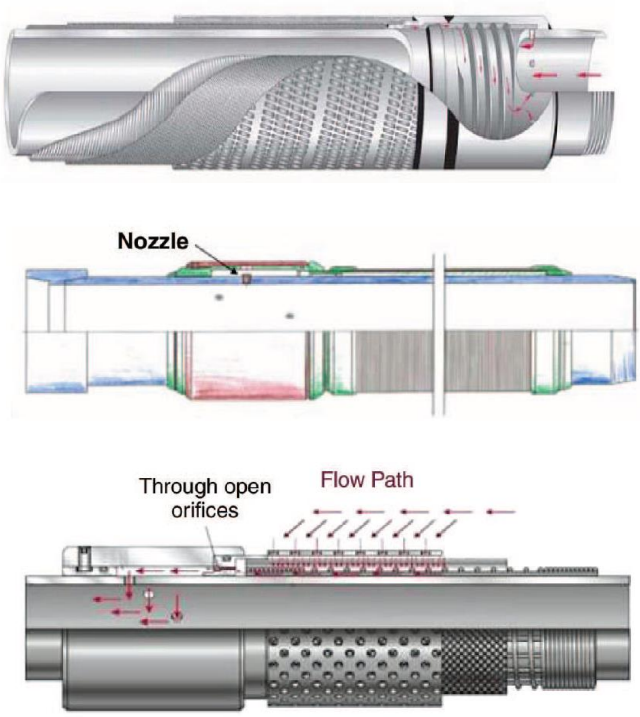

Figure 4: Channel (top), Nozzle (middle) and Orifice (bottom) type ICDs. Adapted from [5]

Even if they are able to delay gas or water breakthrough, they do not contribute to further choking of unwanted fluids once this has happened. Because of this, traditional ICDs only delays coning problems, and does not solve them completely.

1.3.2: Inflow Control Valves

More advanced inflow control systems are Inflow Control Valves (ICV). This type of valve is not designed to choke the initial inflow, but to shut in producing sections completely once breakthrough has occurred. They are connected electrically and hydraulically to the surface, and can be manually shut in by an operator when unwanted fluids enter the system. This kind of completion of sometimes referred to as “Smart Wells”.

ICVs are expensive to implement and maintain, and can only be installed in a limited number of zones. They require more components and installations in the well, and the added complexity might be operationally unstable. In order to use the technology, remote monitoring is required, increasing the time and cost spent on the well [16].

1.3.3: Autonomous Inflow Control Devices

Among the more recent ICD technology are Autonomous Inflow Control Devices. They are ICDs that allow for autonomous selective choking of fluid phases. The geometry of the valve provides an increased pressure drop when low viscous fluids flow through, compared to heavier oils. This means that the valve operate autonomously, i.e. without the need for interaction by an operator.

This allows the AICD to have two functions; Provide a uniform inflow profile (Like traditional ICDs) to delay gas and water breakthrough, and mitigate the effect of breakthrough once it has happened. Zones with gas and water coning will not be shut in, but flow is choked more than zones producing mostly oil.

There are several types of AICD technology, and one of them is the RCP (Rate Controlled Production) valve developed by Statoil. The valve has a flow chamber with a single floating disc, that regulates the maximum flow area for passing fluids [17]. When low viscous fluids

flow through, the disc is moved towards the inlet, thus restricting the flow. Higher viscosity fluids push the disc away from the inlet, and increases the flow.

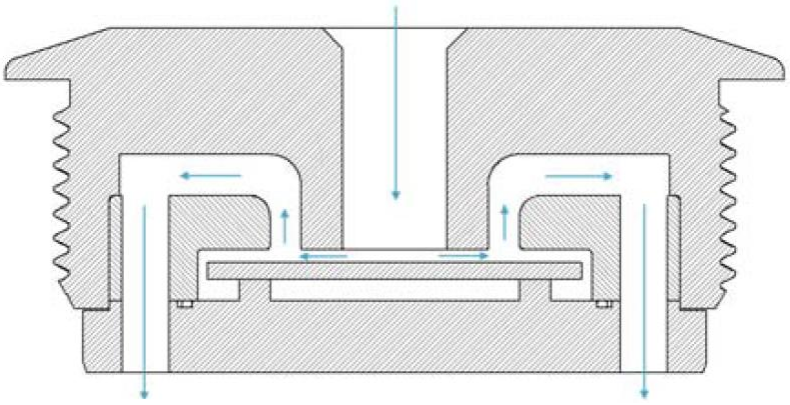

Figure 5: Scetch of the Statoil RCP Valve, with flow path indicators. From [10]

This behavior is explained by the Bernoulli Equation (6), neglecting compressional and elevation effect. Pressure on the flowing side of the disc is low due to the higher fluid velocity, and the rear side of the disc will experience a stagnation pressure where the velocity is zero. Lower viscosity fluids tend to follow different streamlines resulting in a higher stagnation pressure. A cross-section of the valve is shown in Figure 5.

As explained in chapter 1.1, lower viscosity fluids will also experience a lower frictional pressure drop than higher viscosity fluids, if the flow is laminar. This further facilitates a high stagnation pressure on the backside of the disc. These effects combined, results in the disc moving closer to the inlet with lower viscosity fluids. This means that the unwanted fluid flow is never completely shut off, as the valve needs flow though it to trigger the choking.

Statoil has extensively implemented these valves on the Troll field. Wells completed with this technology have been shown to have significantly lower GOR and higher oil recovery than wells with traditional ICDs [9].

1.3.4: Autonomous Inflow control Valve

The newest inflow control technology is the Autonomous Inflow Control Valve, developed by the company InflowControl. It aims to combine the benefits of all previous ICD technology. It can be used to equalize the inflow profile before breakthrough, choke unwanted fluids after breakthrough and shut the valve in once the unwanted fluid fraction is high enough. All this while functioning autonomously, without any interaction from an operator.

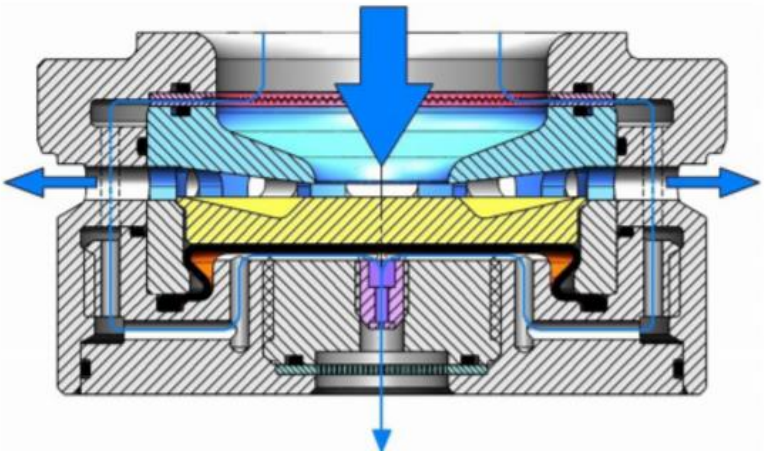

Figure 6: Sketch of the AICV. The large and medium arrows indicate the main flow path. The smallest arrow indicate the pilot flow. The piston marked as yellow. From [19]

The AICV is made with a main flow path and a pilot flow path, both ending in the outlet of the valve. Less than 1% of the total flow is directed to the pilot. A pressure sensitive piston is located in the pilot path, able to completely shut in the main flow path. The piston is triggered by a certain pressure in the pilot flow. A cross-section of the AICV is shown in Figure 6.

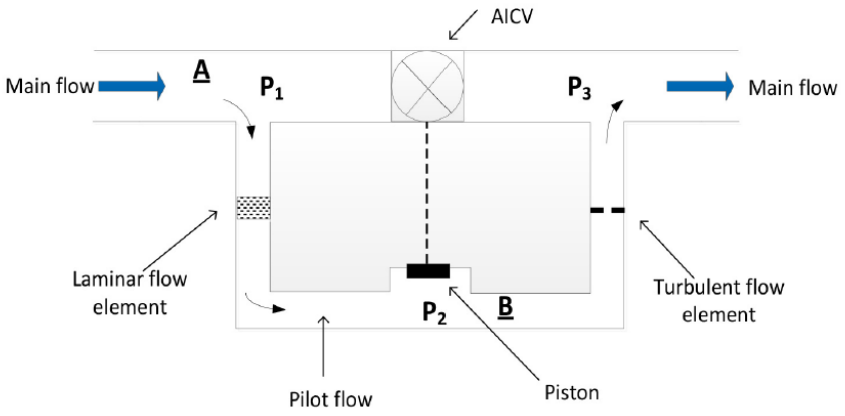

Figure 7: Simplified sketch of the flow paths in the AICV. From [19]

The pilot flow consist of a laminar flow and a turbulent flow element, as shown in Figure 7. High viscosity fluid flow in the pilot will be choked in the laminar section, and the lower pressure will not trigger the piston. Lower viscosity fluids will not be choked as much by the laminar flow element (Figure 8), and the pressure is maintained high enough to trigger the piston. The main flow path will then be shut in completely, and the only flow through the valve is through the pilot flow. If high-viscosity fluid re-enters the valve, it will open again. In this way, the valve is self-regulating and reversible.

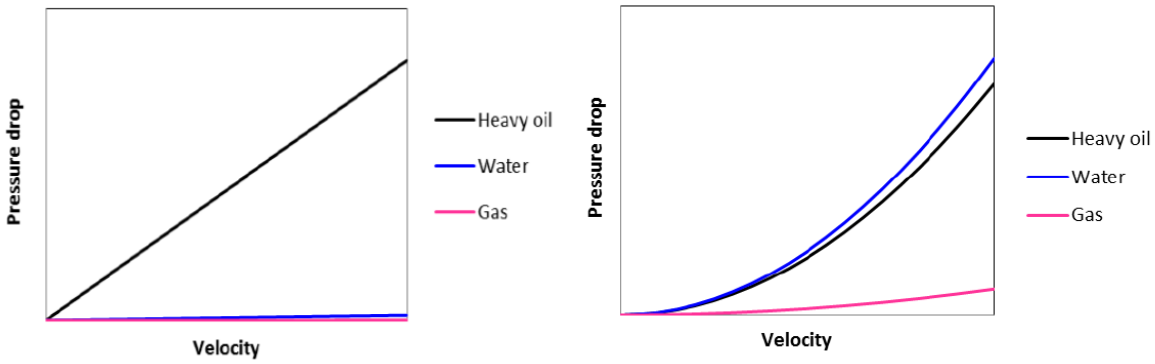

Figure 8: Sketch of typical pressure drop over the laminar flow element (left) and turbulent flow element (right). From [16]

Chapter 2: AICD modelling

In order to assess the benefit if ICD technology, they need to be modelled in reservoir and productions systems. The models used for the ICDs need to be accurate, as they produce a significant pressure and flow variation in the system. The models should capture pressure drop across the valves as a function of flow rate, fluid composition and P, T conditions. ICDs will be exposed to a variety of flowing conditions and compositions, and the models must therefore be able to predict both single- and multiphase flow.

This chapter will evaluate different models for pressure drop across AICDs, based on laboratory test data found in the literature. The devices of interest was originally both AICDs and AICVs, as these are the newest technologies with the least amount of research so far. However, no accurate laboratory test data was found in the literature for AICVs, so the chapter will only consider AICDs. Several papers present experimental results for AICV ([1], [16],[19]) , but almost all are only with single-phase data. A few papers investigate multiphase flow, but none has been found that show accurate results.

The models investigated in this chapter are:

1. Statoil's RCP model
2. Bernoulli choke model
3. Sachdeva's choke model
4. Asheim's choke model
5. (Al-Safran's model) [1]

Model 1 is specifically designed for the RCD-valve, and the rest are originally intended for multiphase flow through chokes. The result of interest is model performance and how the models compare to each other.

[1] Al-Safran's choke model was also considered used, but was discarded. One of the terms in the model include a division with the gas mass fraction [3]. Thus, the model does not work for single-phase oil or water when $x_g = 0$.

2.1: AICD Laboratory test data

There is a limited amount of test data available for AICDs in the literature. Most papers either only present single-phase data, or pseudo-data meant to represent the general behaviour.

Two sets of laboratory test data has been found for AICDs that include a variety of both single- and multiphase data. These are for the two types of devices:

- **Dataset 1:** Statoil's RCP valve, as presented in chapter 1.3.3. Presented in [9].
- **Dataset 2:** Halliburton's Fluidic Diode Valve. This is a valve with vastly different choking mechanisms, but provide the same use as the RCP-valve. Presented in [6].

Both papers present laboratory data in graphical form and this data has been extracted into numerical values using the web-tool WebPlotDigitizer[2].

In order to use the datasets for the models, some adjustments and assumptions were made.

- Both datasets has been converted to units of [m3/s] vs [bar].
- Neither of the datasets give information of the molar mass of the gas used for testing. In order to find the molar mass of the gasses, Equation (36) was used via an iterative process together with Equation (29) for the test P,T-conditions.
- Neither of the datasets give heat capacity values. In order to use the Sachdeva model, the heat capacity values used in [12] was copied and used for both datasets.
- The Statoil RCP data suggest that the valve has an outer size of 5mm, and a nozzle size of 1mm. No such information was found for the Haliburton data. These values have been used for A_1 and A_2 for both datasets. The approximation probably does not accurately represent the valve geometries.

[2] http://arohatgi.info/WebPlotDigitizer/ - Open source web based tool to extract numerical data from plots and images.

2.1.1: Dataset 1 - Statoil RCP Valve

This test in done with Statoil's RCP valve described in chapter 1.3.3. It was done with fluids and test conditions closely representing the Troll field (130 bar, 68 degC), at Statoil's multiphase testing facility in Porsgrunn. Table 1 details the fluid properties for the test.

The data consist of 194 data points, where 144 of them are single-phase, and 50 are multiphase. Multiphase compositions tested are shown in Table 2. The flow rate varies from 0-1.2 m3/hr and the pressure drop from 0-40 bar.

The extracted dataset in its volumetric flow rate form is found in Appendix B.1. Plots of the data are shown in Figure 9 and Figure 10.

Fluid	Density [kg/m3]	Viscosity [cp]	Molar mass [g/mol]	Cv [J/kg]	Cp [J/kg]
Gas	150	0.02	25.0	726	1020
Oil	890	2.7	-	2010	2160
Water	1100	0.45	-	4170	4170

Table 1: Fluid properties at test conditions for Dataset 1

Compositions	Water Cut	Gas Volume Fraction
Oil/Gas 1	0%	25%
Oil/Gas 2	0%	70%
Oil/Gas 3	0%	87%
Oil/Gas 4	0%	96%
Oil/Gas/Water 1	50%	25%
Oil/Gas/Water 2	50%	70%
Oil/Gas/Water 3	50%	87%
Oil/Gas/Water 4	50%	96%

Table 2: Multiphase compositions used Dataset 1

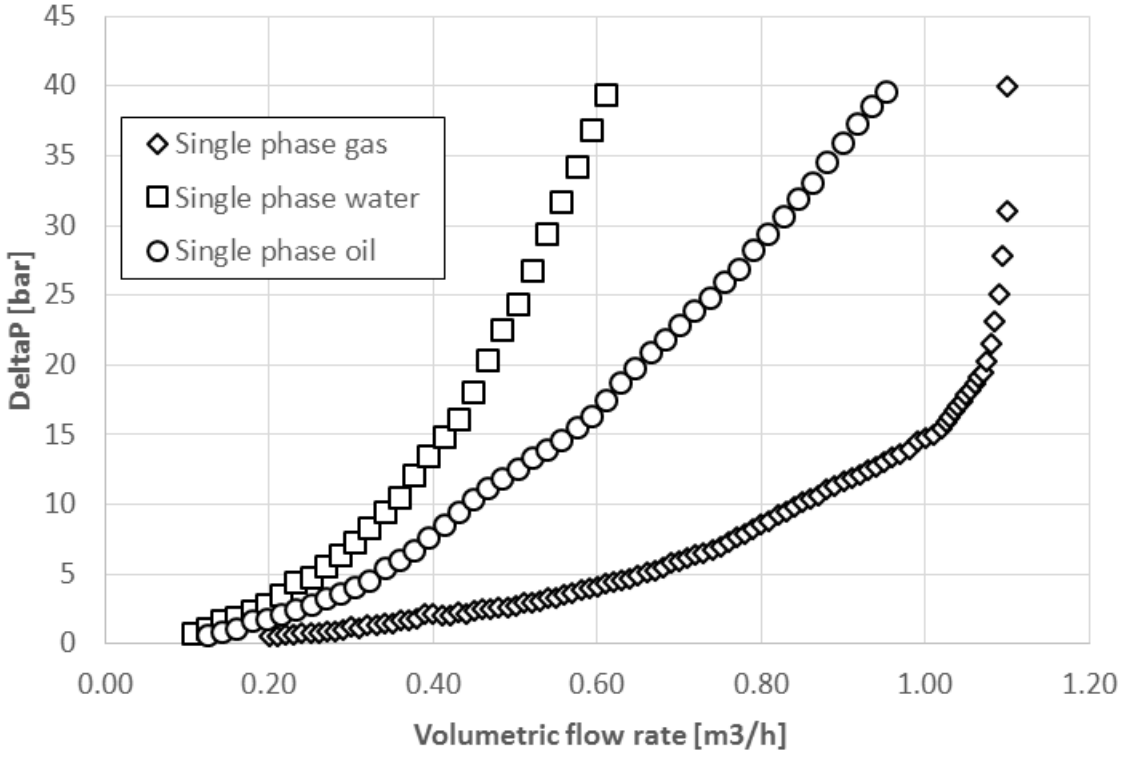

Figure 9: Single-phase test data for Dataset 1.

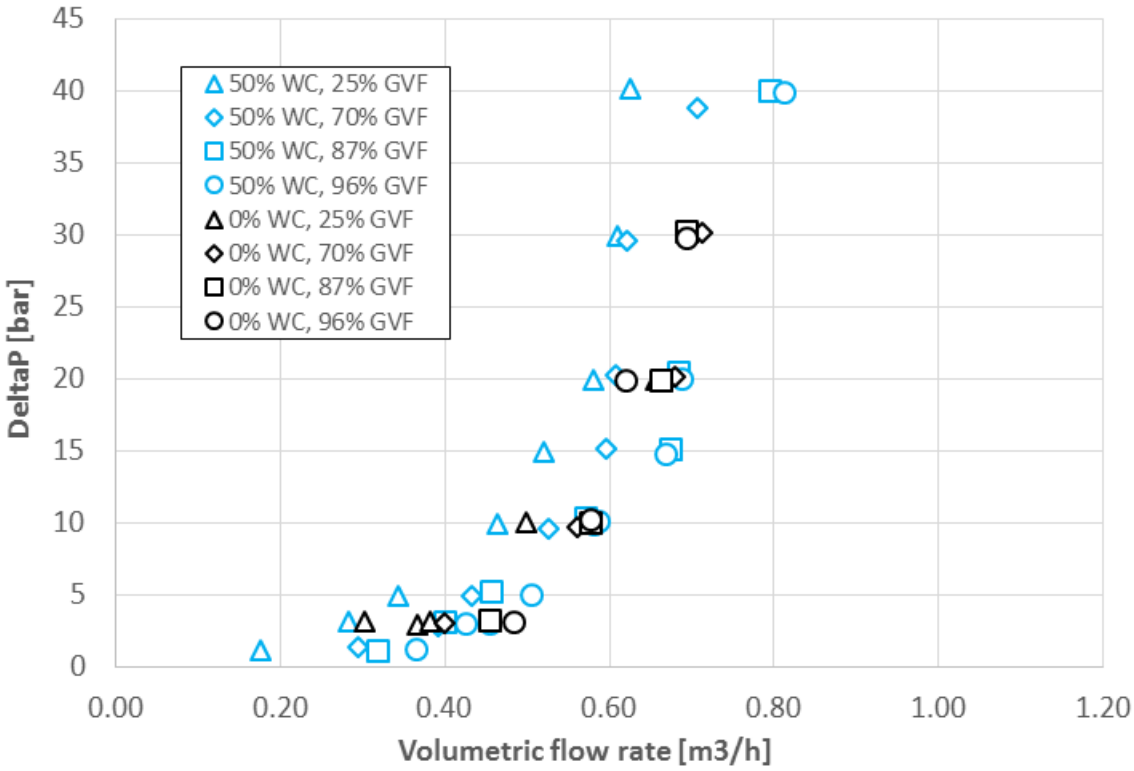

Figure 10: Multiphase test data for Dataset 1

2.1.2: Dataset 2 - Haliburton fluidic diode valve

This test was done at a dedicated flow facility at Southwest Research Institute (SwRI) for Haliburton. The fluids used were Exxsol D60, Nitrogen and water. Test with other fluids were also performed, but they are not of interest for this paper. The authors of the paper write, "*The flow test performance results are generalized and converted into equations*[3]", and then used in reservoir simulators. However, no method or model for this is shown.

Fluid properties at test conditions are given in Table 3, and compositions used in the test in Table 4. Pressure at test conditions was not reported, only the differential pressure. It will therefore be assumed that the inlet pressure is the same as for dataset 1 (130bar), in order to do a close comparison. Temperature was given as 166 degF = 74.4 degC.

The dataset consist of 41 data points, whereof 25 single phase and 16 multiphase. The extracted dataset in its volumetric flow rate form is found in Appendix B.2. Plots are found in Figure 11 and Figure 12.

Fluid	Density [kg/sm3]	Viscosity [cp]	Molar mass [g/mol]	Cv [J/kg]	Cp [J/kg]
Gas	140	0.02	23.9	726	1020
Oil	780	0.7	-	2010	2160
Water	997	0.4	-	4170	4170

Table 3: Fluid properties for Dataset 2

Compositions	Water Cut	Gas Volume Fraction
Oil/Gas 1	0%	25.1%
Oil/Gas 2	0%	50%
Oil/Gas 3	0%	75.1%
Oil/Water 1	49.8%	0%
Oil/Water 2	75.2%	0%

Table 4: Multiphase compositions used for Dataset 2

[3] From [6], at page 8.

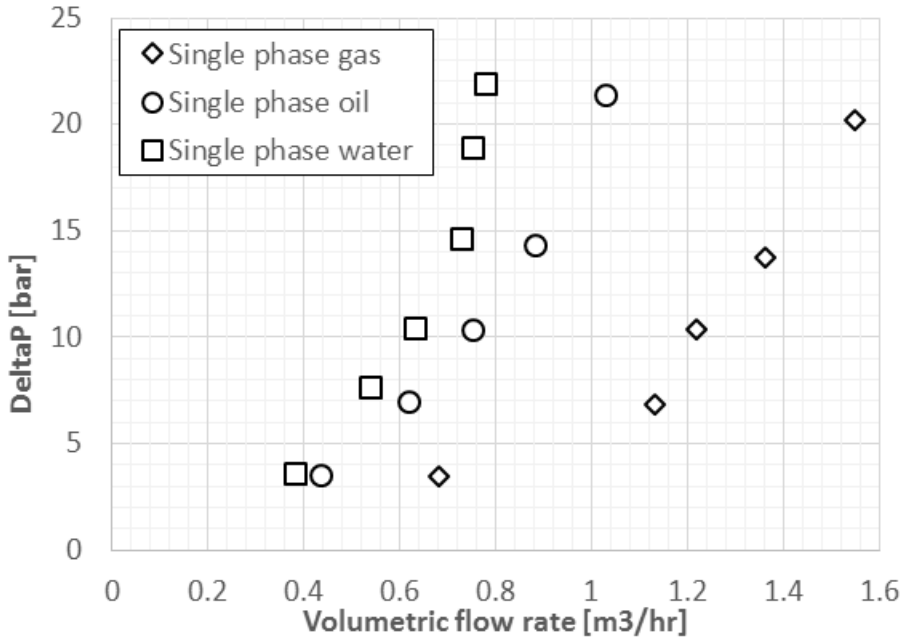

Figure 11: Single-phase test data for Dataset 2

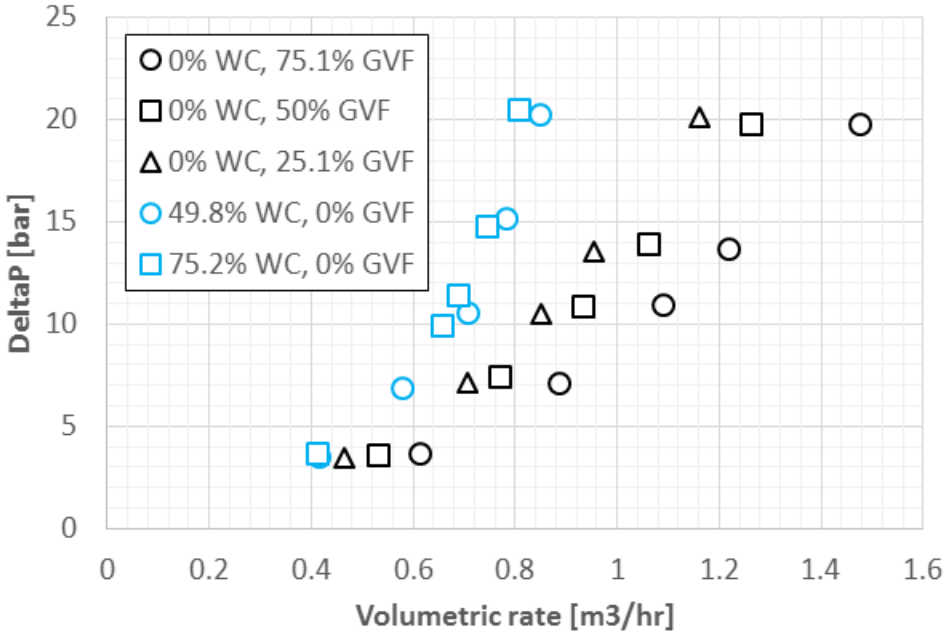

Figure 12: Multiphase data for Dataset 2

2.2: AICD Models

This chapter presents the models used for the analysis. All models except for Statoil's model are designed for mass flow rate. These models have been used in their original form, and iteratively found the pressure drop for a given flow rate. All models are one-dimensional steady state, neglects frictional and gravitational losses and assume constant mass fractions.

2.2.1: Statoil model

Statoil has presented the only model made specifically for AICDs, as of this author's knowledge and research. The model is proposed by Mathiesen et al. (2014) [16], and is specifically designed for Statoil's RCP valve. The model performance for single phases are shown, but no model analysis for multiphase has been provided. The model relates pressure drop as a function of volumetric flow rate, fluid volume fractions, density and viscosity along with a variety of tuning parameters.

The model is not analytically derived, but is based on experimental data:

$$\Delta P = f(\rho, \mu, q) = \left(\frac{\rho_{mix}^2}{\rho_{cal}}\right) \cdot \left(\frac{\mu_{cal}}{\mu_{mix}}\right)^y \cdot a_{AICD} \cdot q^x \tag{31}$$

Where q **is the total local volumetric flow rate.** Mixture density and viscosity is defined as:

$$\rho_{mix} = \alpha_{oil}^a \rho_{oil} + \alpha_{water}^b \rho_{water} + \alpha_{gas}^c \rho_{gas} \tag{32}$$

$$\mu_{mix} = \alpha_{oil}^d \mu_{oil} + \alpha_{water}^e \mu_{water} + \alpha_{gas}^f \mu_{gas} \tag{33}$$

Where α is the phase volume fraction.

And the following parameters are constants, used to optimize the model:

- ρ_{cal} is a calibration density
- μ_{cal} is a calibration viscosity
- a_{AICD} is the AICD strength
- y is a viscosity exponent
- x is a rate exponent
- a-f are phase calibration parameters

This sums up to a total of 11 parameters used to tune the model to experimental data. A simplified version of the model is to set parameters *a-f* to one, as originally presented in *[17]*. This corresponds to the Homogenous mixing as in Equation (14) and (15). The parameters was added to aid in better description of multiphase conditions.

2.2.2: Bernoulli model

The Bernoulli model is simple, and in many cases useful as an approximation. The model is based on the Bernoulli equation, assumes incompressible flow (constant densities), and does not capture critical flow. By substituting $u = \frac{\dot{m}}{\rho A}$, and rearranging the terms the following expression of the mass flow rate is obtained:

$$\dot{m} = A_2 \sqrt{\frac{2\rho(P_1 - P_2)}{1 - \left(\frac{A_2}{A_1}\right)^2}} \tag{34}$$

Where A_2 and A_1 are the maximum and minimum flow area across the contraction. To account for geometries that deviate from smooth curves, as in contractions like valves and chokes, a contraction coefficient is defined.

$$C_c = \frac{A_{vc}}{A_2} \tag{35}$$

Where A_{vc} is the area of the *vena contracta.* This the area within the contraction with the minimum flow area, as the fluid is unable to flow around sharp edges in a contraction. A_{vc} can be thought of as the effective minimum flow area. In order to capture energy dissipation affects in the entrance region, the meaning of the contraction coefficient is expanded to a discharge coefficient C_d. In summary, it is meant to capture non-ideal geometry effects. This parameters is used to tune the model to the experimental data, and is included in further choke models as well.

To account for two-phase flow, a two-phase multiplier is added to the equation. Defined as:

$$\phi_{TP} = \frac{\Delta p_{single-phase}}{\Delta p_{two-phase}} \tag{36}$$

Chisholm and Simpson has presented their versions of this multiplier, both using their respective slip factor. Chisholm's two-phase multiplier is given as:

$$\phi_{TP,Ch} = 1 + \left(\frac{\rho_{liq}}{\rho_{gas}} - 1\right)\left(B x_{gas} x_{liq} + x_{gas}^2\right) \tag{37}$$

Where:

$$B = \frac{\left(\frac{1}{k_{Ch}}\right)\left(\frac{\rho_{liq}}{\rho_{gas}}\right) + k_{Ch} - 2}{\frac{\rho_{liq}}{\rho_{gas}} - 1} \tag{38}$$

Where $k_{Ch}$is given in Equation (21) . Simpson's two-phase multiplier is given as:

$$\phi_{TP,Si} = \left(1 + x_{gas}(k_{Si} - 1)\right)\left(1 + x_{gas}\left(k_{Si}^5 - 1\right)\right) \tag{39}$$

Where k_{Si} is given in Equation (23).

Merging (34) with (36) and (35) gives:

$$\dot{m} = C_d A_2 \sqrt{\frac{\frac{2\rho_{mix}(P_1 - P_2)}{\phi_{TP}}}{1 - \left(\frac{C_d A_2}{A_1}\right)^2}} \tag{40}$$

Where ρ_{mix} is an appropriate mixture density.

2.2.3: Asheim's model

According to [12], Asheim proposed a choke formula based on the acceleration pressure drop in Equation (3). The model does not account for slip, and therefore the densities are based on homogenous density. Liquids are assumed incompressible, and gas expansion is modelled by the real gas law:

$$PV = nRTZ \tag{41}$$

Rearranging terms give the gas density:

$$\rho_{gas} = \frac{PM}{ZRT} \tag{42}$$

Where:

- P is the pressure
- M is the molar mass of the gas
- Z is the compressibility factor
- R is the universal gas constant
- T is the temperature

In this paper, the Z factor was calculated using the Hall-Yarborough correlation (30).

Substituting the homogenous density (18) into the acceleration pressure term (3) gives:

$$u\,du = -\left(\frac{x_{gas}}{\rho_{gas}} + \frac{x_{liq}}{\rho_{liq}}\right)dP \tag{43}$$

Substituting in Equation (42) for the gas density gives:

$$u\,du = -\left(x_{gas}\frac{ZRT}{PM} + \frac{x_{liq}}{\rho_{liq}}\right)dP \tag{44}$$

Integrating this term gives:

$$u_2 = \sqrt{2\left(x_{gas}\frac{ZRT}{M}\ln\frac{P_1}{P_2} + \frac{x_{liq}}{\rho_{liq}}(P_1 - P_2)\right)} \tag{45}$$

Where $u_2 \gg u_1$ and therefore $u_2^2 - u_1^2 \approx u_2^2$ is assumed during the integration. It is assumed that the temperature is constant over the integration, along with M and Z. Substituting $u_2 = \frac{\dot{m}}{\rho_H A_2}$ into Equation (45), and rearranging for the mass rate gives:

$$\dot{m} = \frac{C_d A_2 \rho_{liq} P_2}{x_{gas}\rho_{liq}\frac{ZRT}{M} + x_{liq}P_2}\sqrt{2\left(x_{gas}\frac{ZRT}{M}\ln\frac{P_1}{P_2} + \frac{x_{liq}}{\rho_{liq}}(P_1 - P_2)\right)} \tag{46}$$

Critical flow can be modelled by differentiating equation (46) and finding the maximum flow rate. This has not been done here.

2.2.4: Sachdeva et al. model

The Sachdeva model [22] uses the same starting assumptions as Asheim's model, but assumes polytropic gas expansion instead of using the gas law, and includes a term for critical flow. Polytropic gas expansion is expressed as:

$$\rho_{gas,2} = \frac{1}{\rho_{gas,1}} \left(\frac{P_1}{P_2}\right)^{\frac{1}{n}} \tag{47}$$

Where:

$$n = \frac{k x_{gas} C_{v,gas} + x_{liq} C_{liq}}{x_{gas} C_{v,gas} + x_{liq} C_{liq}} \tag{48}$$

$$k = \frac{C_{p,gas}}{C_{v,gas}} \tag{49}$$

Substituting Equation (47) into Equation (43) and integrating gives:

$$\frac{\dot{m}}{2\rho_{mix,2}^2} = \frac{x_{liq}(1-y)}{\rho_{liq}} + \frac{k x_{gas}}{k-1} \left(\frac{1}{\rho_{gas,1}} - \frac{y}{\rho_{gas,2}}\right) \tag{50}$$

Where $u_2 \gg u_1$ and therefore $u_2^2 - u_1^2 \approx u_2^2$ is assumed during the integration. Solving for the mass flow rate gives the final expression for the model:

$$\dot{m} = C_d A_2 \sqrt{2 P_1 \rho_{mix,2}^2 \left[\frac{x_{liq}(1-y)}{\rho_{liq}} + \frac{k x_{gas}}{k-1} \left(\frac{1}{\rho_{gas,1}} - \frac{y}{\rho_{gas,2}}\right)\right]} \tag{51}$$

Which is an expression based on the mass flow rate. This paper is interested in the pressure drop as a function of the rate. Therefore, with a given flow rate, the downstream pressure is found iteratively.

Critical Flow

The definition of critical flow can be expressed as no change in mass rate with a change in downstream pressure:

$$\frac{d\dot{m}_c}{dP_{2,c}} = 0 \tag{52}$$

Substituting $u_{2,c} = \frac{\dot{m}_c}{\rho_m A_2}$ into equation (3) gives:

$$dP_{2,c} = -\left(\frac{\dot{m}_c}{\rho_m A_2}\right)\rho_m \, d\left(\frac{\dot{m}_c}{\rho_m A_2}\right) \tag{53}$$

Rearranging, and considering Equation (52) gives the following expression:

$$-A_2^2 = \dot{m}_c^{2^2} \frac{d}{dP_{2,c}}\left(\frac{1}{\rho_m}\right) \tag{54}$$

Substituting this into Equation (43) and differentiating with the density as Equation (47) gives;

$$\dot{m_c^2} = \frac{nA_2^2 P_{2,c}\rho_{gas,2}}{x_g} \tag{55}$$

Which is the critical mass flow rate. Combining this with Equation (50) gives:

$$y_c = \left(\frac{\frac{k}{k+1} + \frac{x_{liq}(1-y_c)\rho_{gas,1}}{x_{gas}\rho_{liq}}}{\frac{k}{k+1} + \frac{n}{2} + \frac{nx_{liq}\rho_{gas,2}}{x_{gas}\rho_{liq}} + \frac{n}{2}\left[\frac{x_{liq}\rho_{gas,2}}{x_{gas}\rho_{liq}}\right]^2} \right)^{\frac{k}{k-1}} \tag{56}$$

Which is an implicit expression for the critical flow ratio. This expression needs to be solved iteratively. If the calculated pressure ratio in Equation (51) is lower than the critical flow rate, then the critical flow rate is used as the solution. If the calculated ratio is higher, it is used as the solution.

2.3: Results

2.3.1: Evaluating the model

The basis for evaluation is the measured pressure drop against the modelled pressure drop. The difference between these two is used to measure the error. There are several ways to represent an error in a comparison.

Mean relative error

A relative error normalizes the error to the dataset, and gives a better understanding of how the dataset behaves than an absolute error. It gives the possibility to compare different datasets with each other .The mean relative error takes both positive and negative values, and thus an evenly distributed error in the dataset will yield a 0% mean relative error. It is therefore not representative as an evaluation, but is needed to calculate the standard deviation. It can also show if the data deviates positively or negatively.

$$E_{rel} = \frac{1}{N}\sum_{i=1}^{N}\left(\frac{\Delta p_{test,i} - \Delta p_{model,i}}{\Delta p_{test,i}}\right) \cdot 100\% \tag{57}$$

Standard deviation

The standard deviation represent the spread in the values of a dataset. A high standard deviation means that the errors deviate far both up and down of the mean, while a low standard deviation suggest that most data is centered on the mean.

$$\sigma = \sqrt{\frac{1}{N-1}\left(\sum_{i=1}^{N}\left[\left(\frac{\Delta p_{test,i} - \Delta p_{model,i}}{\Delta p_{test,i}}\right) - \frac{E_{rel}}{100}\right]^2\right)} \cdot 100\% \tag{58}$$

Mean absolute relative error

Taking the *absolute value*[4] of the relative error give a more realistic number as a representation of the model accuracy. When taking the mean of all absolute relative errors, we get a positive number. This is easily understood, and a good way to represent the overall error of the dataset.

$$E_{rel,abs} = \frac{1}{N}\sum_{i=1}^{N}\left|\left(\frac{\Delta p_{test,i} - \Delta p_{model,i}}{\Delta p_{test,i}}\right)\right| \cdot 100\% \tag{59}$$

Sum of squares error

Relative errors, absolute or not, tend to over-emphasize low value data points. A very slight deviation from the measured data can result in a large percentage of relative error. When optimizing a model, higher value datapoints may therefore be under-emphasized. The sum of least squares method can shift this emphasis more evenly across the dataset. It takes the difference between measured and calculated datapoints, and squares the results. This also ensures that that the value is always positive. The sum of the squared errors of all datapoints minimized using an optimization process.

$$E_{SSQ} = \sum_{i=1}^{N}\left(\Delta p_{test,i} - \Delta p_{model,i}\right)^2 \tag{60}$$

[4] Not to be confused with the *absolute error*

2.3.2: Model matching

Excels SOLVER tool was used to match the models to the two datasets. To be able to compare the models directly with each other $E_{rel,abs}$ was the target for optimization. The SOLVER was set to find the minimum value of this by changing the tuning parameter(s). For all models except the Statoil model, the only tuning parameter was the discharge coefficient C_D. For the Statoil model, all 11 parameters was tuned.

Solver convergence

With large, multivariable non-linear problems, the Excel SOLVER can risk converging into a local minimum instead of a global minimum. This means that in theory, an optimization problem can converge on a 'wrong' solution, and thus give unrealistic results. A visualization of the issue is sketched in Figure 13

Using the Multistart option in Excel SOLVER can reduce the risk of finding of converging on a local minimum. Multistart procedures requires an upper and lower bound on the tuning variables, and creates a random population of these to start from. From the different start point, several local minimums can be found, and the solver selects the best fit. This is equal to running the solver manually with many different starting positions, and choosing the best fit manually, and is no guarantee for a global solution.

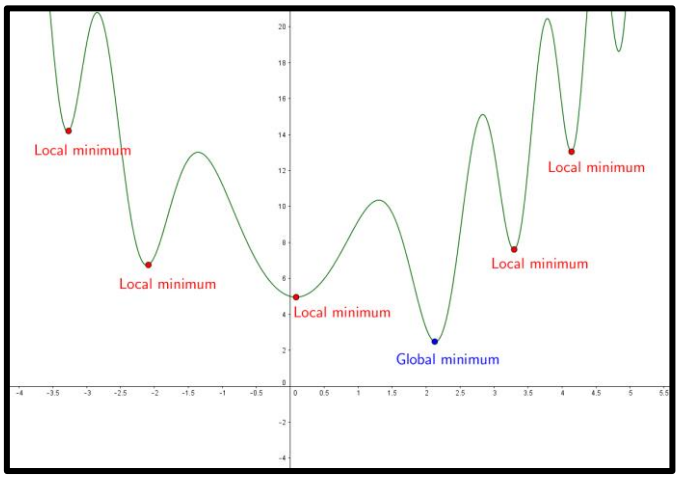

Figure 13: Sketch of a function with several local minimums and one global minimum

2.3.3: Results overview

Both datasets were tuned to all described models using spreadsheets A.1: (Excel sheet "AICD_model_StatoilRCP.xlsm") and A.2: (Excel sheet "AICD_model_Haliburton"). The spreadsheets include all calculations, overview of the results, and all plots. Coding in VBA was done for most calculations. An overview of VBA codes are found in Appendix F.

An overview of the results from dataset 1 and 2 for all models is shown in Table 5 and Table 6. Optimized tuning parameters for the Statoil model is found in Table 7, and for the other models in Table 8. In addition to the overall error of the data, it was of interest to see how the models performed on the single- and multiphase part individually.

Appendix C shows various error plots for both datasets to all models (Figure 40 to Figure 45). The plots types that have been used are:

- Calculated vs measured deltaP. Lines are plotted to represent 0%, 25% and 50% error.
- Relative error vs gas fraction. Both volume and mass fraction is plotted. This plot show deviation both positive and negative.
- Relative error vs deltaP. This plot show deviation both positive and negative.

Model	Total mean relative Error	Standard deviation	Maximum relative error	Single-phase Error	Multiphase Error
Statoil Homogenous	21.8%	19.3%	97.6%	18.5%	31.0%
Sachdeva	28.5%	20.5%	127.8%	23.3%	43.5%
Asheim	29.9%	27.6%	160.3%	46.4%	25.6%
Bernoulli Homogenous	30.2%	19.2%	115.3%	25.2%	43.8%
Bernoulli Simpson	48.3%	28.8%	86.0%	45.4%	56.3%
Bernoulli Chisholm	48.6%	28.7%	85.5%	45.4%	57.4%

Table 5: Model performance results for Dataset 1

Model	Total mean relative Error	Standard deviation	Maximum relative error	Single-phase Error	Multiphase Error
Statoil	11.3%	10.3%	38.4%	6.0%	14.3%
Sachdeva	13.7%	13.9%	56.9%	17.4%	7.5%
Asheim	14.9%	13.8%	54.4%	18.6%	8.4%
Bernoulli Homogenous	14.6%	14.4%	56.9%	18.0%	8.6%
Bernoulli Simpson	32.2%	34.2%	175.7%	42.9%	13.7%
Bernoulli Chisholm	30.3%	33.9%	172.2%	43.1%	8.1%

Table 6: Model performance results for Dataset 2

Statoil model parameters	Statoil dataset	Haliburton dataset
A	1.02	0.12
B	0.14	0.33
C	1.26	0.89
Calibration density	261.41	2264.80
D	1.00E-04	1.19
E	1.01E-03	1.00E-03
F	1.34	0.54
Viscosity exponent	0.482	0.763
Calibration viscosity	1.38	0.64
ICD strength	2.2E+12	5.1E+11
Rate exponent	2.528	2.240

Table 7: Tuning parameters for optimized solution, Statoil model

Model	Statoil dataset	Haliburton dataset
Sachdeva	0.0302	0.0495
Asheim	0.0284	0.0490
Bernoulli Homogenous	0.0309	0.0491
Bernoulli Simpson	0.0623	0.0575
Bernoulli Chisholm	0.0622	0.0579

Table 8: Tuning parameters for optimized solution, Bernoulli, Asheim and Sachdeva model

2.4: Discussion

Overall, none of the models are able to completely replicate the test data. The average error for dataset 1 is above 20% for all models, with high standard deviations and maximum errors. Results from dataset 2 is better, but still not completely accurate. There is reason to believe that this can cause errors when using the models in reservoir and production simulators.

2.4.1: Model performance

Statoil model

The Statoil model had the best results for both datasets. For dataset 1, the Statoil model is significantly better that all the other models. For dataset 2, there is less spread in the performance, and the Statoil model is only 2 percentage points away from the Sachdeva model. This, despite that the model was not specifically made for the Haliburton Valve. It was not unexpected that the Statoil model would be the best, as it is specifically developed for AICDs. It is also the only model that includes fluid viscosity, which is the driving principle behind AICD selective choking.

Sachdeva and Asheim

The Sachdeva and Asheim models were very similar, which is probably due to their similar derivations. The Sachdeva model is supposed to predict critical flow, but the calculations were not able to capture this. This added complexity of the model might be considered redundant. However, assumptions of heat capacities affect the modelling of critical flow. Proper heat capacity data might have been able to model critical flow correctly. For dataset 2 single phase gas has the highest error.

Bernoulli model

The Bernoulli model showed very different results with and without slip. The simple, original Bernoulli model was far better than when considering slip, for both Simpsons and Chisholm's slip model. Both the Simpson and Chisholm slip model seems to throw the Bernoulli model far off in terms of performance for this use. For dataset 1 the model has an even error across all data, while for dataset 2 the single phase gas has the highest error.

2.4.2: Comparing the models

For dataset 2, Bernoulli, Sachdeva and Asheim all have the highest error at single-phase gas. This shows that gas flow through the AICD deviates from regular choke behavior, and is probably an indication that the AICDs works as intended.

Interestingly, the Bernoulli model is nearly as good as the Sachdeva and Asheim models. For the Haliburton dataset, the Bernoulli model is actually better than Asheim's model. Given the simplicity of the original Bernoulli equation, it performs very well against the more 'advanced' models.

It must be noted that the Statoil model has 11 tuning parameters compared to one parameter for all the other models. For more accuracy, more tuning parameters will in most cases give better results. However, the difference from the Statoil model to the Sachdeva model (second best) is not large (7 and 2 percentage points for dataset 1 and 2). With so many parameters available, perhaps 'any' model would be able to capture the test data.

If the preference of a model is to be as precise as possible, then the Statoil model is the clear choice. If a compromise of accuracy and simplicity is preferred, then the Bernoulli model is

surprisingly accurate. A modification of the Bernoulli model to include viscosity differences in the choking could maybe allow for a new, superior model.

2.4.3: Sources of error

The Haliburton dataset was much better fitted than The Statoil dataset. The results are almost doubled in accuracy. The author believes that the test data provided by Statoil can be criticized. It seems very unlikely that the multiphase flow will behave as different to single-phase flow as presented in the dataset. Performance curves for multiphase flow with 96% GVF are far away from the 100% GVF curve. Intuitively, the multiphase flow curves should collapse onto the single-phase curves when volume fractions approach unity. This does not seem to be the case for dataset 1. It would be interesting to see a test with 100% gas or Oil and gradual introduction of another phase. Future tests of the AICDs should include this.

The Haliburton test data seems more consistent on this part. Oil water mixture curves are placed between oil and water curves, and gas-oil mixture curves are placed between gas and oil curves. There might be a possibility that inaccuracies in the test data affect the overall analysis of the models.

The number of datapoints in the datasets should also be addressed. For dataset 1, the number of single-phase datapoints are significantly higher. This results in an optimization that naturally favors single-phase, as they are averages over all datapoints. Small deviations from single-phase behavior results in large errors in the model. This is probably why we do not see the same error for single phase gas in both datasets.

Chapter 3: VFP tables method for modelling AICDs

The standard way to model AICDs in Eclipse is to use the Statoil model equation presented in chapter 2.2.1 [23]. As shown, the accuracy of the model may not be good enough to represent the AICDs in a good manner. This can affect the accuracy of reservoir and production simulations when planning well completion. If models are not good enough, the technology needs to be tested by trial and error, which can prove very expensive.

Since no other models were shown to have better accuracy than the Statoil model, they are not considered any further. This chapter will propose a new method of modelling AICDs in Eclipse, using a VFP-table approach based on a modified version of the Statoil model.

3.1: Vertical Flow Performance tables

Vertical Flow Performance[5] (VFP) tables are generally used in reservoir simulators to represent tubing flow from the bottomhole to the tubinghead. The tables tabulate bottomhole pressure as a function of oil, gas and water rate together with the flowing tubinghead pressure. To represent the rates, a combination of basis flow rate (oil, gas or liquid), gas fraction (Gas oil ratio, oil gas ratio, gas liquid ratio) and water fraction (water oil ratio, water gas ratio, water cut) is used. Many production simulations software allow for up to 50 nodes of each variable [23].

The table consist of a discrete set of nodes containing all combinations the four variables and the output BHP. In order to obtain the values in between the nodes, most reservoir simulators use multilinear interpolation. For this reason, VFP tables need to be sufficiently dense in nodes to account for non-linearity in the model. Should the simulator need values outside the range of the table, it will linearly extrapolate. This should be avoided, by creating the range of the table to cover all conditions the simulation will encounter.

VFP tables in Eclipse

In addition to Vertical Flow, it is possible to use VFP-tables for representing pressure drop in a pipe segment. Therefore, in theory, a VFP table can be made to represent the pressure drop through an AICD placed in a well segment.

Every reservoir simulator has its own structure for its own compatible VFP-tables, but the basic principle is still the same. The four variables are represented in combination together with their corresponding output in table form. Eclipse has its own specific structure (Figure 14).

[5] Also called Vertical Lift Performance tables, Tubing Head Pressure tables and several other definitions. VFP is the terminology used in this paper.

```
VFPPROD

1       1036  LIQ     WCT    GOR    THP    ''       METRIC       BHP                 /

--Where       LIQ = Liquid rate
--            WCT = Water Cut
--            GOR = Gas Oil Ratio
--            THP = Tubinghead pressure

FLO(1)        FLO(2)        FLO(3)        ...   FLO(n)        ...   FLO(N)        /
THP(1)        THP(2)        THP(3)        ...   THP(m)        ...   THP(M)        /
WFR(1)        WFR(2)        WFR(3)        ...   WFR(k)        ...   WFR(K)        /
GFR(1)        GFR(2)        GFR(3)        ...   GFR(l)        ...   GFR(L)        /

--Where       FLO = Flow rate
--            THP = Tubinghead pressure
--            WFR = Water fraction
--            GFR = Gas fraction

--And         n = 1 to N
--            m = 1 to M
--            k = 1 to K
--            l = 1 to L

1 1 1         BHP(1,1,1,1)          BHP(2,1,1,1)   ...   BHP(N,1,1,1)          /
1 1 2         BHP(1,1,1,2)          BHP(2,1,1,2)   ...   BHP(N,1,1,2)          /
1 1 3         BHP(1,1,1,3)          BHP(2,1,1,3)   ...   BHP(N,1,1,3)          /
...
1 1 L         BHP(1,1,1,L)          BHP(2,1,1,L)   ...   BHP(N,1,1,L)          /
...
m k l         BHP(1,m,k,l)          BHP(2,m,k,l)   ...   BHP(N,m,k,l)          /
...
M K L         BHP(1,M,K,L)          BHP(2,M,K,L)   ...   BHP(N,M,K,L)          /

--For a total of N*M*K*L entries
```

Figure 14: Pseudocode of the VFP-table format in Eclipse (.ECL). Producing well in metric units.

Adapted from Eclipse Manual [23]

3.2: The Black Oil model

Equations (31) to (33) for the AICD all require flow rates and fluid properties to be in local (P, T) conditions. A phase behavior model is needed to convert from standard to local rates. The two most used methods for phase behavior are the Black-Oil (BO) model and Compositional models. The Black-Oil model uses three phases (oil, gas and water) and sets of variables and correlations to relate their properties from standard conditions to local (P,T) conditions.

In contrast, a Compositional model uses thermodynamic Equations of State (EOS) to each hydrocarbon component or pseudo-component. It is more accurate than the Black-Oil model. However, the Black-Oil model more widely used in the industry, because it is simpler to use, and has less computational time.

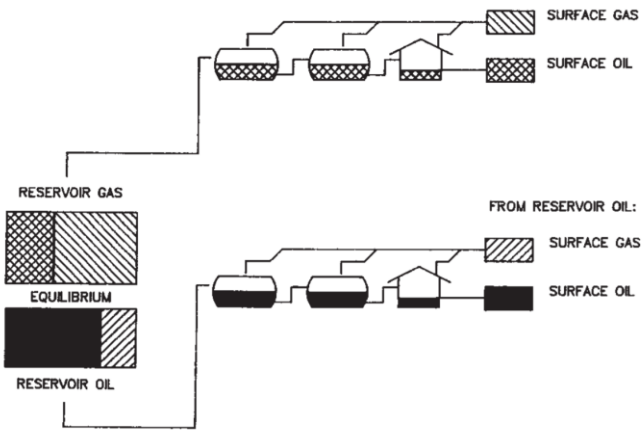

Figure 15: Sketch of a surface process for obtaining surface phases from reservoir phases. From [27]

Consider separate samples of oil and gas at local (P, T) conditions taken to surface conditions through a specific process (Figure 15). The oil volume at local conditions (V_o), will generate a volume of surface oil from oil ($V_{\overline{o}o}$)[6], along with a volume of surface gas from oil which ($V_{\overline{g}o}$), was previously in solution in the oil. The same applies for a local gas volume (V_g). It will yield a surface volume of gas from gas ($V_{\overline{g}g}$), and a surface volume of oil from gas ($V_{\overline{o}g}$).

[6] Dashes indicate surface conditions, and the second subscript indicate the origin of the property.

This behavior is summarized in the black oil variables:

- Solution oil gas ratio $$r_s(p,T) = \frac{V_{\overline{o}g}}{V_{\overline{g}g}} \quad (61)$$
- Solution gas oil ratio $$R_s(p,T) = \frac{V_{\overline{g}o}}{V_{\overline{o}o}} \quad (62)$$
- Gas formation volume factor $$B_g(p,T) = \frac{V_g(p,T)}{V_{\overline{g}g}} \quad (63)$$
- Oil formation volume factor $$B_o(p,T) = \frac{V_o(p,T)}{V_{\overline{o}o}} \quad (64)$$

In addition, fluid viscosities and interfacial tension are acquired through the Black Oil Model.

Dependency on pressure

The Black Oil variables will have very different behavior depending on pressure and temperature. Especially if the pressure is above (undersaturated) or below (saturated) the bubblepoint P_b at the given temperature, mainly due to the different compressibility of liquid and vapor. Variables related to gas are undefined above the bubblepoint, as there is no free gas present. The behavior is summarized in Figure 16.

The solution oil gas ratio $\mathrm{r_s}$ is a relatively new term, as it was not part of the originally formulated Black-Oil model. When dealing with volatile oil or gas condensate, it is a very important term. For heavier oil, the effect of this factor is very low. In this paper, it has been set to zero in relevant calculations.

Water is in this paper assumed to have negligible compressional effects. This means that the density is constant and the standard rates are equal to the local rates.

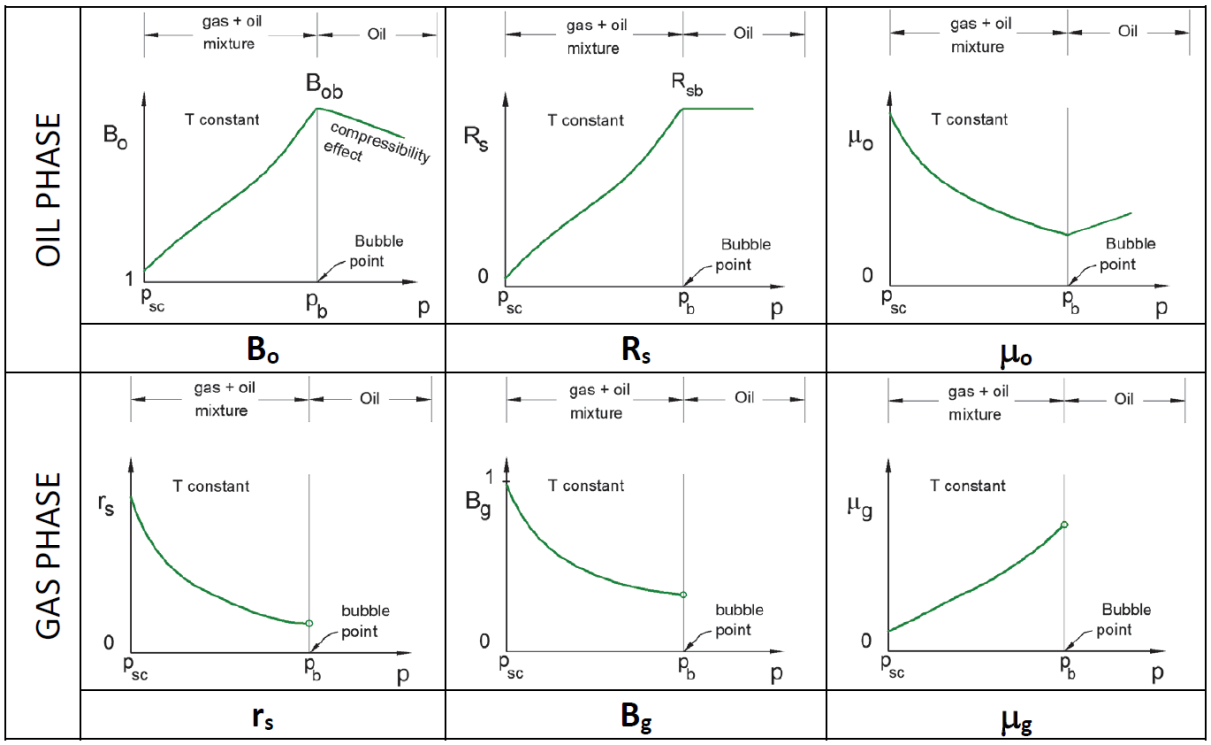

Figure 16: Black-Oil parameter behaviour with relation to pressure, with consant temperature From [24]

Black Oil Tables

The process of identifying the Black Oil variables uses one constant hydrocarbon stream composition, and is therefore only valid for this composition. A change in composition will result a change in the BO-parameters (Figure 17)

If the production stream is expected to change composition, typically due to increasing producing GOR in the well, the Black Oil parameters are usually described in table form. If the change in composition comes from the same original fluids, and is only a mixture of these, a single Black Oil Table can be produced to cover all compositions in the life of the well. If the well expects mixing of new fluids, tables need to be made for each composition, and related with mixing ratios. This may be due to gas injection or producing from different compositional well sections.

Reading Black-Oil Tables

Black-Oil tables consist of an oil table and a gas table. Oil tables tabulate multiple GORs (R_s) at their bubble-point along with the corresponding properties (B_o, μ_o). This represent the saturated values of the oil. Undersaturated values are given for each GOR in the table for pressures above the bubblepoint. Gas tables tabulate the same with r_s and dewpoint pressure, and these are the values used in this paper.

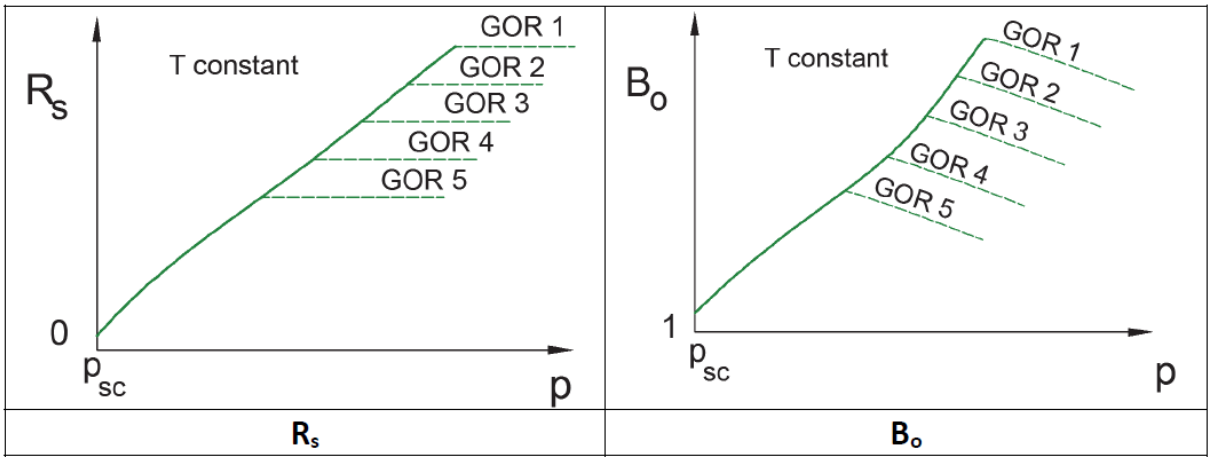

Figure 17: Black-Oil parameter variation with different compositions (GORs). From [24]

Procedure to read Black Oil Tables

- Oil values:
  1. Identify producing GOR
  2. Identify if the local pressure is above or below the bubblepoint
     a. Pressure above bubblepoint (undersaturated):
        i. Use the closest undersaturated values (above and below) to interpolate for the given pressure and GOR (Bilinear interpolation)
     b. Pressure below bubblepoint (saturated):
        i. Interpolate between closest saturated values to interpolate for the given pressure (Linear interpolation).
- Gas values:
  - Interpolate closest values with the given pressure.

Use of the properties

Once obtained, the Black-Oil variables are used to convert volumetric properties, (i.e. rates and densities) from standard conditions to local PT conditions, and vice-versa. Pressure and flow calculations require local volumetric rates as input. Equations (65) to (68) show the relation between standard and local properties.

$$q_g = q_{\overline{g}} \frac{B_g}{1 - R_s r_s} - q_{\overline{o}} \frac{B_g R_s}{1 - R_s r_s} \approx q_{\overline{g}} B_g - q_{\overline{o}} B_g R_s \tag{65}$$

$$q_o = -q_{\overline{g}} \frac{B_o r_s}{1 - R_s r_s} + q_{\overline{o}} \frac{B_o}{1 - R_s r_s} \approx q_{\overline{o}} B_o \tag{66}$$

$$\rho_g = \rho_{\overline{g}} \frac{1}{B_g} + \rho_{\overline{o}} \frac{r_s}{B_g} \approx \frac{\rho_{\overline{g}}}{B_g} \tag{67}$$

$$\rho_o = \rho_{\overline{g}} \frac{R_s}{B_o} + \rho_{\overline{o}} \frac{1}{B_o} \tag{68}$$

3.3: Statoil Hybrid model in VFP format

Eclipse allows for the use of multi-segment wells, each of which can be equipped with AICDs. The idea is to assign a VFP-table to capture the pressure drop from AICDs in each section instead of using the Statoil model directly. A single VFP table is made, that can be assigned to all individual AICDs.

Converting a model into VFP format will always decrease the accuracy of the model. This because of the discretization from algebraic to table form takes away the smoothness of the model. Therefore, an alternative solution is proposed. The Statoil model will be split into four separate models, each individually matched for the respective categories:

- Single phase oil
- Single phase gas
- Single phase water
- Multiphase

Dataset 1 is used for the matching. By matching the model to each individual sub-dataset, this will result in four individual sets of tuning parameters. This will give four independent Statoil models that are best fit for their respective phase. The single-phase models will be very accurate, as it is easy to tune a model to a single performance curve. The multiphase model will still have errors, but much less than if the model was tuned to single and multiphase simultaneously.

In calculating and creating the VFP-table, the multiphase model will be used as a default. A volume fraction limit is introduced, and when a certain phase is above this limit, the model will use the model corresponding to this phase. The limits used are given in Table 9.

For example, a data section with increasing GOR will initially use the multiphase model. When the GOR gets high enough that the gas volume fraction is above a certain limit, the table will calculate using the single-phase gas model. It should be noted that this value is semi-arbitrary, does not necessarily represent the actual behavior. For gas, a value of 96% is chosen, since this is the highest gas fraction presented in the dataset.

Fluid	Volume fraction [frac]
Gas	0.96
Oil	0.99
Water	0.99

Table 9: Limit volume fractions chosen for the Hybrid model to use single-phase parameters

Troll fluid - Black Oil table

VFP-tables tabulate surface rates, and subsequent pressure drops are calculated from local rates. A Black Oil Table was used for this conversion. The Statoil RCP test data was originally made for Troll fluid properties, so the BO-table was made for the same fluid. Supervisor Curtis H. Whitson used his existing Troll EOS model to create a black oil table. The black oil table files are attached in A.7: (ZIP-file "BOPVT-Troll.ZIP"). Fluid properties are given in Table 10. Water is assumed to have constant density and viscosity. Oil and gas properties are found via the BO-table and equations (65) to (68).

Fluid	Density [kg/sm3]	Viscocity [cp]	FVF [m3/sm3]
Gas	0.775	BO-table	BO-table
Oil	874.15	BO-table	BO-table
Water	999	0.45	1.0

Table 10: Fluid properties from the Black Oil Table.

Matching the model

The VFP-table is created using the spreadsheet A.3: (Excel sheet "VFP_table_generation.xlsm"). The spreadsheet was designed with the following functions:

- Match the experimental data to the Statoil model for each phase
- Write a VFP-table using the matched data and BO-table
- Write the result into a VFP-table file for Eclipse (.ECL)

Each individual dataset is matches to its respective model. The resulting tuning parameters and errors of the matching is found in Table 11 and Table 12.

Figure 18 show the measured data vs the modelled data graphically.

Statoil model parameters	Oil phase	Gas phase	Water phase	Multi-phase
A	1.00	1.00	1.00	1.04E-01
B	1.00	1.00	1.00	3.82E+00
C	1.00	1.00	1.00	1.08E+00
RHO_CAL	1.24	659.27	1.11	7.24E-04
D	1.00	1.00	1.00	2.90E-09
E	1.00	1.00	1.00	9.96E-01
F	1.00	1.00	1.00	2.54E+00
Y	0.316	0.868	0.000	5.34E-02
MY_CAL	0.71	1.17	0.65	6.21E+00
A_AICD	1.9E+03	8.5E+05	2.2E+04	2.49E+07
X	2.032	2.203	2.332	4.03E+00

Table 11: Optimized tuning parameters for the Statoiul Hybrid model

Fluid	$E_{rel,abs}$ [%]	Max absolute error [bar]
Gas	9.48%	22.0
Oil	4.78%	2.28
Water	3.44%	1.12
Multiphase	19.90%	9.42

Table 12: Error results for the different phases in the optimized Hybrid Model

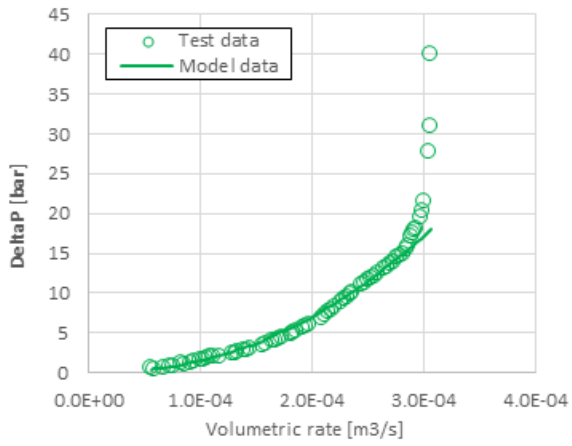

(a) – Gas: model vs test data

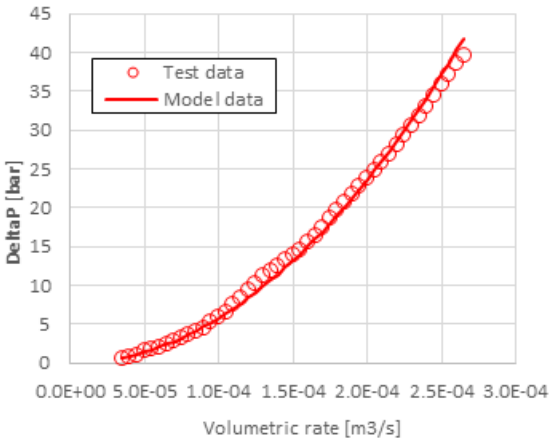

(b) – Oil: model vs test data

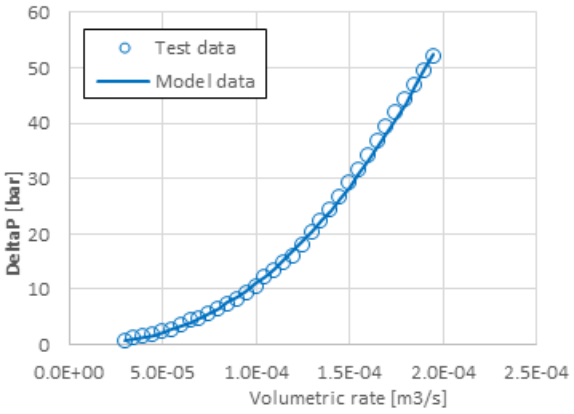

(c) – Water: model vs test data

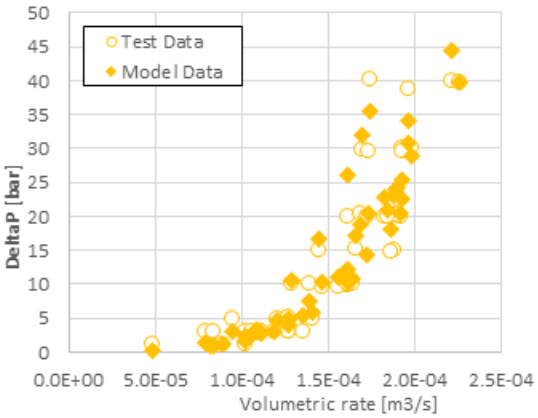

(d) – Multiphase: model vs test data.

Figure 18: Statoil Hybrid Model performance to test data, split into the four different phases.

Creating the VFP table

For the creating of the VFP table itself, the spreadsheet takes in upper and lower values of the VFP-parameters and the number of values. The values are distributed linearly, and all possible combinations of values are calculated. The values can be seen in Table 13.

Variable range	Outlet pressure [bar]	Water Cut [frac]	Gas Oil Ratio [sm3/sm3]	Liquid rates [sm3/d]
Lower Value	80	0.00	1.00	0.10
Upper Value	158	1.00	10 000	40.00
Number of Values	5	10	40	50

Table 13: VFP-table parameter distribution used.
Linear distribution between the upper and lower bound

The values in the VFP-table are chosen to get a good variation in the fluid compositions in the VFP-table. It is of interest to include all single phases and various compositions of multiphase. In order to have single-phase gas, a very high GOR is needed. With typical FVFs for oil and gas, a GOR of at least 4000 sm3/sm3 is needed to achieve 98% gas fraction.

The calculated table is written to a VFP–file for Eclipse (.ECL) by the macro 'writeVFPtable' in F.2: VFP-table generation spreadsheet. The procedure is similar to the pseudocode presented in Figure 14. The variables are combined into table form, and the corresponding inlet pressure is given. The desired file path for the file is input by the user. The Eclipse file is made in metric units, with WC, GOR and LIQ (Liquid Rate) as the parameters. This not an option to change in the spreadsheet, it is built in the VBA macro.

In addition to the main VFP-table, a secondary VFP-file was written only using the multiphase. This is based on the idea that a well will practically always have more than one phase flow. Completely pure single-phase flow is rare.

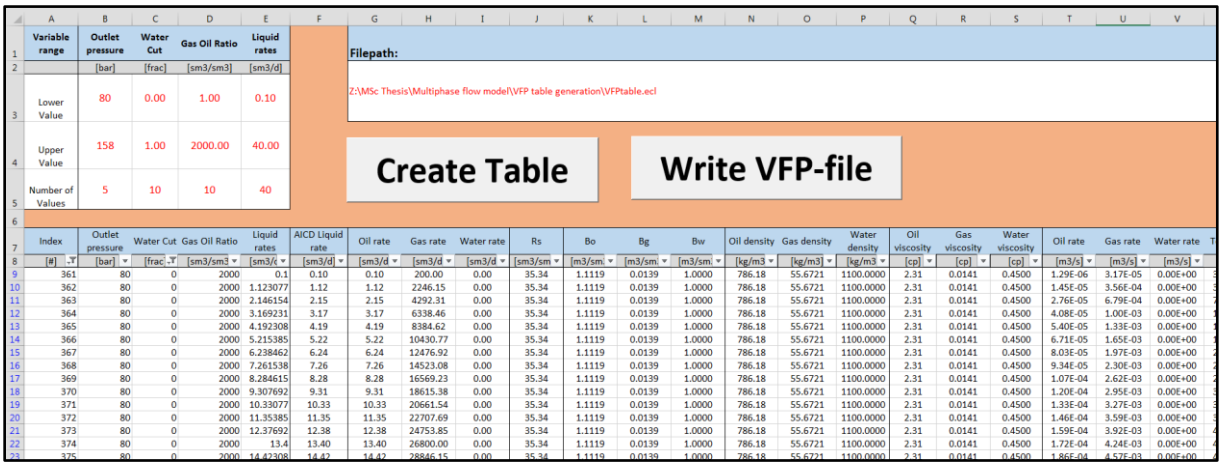

Figure 19: Screenshot from the spreadsheet used for creating and writing VFP tables

3.4: Results and discussion about the method

The two Eclipse VFP-files are found in the attachments A.5: (Eclipse VFP-file "VFPtable_primary.ECL") and A.6: (Eclipse VFP-file "VFPtable_multiphase.ECL"). Figure 20 show the full Hybrid Model VFP-table nodes plotted against the test data. VFP-data points can be seen following mainly the behavior of the multiphase model, and some of the datapoints seems to replicate the single-phase curves.

The reason the curves do not completely replicate the single-phase curves, is because the fluid properties are slightly different from the test data and from the BO-table. Water data point replicate the model perfectly, since the fluid properties are identical.

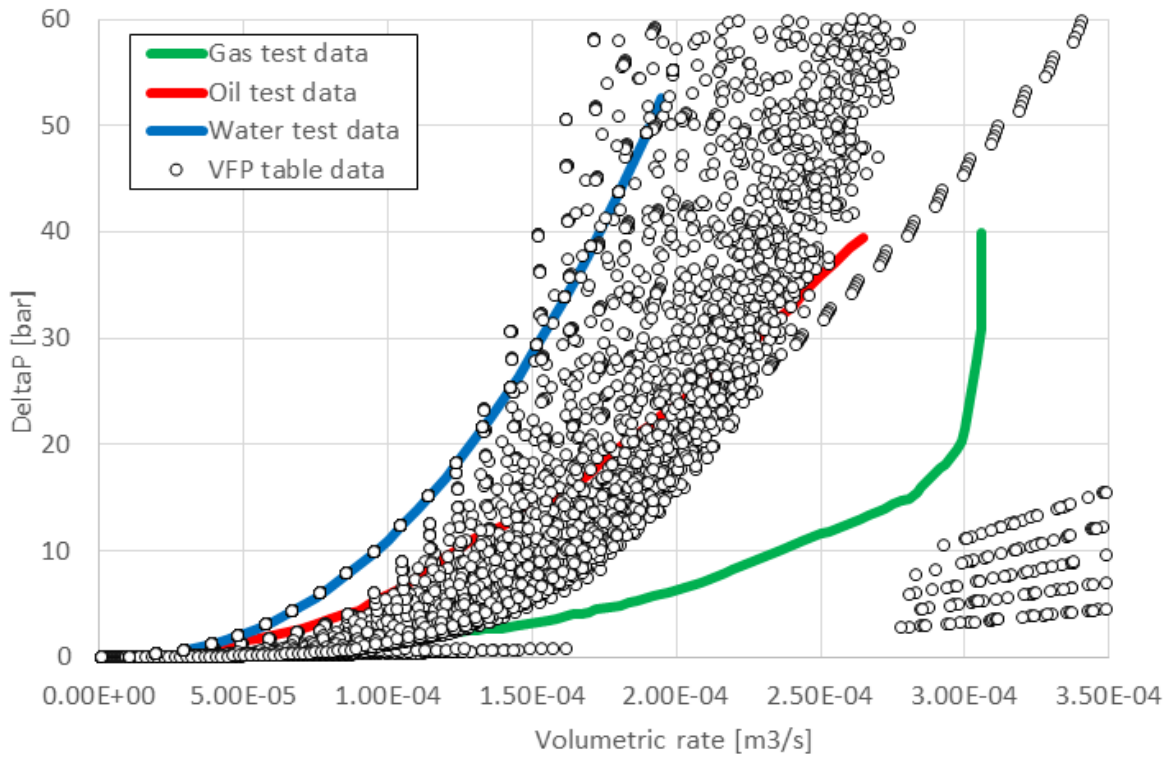

Figure 20: Graph relating test data and datapoint from the VFP table.

An 'empty' space can be seen between the single-phase gas curves and the multiphase data. This is due to the test data not covering gas fractions above 96%, and the model limit is set at this value. Had the test data shown gas fractions between 96-100%, a more realistic table could probably be made. The single-phase gas curves is sparse at low rates, and this is due to sparseness of the liquid rates at low values. Most likely, the liquid rates chosen should be geometrically distributed instead of linearly. This could have been an improvement to the Excel sheet.

Potential pitfalls

When converting a model into VFP-format, accuracy will always be lost. This is because the model goes from continuous to discrete form, and any non-linearity will give a deviation from the original when interpolating. One can never completely avoid this issue; only limit the problem as much as possible. This needs to be done by choosing nodes carefully and dense enough that the table does not need in interpolate too far.

The idea behind this solution is that the merging of different models will provide an increase in accuracy that is higher than the accuracy lost by discretization. However, the jump from one model to the next could give unphysical results. In a scenario where Eclipse interpolates between nodes that use different models, the result could be poor. This has not been tested in this thesis, but needs to be addressed as a weakness of the method.

Another remark against this method is the need for a complicated model in the first place. If the complicated model is discarded and simplified into tables, is the complicated model needed in the first place? Could a simpler model perform the same in VFP-table form? Could test data be directly implemented into VFP-table form? This would be interesting for future work.

Plans of testing the method

The original intent was that the VFP table should be tested in Eclipse. The plan was that Statoil personnel would test the model using both the original model, and the VFP approach, and compare the results. Due to time constraints and holidays, this was unfortunately not done. The author strongly recommends anyone interested in the subject to test the VFP-files in Eclipse.

If the method had been tested, the following reasoning could have been done:

Outcome 1: Results from original model and VFP tables are equal or deviate slightly:

This would indicate that the VFP-method would have been valid to use in simulation. This would mean that the practical modelling works. One cannot accurately determine if the method is an improvement or not. Further investigation could have been done to determine this.

Outcome 2: Results from original model and VFP tables massively deviate.

This could lead to two conclusions. Either the original model is correct, while the VFP-method does not work, or vice-versa. One could analyze both results, and try to logically determine if one of them are inaccurate. A third option is that both methods are wrong.

If a VFP-table approach is determined valid, this could be a big improvement in modelling AICDs in reservoir simulators.

Chapter 4: AICD in well performance

This chapter covers an analysis of the effect of AICDs on oil production in wells with gas coning issues. A one-dimensional steady state flow analysis of a producing well is performed, to estimate well performance. The analysis is similar to the commercial software NetTool. Results of interest is the relation between oil and gas production and well completion strategies.

The analysis is done in three different points in time, representing increasing gas coning tendency. Each with the well equipped with three different completions:

- Open Hole
- AICD
- AICV

The Statoil AICD Hybrid model presented in chapter 3.3 is used in the analysis. Since the data is made for Troll field production, a dummy well resembling a Troll well will be made. The properties of the well are within a rough order of magnitude, and may not accurately represent an actual Troll well. However, the general trend in production can be found, as a "within the ballpark" estimate.

Water production is neglected, to simplify the analysis further. Only oil and gas production will be covered, as this is the main issue on the Troll field. Therefore, all water production is set to zero.

4.1: Well Performance Theory

Fluid in a production well flow from the reservoir to the surface, via several stages in the system (Figure 21). Pressure differentials drive the fluid flow, and specific pressure drops can be associated to the different processes. The pressure drop processes of importance from reservoir to separator are:

- ΔP_{IPR} From the reservoir to the well
- $\Delta P_{completion}$ Through the outer well completion
- $\Delta P_{tubing,hor}$ In horizontal tubing section
- $\Delta P_{tubing,ver}$ In vertical tubing section
- ΔP_{choke} Through wellhead choke (not considered here)

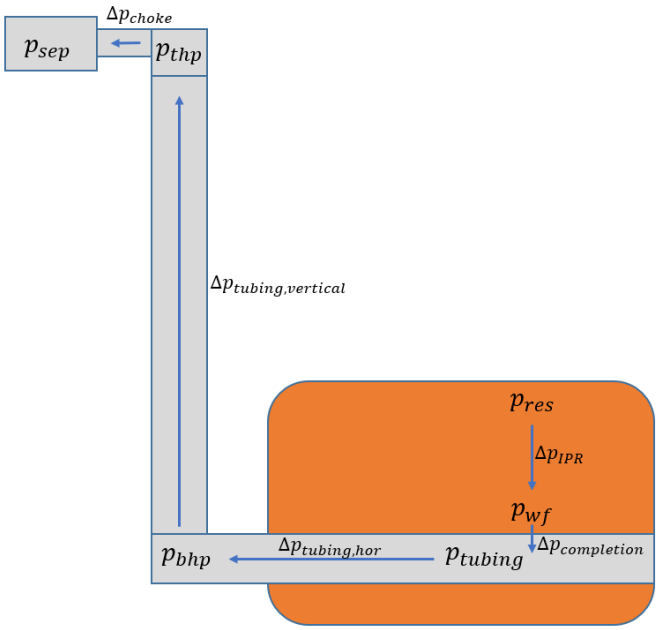

Figure 21: Sketch of a horizontal producing well system

4.1.1: Inflow Performance Relationship (IPR)

An IPR represents the inflow from the reservoir to the wellbore, given a specific reservoir and bottomhole pressure. The pressure differential between reservoir pressure and wellbore pressure is called the drawdown. For undersaturated oil wells, the relation between inflow rate and drawdown is linear, and can be described as:

$$J = \frac{q_{oil}}{P_{res} - P_{wf}} = \frac{q_{oil}}{\Delta P_{drawdown}} \tag{69}$$

Where the oil rate is expressed in surface rates and J is the productivity index (PI), with units $\frac{\frac{sm^3}{d}}{bar}$. The PI is a collective term that describes both reservoir and fluid properties that affect the inflow. If the conditions in well are constant, then the PI will stay constant, and define the slope of a plot of inflow rate vs wellbore pressure (Figure 22). Alteration in the reservoir will change the PI positive or negative such as for example fracturing/stimulation or scale/cementation problems.

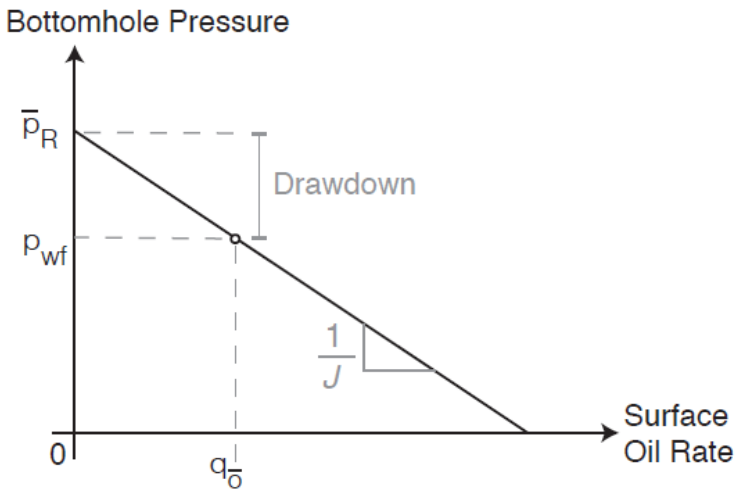

Figure 22:Single-phase linear inflow performance relationship. From [25]

When the oil is saturated, or gas breakthrough occurs, the gas will enter the wellbore, and limit oil production. This causes the IPR to deviate from linear behavior, as shown in (Figure 23). Oil production will no longer increase proportionally to drawdown, but curve down toward a theoretical maximum oil rate. Two –phase IPRs are generally empirical, and need well-testing data to be accurate.

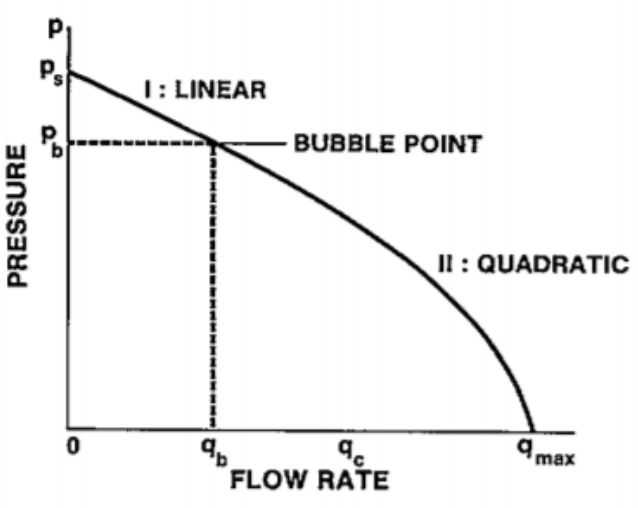

Figure 23: Multi-phase inflow performance relationship. From [21]

4.1.2: Pressure drop through outer completion

Fluid enters wellbore through the outer completion. In this case, it consist of an outer sand screen, annular flow between the tubing and screen before it flows through eventual Inflow Control Devices (Figure 24). The pressure drop though the screen and annulus is very low compared to the ICDs, and can be considered negligible [10].

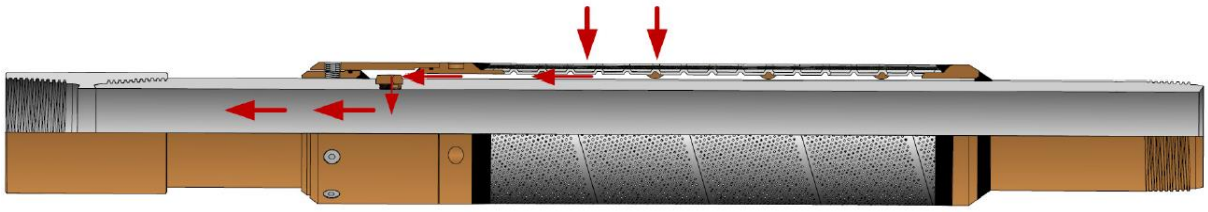

Figure 24: Sketch of typical AICD completion. Arrows indicate flow through sandscreen, annulus, AICD and tubing. From [9]

4.1.3: Horizontal Pipe flow:

The fluid flow in the tubing can be described by pressure drop equations in chapter 1.1. Pressure and temperature conditions will vary along the wellbore, and thus affect the fluid properties. In order to accurately represent pipe flow under varying conditions, the pipe is usually discretized into segments. Fluid properties are assumed constant in the every segment. Average pressure and temperature is used to determine fluid properties through a phase behavior model, which along with flow data determine the pressure drop in the segment.

Acceleration pressure drop is considered negligible, and the total tubing pressure drop can be describes as a sum of Equation (2) and Equation (4):

$$\Delta p_{pipeflow} = \rho_{mix} g h + f \frac{L}{D} \frac{\rho_{mix} u^2}{2} \tag{70}$$

Mixture properties are determined by an appropriate approximation, and friction factor is determined by either Equation (9) or Equation (11), depending on the flow regime. For simplicity, this chapter uses homogenous volumetric averages in Equation (14) and Equation (15) for density and viscosity.

4.1.4: Vertical pipeflow

Flow in the vertical tubing is more complex than horizontal flow, as more complex flow regimes can develop due to gas and liquid holdup. In production simulation software, various correlations are used for different kinds of vertical flow. For simplicity, this paper treats vertical flow equally to horizontal flow, and uses equation (70).

The vertical flow is considered as one pipe segment. Average values of pressure and temperature between the bottomhole and the wellhead is used as the flowing conditions, and fluid properties are defined from these.

However, as the tubinghead pressure is defined by the vertical flow pressure loss, and the fluid properties are defined by the average pressure, an iterative process is used to determine the average pressure. This process is described in Figure 25.

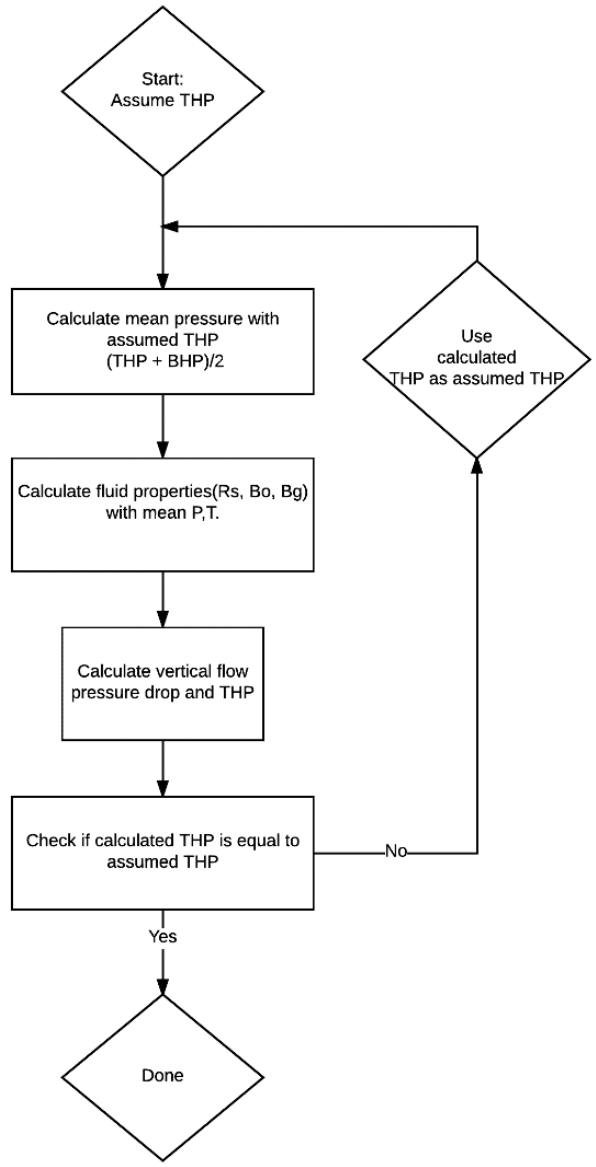

Figure 25: Flow chart showing the iteration process of finding the Tubinghead pressure

4.2: Modelling a typical Troll well

The modelling of the Troll well is based on public papers on the field. Some properties are taken from different wells, and this may or may not produce a completely realistic combination. When in doubt, properties are chosen in a fashion that allows realistic results to be obtained.

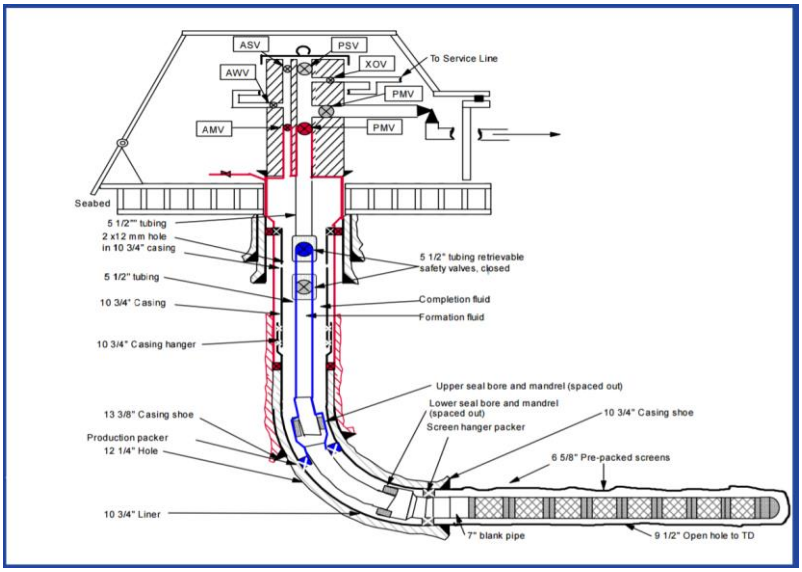

Figure 26: A typical Troll well. From [8]

4.2.1: Well geometry

Modern Troll wells are often multilateral, with several kilometer long branches. For simplicity, our well has one perfectly horizontal branch of 2000m at a depth of 1580m. Papers on AICDs suggest that wells are equipped with 200-400 AICDs, and a well may have 30 producing sections separated by swell packers. A number of 12 devices per section was chosen, resulting in 360 devices in the well. This allowed for realistic amounts of fluid flow through each device.

Property	Value	Unit	Reference
Depth	1580	m	[8]
Horizontal length	2000	m	[15]
Tubing diameter	5 ½	Inches	[8]
Roughness	0.006	Inches	Industry standard
Number of sections	30	/well	[10]
Number of AICDs	360	/well	[17]

Table 14: Well geometry for a typical Troll well

4.2.2: Production

In the oil-producing province of the Troll field, gas-handling capacity due to coning is the major production constraint. The reservoir is highly productive, with a productivity index ranging from 5-10,000 sm3/d/bar. The drawdown is therefore typically very low, from 0.5-1.5 bar. Figure 27 shows the production of a typical well, with 2000-2500 sm3/d of oil production until gas breakthrough. After breakthrough, the well has a gas handling capacity around 400,000 sm3/d. Oil rate is maximized as much as possible while keeping the gas production within limits.

Property	Value	Unit	Reference
Oil rate	500-4000	Sm3/d	[13]
GOR	56-2000	Sm3/sm3	[13]
Water Cut	0	%	[13]
Productivity Index	5 – 10 000	Sm3/d/bar	[15]/[13]
Drawdown	0.5-1.5	bar	[15]
Tubinghead pressure	30-110	bar	[13]
Tubinghead temperature	40-60	degC	[13]
Gas handling capacity	400,000	Sm3/d	[13]

Table 15: Production data and properties for a typical Troll well

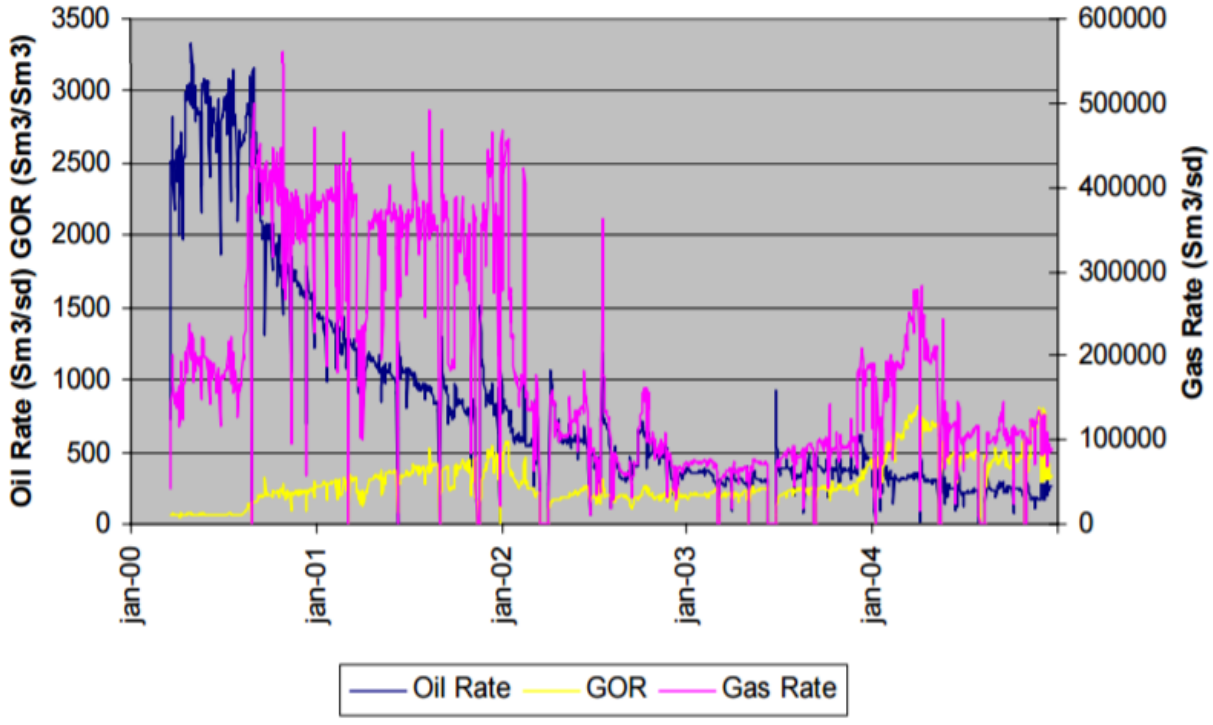

Figure 27: Production data for a typical Troll well. From [13]

4.2.3: Fluid properties

Fluid properties are modelled by the same BO-table as described in Chapter 3.2, as both chapters are based on Troll fluids. Standard fluid properties are therefore the same as given in Table 10.

4.2.4: Reservoir and Inflow Performance

Reservoir pressure and temperature was chosen to mimic the AICD test data, summarized in Table 16. Reservoir pressure is assumed constant for all sections. Temperature is assumed constant in the entire horizontal section.

Property	Value	Unit	Reference
Reservoir pressure	130	bar	[13]
Reservoir temperature	68	degC	[13]

Table 16: Reservoir conditions

Other reservoir properties are captured by in the chosen Inflow Performance Relation. The reservoir is assumed to have individual inflow models for each of the 30 producing sections of the well. This is not considered an unreasonable suggestion, as wells often are completed with section for the different heterogeneous reservoir sections.

A typical Troll well produce single-phase oil for a given time until gas (or water) breakthrough. In the time before breakthrough, oil is produced at a linear rate, and can be described by Equation (69). Here, oil inflow is assumed linear even after breakthrough. The time of gas breakthrough is often described by a *critical flow rate*[7], meaning that production above this rate produces a pressure drop high enough that gas cones into the wellbore. A further increase above this rate will results in an increasingly higher GOR. This can be seen in Figure 27, where breakthrough occurs sometime around September 2000.

[7] Not to be confused with the critical flow rate through chokes.

Statoil has developed a Gas Oil Ratio Model (GORM) for gas coning wells, which relate oil rate with GOR. This is used to predict gas coning and the resulting increase in GOR. Figure 28 shows the GORM for the same well as in Figure 27 at three different times. All three times has a specific critical oil rate, and a corresponding function for GOR development. Note that as time goes on, the coning increases in severity, the critical rate gets lower, and the GOR relation is steeper. Also, note that prior to breakthrough, the GOR is equal to the solution gas oil ratio R_s. In the analysis, the value of R_s is calculated from the BO-table at reservoir conditions, and differ slightly from the figure.

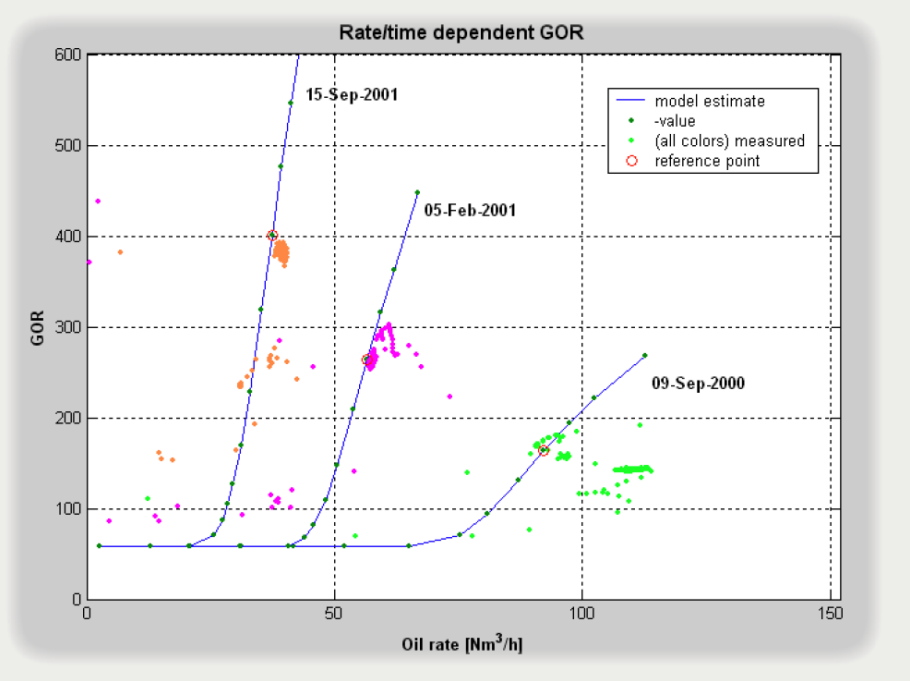

Figure 28: Gas Oil Ratio model for a typical Troll well. Modelled at different points in time. From [13].

Using GORM to model coning

The GOR behavior in Figure 28 is a representation of the entire well. It will be assumed that this can be scaled down to each of the 30 producing sections, and that all sections behave equally in terms of coning potential. The units of the original figure is [sm3/hr], and must be scaled to [sm3/d]. Since the analysis uses 30 sections, a scaling factor of $\frac{24\frac{\text{hr}}{\text{d}}}{30}$ should be used,

given that previous assumptions are valid. A further simplification is made, and setting the scaling factor to unity. This means that the values in Figure 28 are set to each reservoir section with the units [sm3/d]. This simplifies data extraction and fitting.

This means that all section will have the same critical rate and GOR development with oil production. The only difference in the sections is the Productivity Index, which controls the oil inflow rate. As such, sections with higher productivity has a higher chance of surpassing the critical rate, leading to gas coning. This assumption is assumed well enough for this analysis. In a more realistic scenario, the higher permeability sections will probably also have a lower critical rate and higher GOR development due to gas mobility.

The three different curves will be used as three points in time for the analysis, representing an increase in gas coning severity. GORM 1-3 will respectively represent early, intermediate and late time (and coning severity).

Extracting GORM data

In order to create replicate the GORM, data from the graphs in Figure 28 was extracted. Below critical rate, the well is producing with Solution GOR R_s for the reservoir conditions. The critical rate can be found by identifying where the GOR starts to increase. An empirical model was suggested by this author to represent the data (71), and fitted in Excel to replicate the curves. Parameters for the model is given in Table 17, and a plot of the model is given in Figure 29.

$$GOR = \begin{cases} R_s & q_{oil} \leq q_{oil,crit} \\ R_s + \left(\left(q_{oil} - q_{oil,crit} \right) * A \right)^B & q_{oil} > q_{oil,crit} \end{cases} \quad (71)$$

Where:

- A and B are tuning constants
- R_s is found through the BO-table at reservoir conditions.

Gas breakthrough stage	Critical rate [sm3/d]	A – Multiplier [-]	B- Exponent [-]
GORM 1 – Early	65.20	0.641	1.628
GORM 2 – Intermediate	41.50	2.255	1.505
GORM 3 – Late	25.96	6.251	1.360

Table 17: Tuning parameters for replicdating the GOR-Model

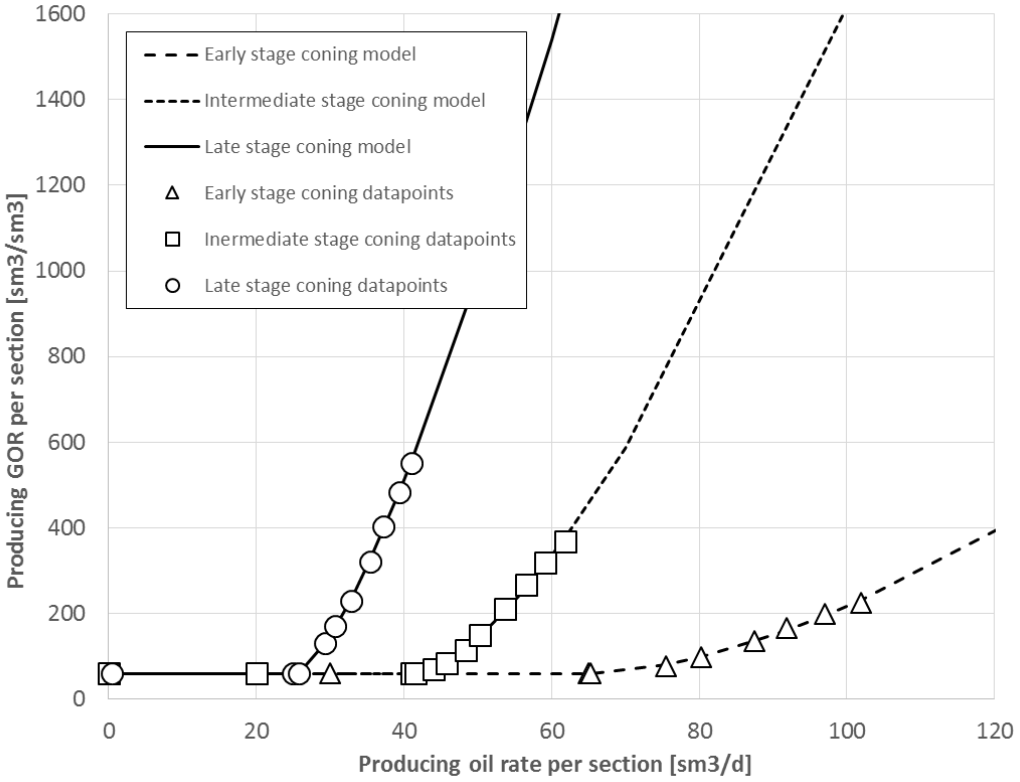

Figure 29: Optimized expressions for replicating the Troll GOR-Model

Productivity Index distribution

The Troll reservoir mainly consist of two alternating layers of sandstone. C-sand is highly productive in order of 1-30 Darcy, while M-sand are more compacted ranging from 10-1000mD. A well may go through several sections of the two sands, resulting in a strongly heterogeneous reservoir, as shown in Figure 30.

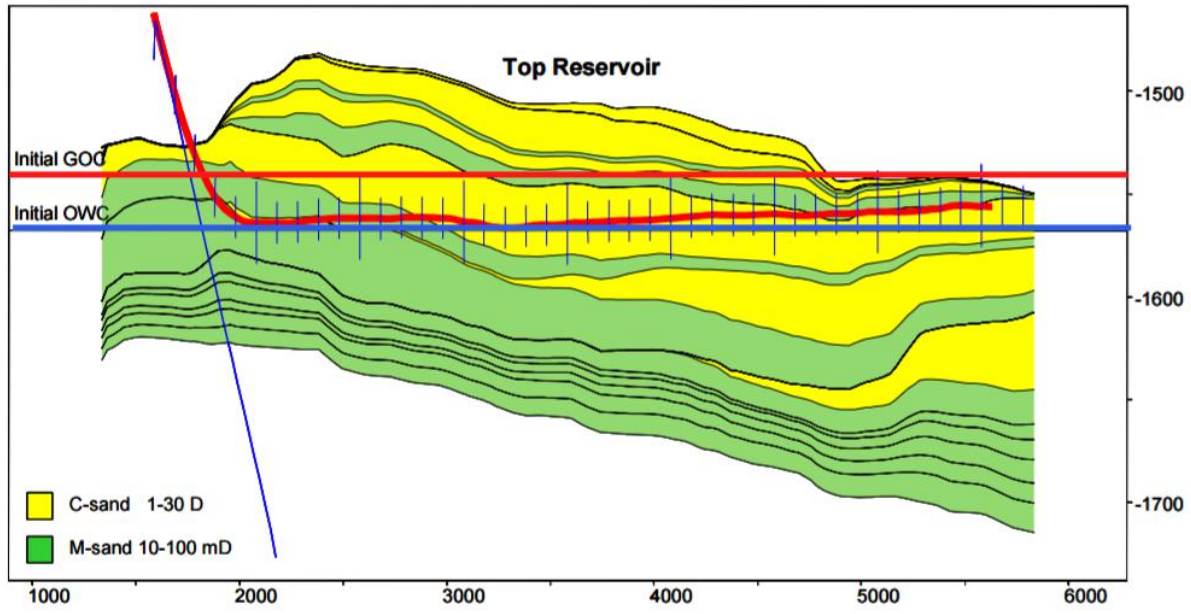

Figure 30: Geological cross sectio for a typical Troll well. From [7]

Three different "reservoirs" are suggested to use in this analysis. Each has a unique PI distribution for each of the sections. The sum of all PI from all sections represent the total productivity of the well, and should represent a realistic well productivity. 5000 sm3/d/bar has been chosen as a realistic baseline. The Productivity Index distributions for the different reservoirs are given in Table 18, and in Figure 31.

- Reservoir 1: Homogenous reservoir

  All sections have the same PI. This is used to compare against the other heterogeneous reservoirs.

- Reservoir 2: Normal distributed reservoir

  A normal distribution multiplied with the total well productivity. In this case, the normal distribution was shifted with the peak (mean) closer to the toe of the reservoir.

- Reservoir 3: Manual distribution

  Segments have either very low or very high productivity. Chosen as 1000 and 10 sm3/d/bar. This is to replicate the behaviour of C-sands and M-sands on Troll.

	Reservoir 1	Reservoir 2	Reservoir 3
Section	PI distribution [sm3/d/bar]	PI distribution [sm3/d/bar]	PI distribution [sm3/d/bar]
1 (Toe)	166.67	83.95	10.00
2	166.67	115.92	10.00
3	166.67	154.73	1000.00
4	166.67	199.19	1000.00
5	166.67	246.97	10.00
6	166.67	294.69	10.00
7	166.67	338.22	10.00
8	166.67	373.27	10.00
9	166.67	396.04	10.00
10	166.67	403.94	10.00
11	166.67	396.04	10.00
12	166.67	373.27	10.00
13	166.67	338.22	10.00
14	166.67	294.69	10.00
15	166.67	246.97	10.00
16	166.67	199.19	10.00
17	166.67	154.73	10.00
18	166.67	115.92	10.00
19	166.67	83.95	10.00
20	166.67	58.99	10.00
21	166.67	40.47	10.00
22	166.67	27.39	10.00
23	166.67	18.58	1000.00
24	166.67	12.92	1000.00
25	166.67	9.43	1000.00
26	166.67	7.38	10.00
27	166.67	6.23	10.00
28	166.67	5.61	10.00
29	166.67	5.29	10.00
30 (Heel)	166.67	5.13	10.00

Table 18: Productivity Index distribution for the suggested reservoirs

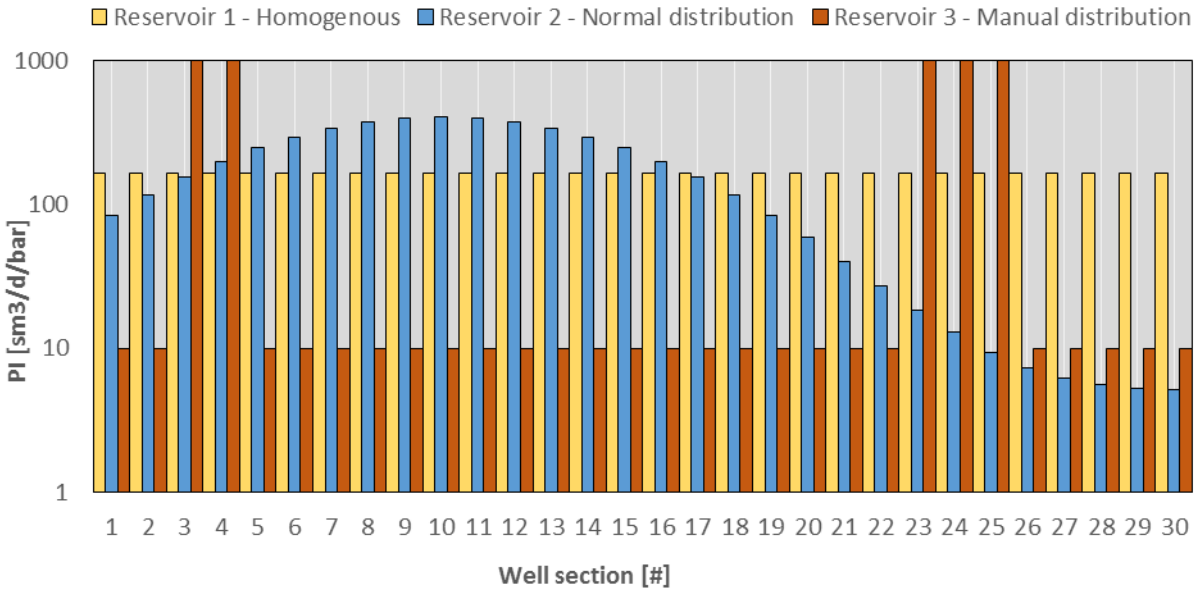

Figure 31: Productivity Index distribution for the suggested reservoirs. Section 1 is the toe, and section 30 is the heel of the well.

4.2.5: AICD modelling

When considering cases with open-hole production, there will be assumed no pressure drop across the completion. Inflow Performance and tubing flow are the only factors in this analysis.

For AICD cases, the Hybrid model will be used. The tuning parameters presented in Table 11 will be used for this analysis, as they are representative for a Troll fluid. The model requires a volume fraction limit to determine if the flow is single or multiphase, and this has been set to 98% for all fluids.

Since this paper does not have models for AICVs, they will be modelled based on the AICD model. They are assumed to behave identically, except that the AICD will completely shut in once single-phase gas or water is reached. The volume fractions for this is also set to 98%. This value for shut in limit is suggested in [19]. When the AICV is shut in, it is assumed that no flow goes through it. In reality, around 1% of the flow is let through. It is also assumed that

there is no pressure connection between the reservoir and the wellbore, when an AICV section is shut in. This means that the pressure drop across the closed AICV is zero.

4.3: Production Network

For a well with *N* producing sections, the corresponding production network will look like Figure 32. Each of the nodes correspond to a specific pressure in the system, and the lines between them represent the pressure drop determined by a specific process. The fluid flow will only travel along these lines. It is assumed that crossflow or flow in the annulus does not happen. The reservoir pressure is assumed average and equal for all sections of the well, thus being one of the boundaries of the system. The other boundary will be the tubing head pressure at the top.

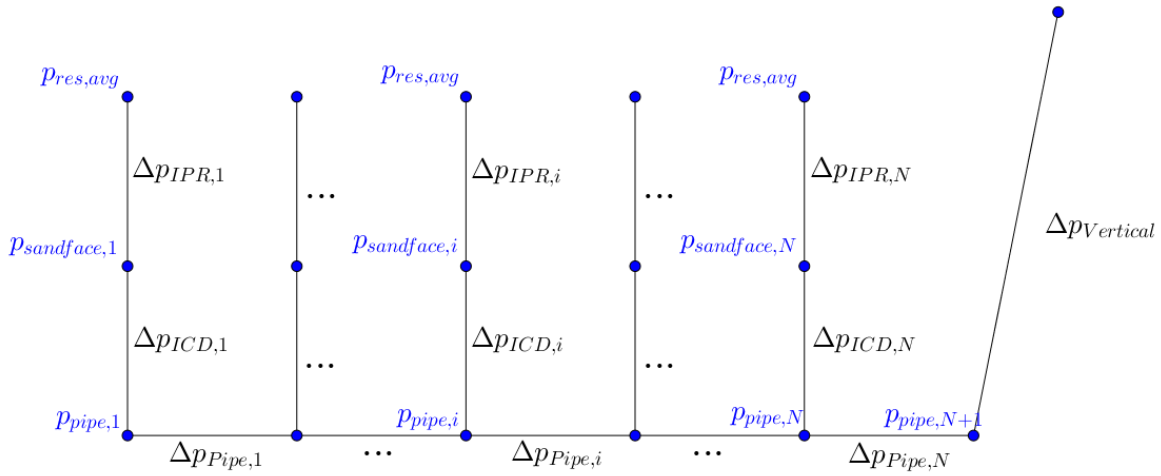

Figure 32: Nodal production network sketch

The pressure drawdown determines inflow rates for each section, and thus sets up all the other pressure drops in the system. For a given section, the drawdown determines the inflow rate, which again determines the pressure drop in the outer completion. The flow continues to the pipe, and merges with the cumulative flow from the previous sections. This cumulative flow determines the pipe pressure drop from this section to the next.

Consider a node pressure $p_{pipe,i}$ in the system. The two ways to calculate the node is:

$$p_{pipe,i} = \begin{cases} p_{pipe,i-1} - \Delta p_{pipe,i-1} & calculated\ from\ inflow \\ p_{res,avg} - \Delta p_{inflow,i} & calculated\ from\ previous\ pipe\ section \end{cases}$$

Where:

$$\Delta p_{inflow,i} = \Delta p_{IPR,i} + \Delta p_{ICD,i}$$

Except for the first and last pressure node in the pipe, all of the pressure nodes in the pipe is defined both from the inflow process and from the previous pipeflow process. This can be seen in Figure 33, as all nodes with more than one inlet pressure drop. A system in equilibrium demands that both calculations give the same pressure.

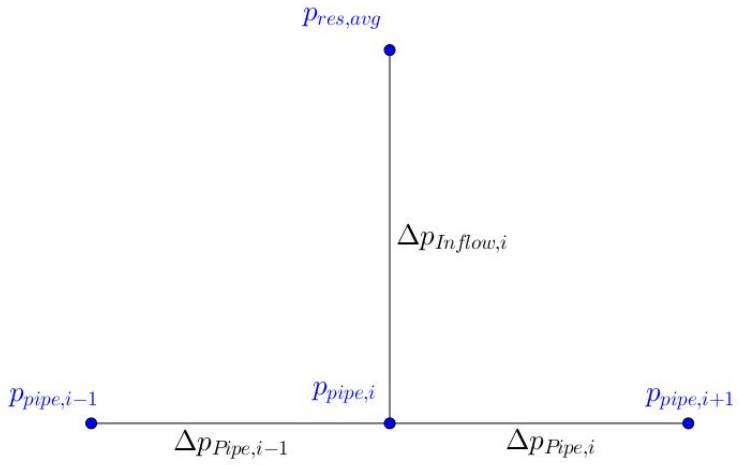

Figure 33: Convergence on Network node sketch. Pressure calculations from both inflow directions must give the same result.

In a production network analysis, each of the nodes in the system is analyzed with both equations. By taking sum of squared error between both results from all nodes, an estimate of the error in the system is obtained.

$$SSQ_{pipe} = \sum_{i=2}^{N-1} \left(p_{pipe,i,"inflow"} - p_{pipe,i,"pipeflow"} \right)^2$$

The last node that needs evaluation is the tubinghead pressure. This is the second boundary of the system, along with the reservoir pressure.

$$SSQ_{THP} = \left(p_{tubinghead,i,"pipeflow"} - p_{tubinghead,i,"defined"} \right)^2$$

Note that the boundary node can also be set as the bottomhole pressure, i.e. the last node in the pipe $P_{pipe,N+1}$, or a production target rate. If this is the case, vertical flow should still be evaluated, and note if the resulting tubinghead pressure is physically reasonable. This can be of interest if the vertical flow is of less importance, for example if some form of artificial lift is planned.

The total error in the system is defined as the sum of equation 1 and 2:

$$SSQ_{total} = SSQ_{THP} + SSQ_{pipe}$$

With the Excel SOLVER, SSQ_{Total} is driven to zero by adjusting the pressure drawdown in all of the sections. Once $SSQ_{Total} = 0$, the system is in equilibrium.

4.4: Well performance analysis

The Troll well analysis was done in the Excel file **A.4: (Excel sheet "Network_Analysis.xlsm")**, by tuning the pressure drawdown for all 30 sections simultaneously. The analysis was done for each of the reservoirs with all three coning models. All combinations was performed for open hole, AICD and AICV completion. Table 19 shows an overview of all the cases.

ANALYSIS	Open hole	AICD	AICV
Reservoir 1	Case 1-3	Case 4-6	Case 7-9
Reservoir 2	Case 10-12	Case 13-15	Case 16-18
Reservoir 3	Case 19-21	Case 22-24	Case 25-27

Table 19: Overview of analysis cases. All three reservoirs are analyzed for three completions, and each for three GOR-Models.

The cases was optimized by targeting the maximum oil rate possible while staying below the gas handling capacity. The main result of interest in the maximum oil rate obtainable at the max gas handling capacity.

In practice, this worked best by solving the system for gas rate equal to 400,000 sm3/d, and reading the respective oil rate. Bottomhole and tubinghead pressure was not considered in the optimization, but calculated and noted in the results.

In addition to these cases, a final analysis was done using Reservoir 3 with variable GOR models for the different sections. The low permeability (PI = 10) sections was assigned the early stage (high critical rate, low GOR increase) GOR model, and the High permeability (PI = 1000) section was assigned the late stage (low critical rate, high GOR increase). This was done to investigate even higher effects of heterogeneous coning, since the other reservoir models assume that section have the same coning behavior. This analysis was done for open hole, AICD and AICV completion (Case 28-30).

Solving the system

In practice, the system was difficult to solve in Excel. A variety of factors added to the complexity of the problem in such a way that the SOLVER had a hard time converging without good starting suggestions from the user.

- The very high drawdown sensitivity on inflow rate. In high productivity sections, a very small change in drawdown have a large effect in inflow rate and consecutive pressure drops in the system.
- The discrete nature of the both the GOR model and the AICD model. After a certain drawdown or volume fraction threshold, the model changes its nature, and the SOLVER is thrown off.
- Very low pressure drop in the horizontal section.

For some cases, the system was accepted as solved with a lower threshold for convergence, in order to get results.

Another issue encountered was that gas rates per section never got high enough to trigger the AICV shut in. To reach a gas volume fraction of 98% for a given section the GOR needs to be around 4000sm3/sm3. This was never achieved naturally in the analysis of open hole or AICD. In order to get an approximation of AICV behavior, the highest gas producing reservoir sections was shut in manually, even if the gas fraction was lower than needed. The sections that were shut in:

- Reservoir 1: Sections 28-30. The three sections closest to the heel
- Reservoir 2: Section 9-11. The three higher gas producing sections.
- Reservoir 3: Sections 3-4 and 23-25. The five sections with extremely high PI.

4.5: Results

Results are summarized in Table 20 to Table 23. Oil rate, GOR, BHP and THP are tabulated at the maximum gas rate. Each table represent one reservoir analysis, with different completions and GOR-Models. Figure 34 to Figure 37 represent the results graphically.

The oil and gas inflow for all sections can be found in Figure 46 to Figure 55. Pressure distribution for the solved system for each case is represented graphically in Figure 56 to Figure 65, in order of cases. The pressures are represented in column chart form, with Reservoir, Sandface and Tubing pressure for each section. Bottomhole pressure at the heel section is plotted for reference. From the charts, one can deduce the representative pressure drops for each process. Pressure drops from the sandface to the tubing is represented by the AICD/V pressure drop.

The drawdown distributions found to converge each analysis is found in Table 27 to Table 30. If the reader is interested in other data for each case, the pressure drawdown for the case of interest should be copied into the Excel sheet A.4: (Excel sheet "Network_Analysis.xlsm")

		Reservoir 1 – Homogenous reservoir				
		Oil rate [sm3/d]	GOR [sm3/sm3]	Gas rate [sm3/d]	BHP [bar]	THP [bar]
No ICD	GORM 1	1843.7	216.9	4.00E+05	128.8	69.9
	GORM 2	1225.8	326.3	4.00E+05	129.2	82.6
	GORM 3	879.3	454.9	4.00E+05	129.5	90.5
AICD	GORM 1	2694.7	148.4	4.00E+05	115.6	46.9
	GORM 2	1665.5	240.1	4.00E+05	122.2	68.8
	GORM 3	1093.7	365.5	4.00E+05	124.8	82.0
AICV	GORM 1	2482.1	161.1	4.00E+05	111.2	47.3
	GORM 2	1528.4	261.7	4.00E+05	119.6	69.6
	GORM 3	1006.4	397.5	4.00E+05	122.9	82.5

Table 20: Results from analysis on Reservoir 1

		Reservoir 2 – Normal distribution'				
		Oil rate [sm3/d]	GOR [sm3/sm3]	Gas rate [sm3/d]	BHP [bar]	THP [bar]
No ICD	GORM 1	1934.7	206.8	4.00E+05	126.1	66.7
	GORM 2	1199.9	333.3	4.00E+05	127.6	81.9
	GORM 3	814.7	491.1	4.00E+05	128.3	91.2
AICD	GORM 1	2686.4	149.0	4.00E+05	111.1	43.1
	GORM 2	1660.7	240.9	4.00E+05	119.4	67.0
	GORM 3	1091.5	366.5	4.00E+05	123.0	80.6
AICV	GORM 1	2478.3	161.8	4.00E+05	106.9	44.3
	GORM 2	1526.0	262.1	4.00E+05	117.1	67.9
	GORM 3	1005.3	397.9	4.00E+05	121.4	81.3

Table 21: Results from analysis from Reservoir 2

		Reservoir 3 – Manual distribution				
		Oil rate [sm3/d]	GOR [sm3/sm3]	Gas rate [sm3/d]	BHP [bar]	THP [bar]
No ICD	GORM 1	687.8	581.6	4.00E+05	129.3	95.0
	GORM 2	409.7	986.3	4.00E+05	129.5	102.6
	GORM 3	284.2	1407.3	4.00E+05	129.6	106.3
AICD	GORM 1	2689.7	148.0	4.00E+05	106.9	40.9
	GORM 2	1665.1	240.6	4.00E+05	117.1	65.4
	GORM 3	1093.4	365.8	4.00E+05	121.6	79.5
AICV	GORM 1	2328.4	168.7	4.00E+05	96.7	40.0
	GORM 2	1435.8	278.6	4.00E+05	111.1	65.4
	GORM 3	947.2	422.2	4.00E+05	117.4	79.6

Table 22: Result from analysis from reservoir 3

	Reservoir 3 – Manual distribution, with varying GORM per section				
	Oil rate [sm3/d]	GOR [sm3/sm3]	Gas rate [sm3/d]	BHP [bar]	THP [bar]
No ICD	291.7	1371.1	4.00E+05	129.6	106.0
AICD	2391.3	168.1	4.00E+05	109.1	47.4
AICV	2338.5	171.3	4.00E+05	95.3	39.3

Table 23: Results from analysis from reservoir 3 with varying GOR-Model per section

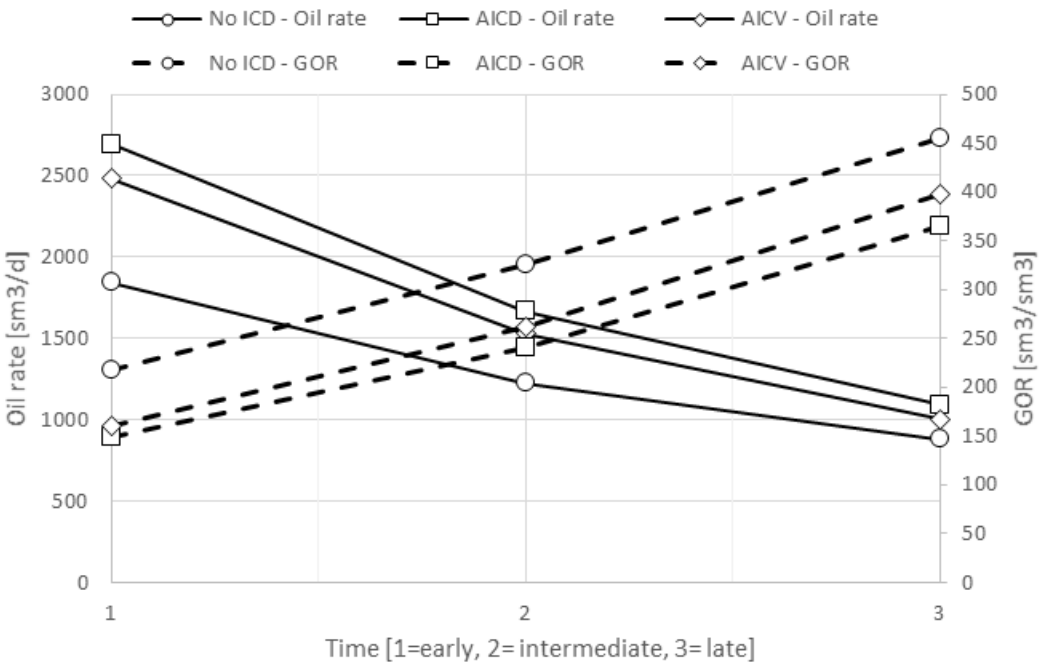

Figure 34: Results from analysis on reservoir 1

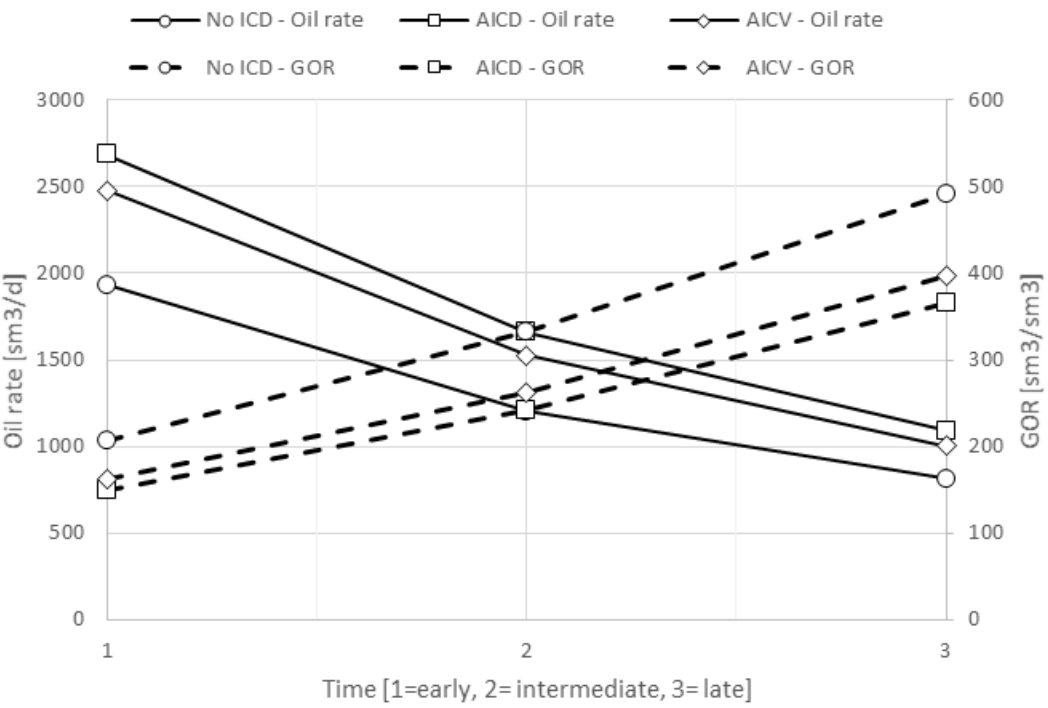

Figure 35: Results from analysis on reservoir 2

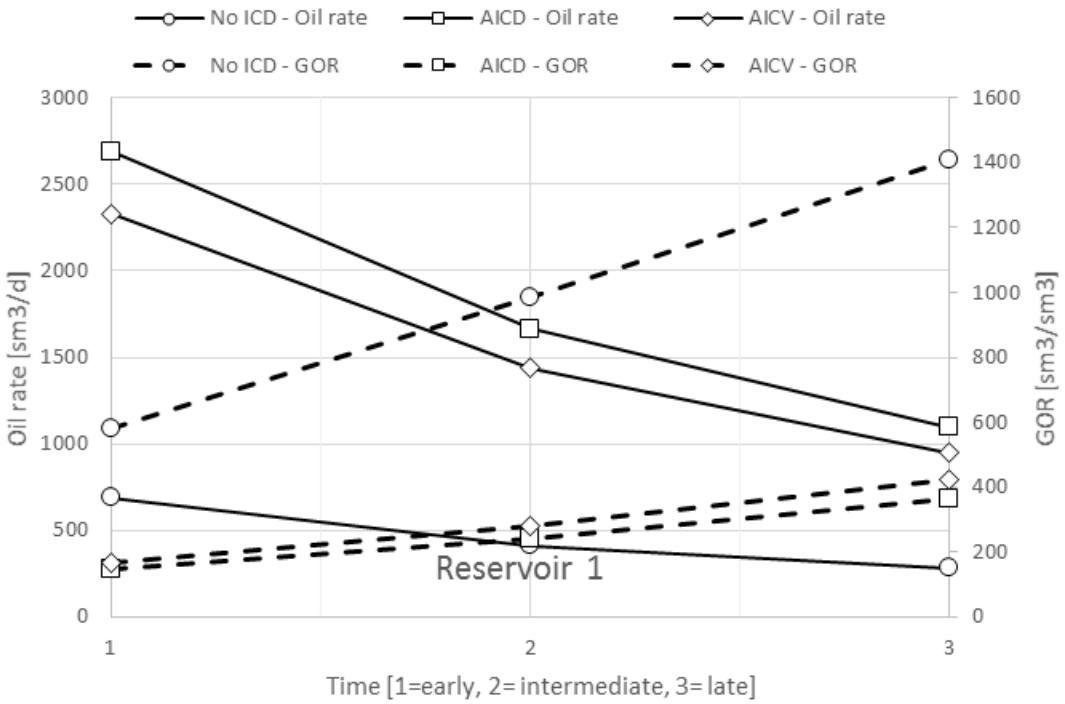

Figure 36: Results from analysis on reservoir 3

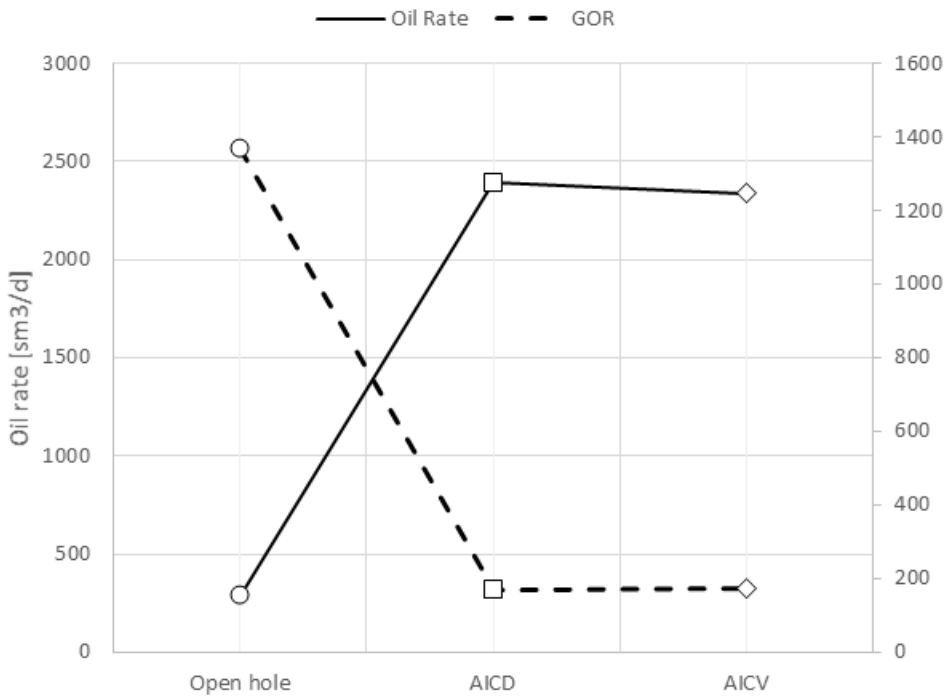

Figure 37: Results from analysis on reservoir 3 with varying GOR-Model per section

4.6 Discussion

On some cases, the analysis did not converge 100%. This can be seen in Figure 49 (c) especially, where the inflow rated are not stabilized. Still, the result would not have deviated far from this.

The pressure distribution plots show that in open hole completion, the pressure drawdown increases more and more towards the heel. This as expected, due to frictional losses in the tubing. This in turn causes the inflow to increase dramatically towards the heel. This is well seen in Figure 46. Both AICD and AIVD functions well in evenly distributing the inflow.

Comparison of completions

The results show that completion with both AICD and AICV greatly outperform open-hole completion, as expected. More surprising, however, was that AICV completion consistently produced with a higher GOR that the AICDs.

This is probably because when one section is shut in, other sections need to produce with a higher drawdown in order to reach the same rate. High productivity sections give a high inflow of *both oil and gas.* When other sections need to produce with a higher drawdown, they produce with a higher GOR than before. In summary, this analysis suggest that when severe coning is stopped in section, *other sections will increase their coning problems to produce the same rate.*

The reason can possibly also be blamed on the assumptions of the analysis:

- Because of the lack of models and data for AICV, it is assumed to act as AICDs when producing, and this is probably not the case. With detailed test data of AICVs, better analysis can be performed.

- The GOR-Model is empirical and scales to sections, and does not necessarily behave as assumed for each section.
- Oil rate is assumed to have linear inflow, and increasing gas rate as a function of oil rate. Figure 23 shows that oil rate would in reality decline.
- AICVs are shut in 'manually'. In the analysis, the gas rates are never high enough to surpass the 98% volume fraction of gas. This means that sections are shut in before they would in reality, and they may have contributed more to oil production.

The final analysis (case 28-30) also showed a higher oil production with AICDs than ICDs. In this case, the high productivity sections was given an even higher GOR-Model. Even with relatively higher gas producing section shut off, the well did not produce more oil before gas capacity was reached.

Other suggestions for analysis

Other constraints for the analysis might also have given different results. The analysis was now based on a limit gas rate, with the objective of getting as much oil production as possible. A different approach could have been to set a target oil rate, and investigate the associated gas rate. This may or may not have given different results.

It should also be noted that the analysis did not include traditional ICDs. This could have given a better comparison of ICD technology, since all is expected to perform better than open-hole completion. A more complete analysis would include this as well.

Chapter 5: Recommendations for future work

This chapter includes recommendations for future work, both for people in the industry and for students that want to further investigate this topic.

Chapter 2

- Multiphase testing of AICDs
    - Test from pure single-phase gradually into multiphase to observe behavior.
    - Test of a larger variety of multiphase compositions
- Multiphase testing of AICVs
    - Same as for AICDs
    - Make the test data public
- Finding a better AICD model
    - Investigate if the original Bernoulli model can be modified to fit the test data better. This probably involves introducing a viscosity term in the model.
    - Find a completely new model that performs better

Chapter 3

- Test a VFP table created from AICD data, in Eclipse. Files in the attachments of this thesis can be a place to start

Chapter 4

- Perform similar analysis as described in chapter 4 with:
    - Better reservoir/Inflow model to capture a coning reservoir better
    - A proper model for AICV
    - Compare against traditional ICD
    - Perform the analysis with other targets that maximum gas rate.
    - Perform the analysis before coning, and longer after coning.

Chapter 6: Conclusions

Chapter 2

- Statoil's AICD model does not accurately represent the laboratory test data. Results show that the errors can be expected to be at least 10-20% on average.
- Statoil's AICD model can model other AICDs than the RCP Valve at least as accurate as the RCP Valve.
- None of the other models investigated performed better than the Statoil model
- Halliburton's dataset was fitted better than Statoil's dataset for all models
- The original Bernoulli equation performs almost as good as other, more complex models.

Chapter 3

- Optimizing the Statoil model to separate datasets significantly increases the model accuracy.
- A tool for creating VFP-tables for AICDS in Eclipse format has been made.
- VFP-tables for AICDs in Eclipse has been created, but not tested.

Chapter 4

- The analysis suggest that both AICDs and AICV significantly increases oil recovery compared to open-hole completions.
- The analysis suggest that AICVs does not increase oil recovery compared to AICDs
- AICV require a very high GOR to shut in, in the order of 1000s sm3/sm3.

Nomenclature

Abbreviations:

AICD/V	-	Autonomous Inflow Control Device/Valve
BHP	-	Bottomhole pressure
BO	-	Black Oil
EOS	-	Equation of State
FVF	-	Formation Volume Factor
GOR	-	Gas-Oil-Ratio
GORM	-	Gas Oil Ratio Model
GVF	-	Gas Volume Fraction
ICD/V	-	Inflow Control Device/Valve
IPR	-	Inflow Performance Relationship
PI	-	Productivity Index
RCP	-	Rate Controlled Production
SSQ	-	Sum of squared errror
SwRI	-	Southwest Research Institute
THP	-	Tubinghead pressure
VBA	-	Visual Basic for Applications
VFP	-	Vertical flow performance
WC	-	Water Cut

Nomenclature and Symbols

a	-	Constant in Simpson Slip Factor
A	-	Flow area
A-F	-	Statoil tuning parameters
B	-	Formation Volume Factor
C	-	Heat capacity
C_d	-	Discharge coefficient
E	-	Error
f	-	Darcy friction factor
g	-	Acceleration of gravity
H	-	Height
J	-	Productivity Index
k	-	Slip factor
K	-	Adiabatic exponent
L	-	Length
$\dot{m}$	-	Mass rate
M	-	Molecular weight
n	-	Moles, amount
n	-	Polytropic exponent
P	-	Pressure

q	-	Volumetric flow rate
R	-	Universal gas constant
Re	-	Reynolds number
r_s	-	Solution Oil gas ratio
R_s	-	Solution Gas oil ratio
T	-	Temperature
u	-	Velocity
Y	-	Pressure ratio
Z	-	Gas compressibility factor
α	-	Volume fraction
ε	-	Pipe roughness
ρ	-	Density
μ	-	Viscosity
σ	-	Standard deviation
χ	-	Mass fraction
γ	-	Specific gravity
ϕ_{TP}	-	Two phase multiplier

Subscripts

Abs	-	Absolute
c	-	Critical
Cal	-	Calibration
Ch	-	Chisholm
gas	-	Gas
H	-	Homogenous
liq	-	Liquid
O	-	Oil
Pc	-	Pseudocritical
Pr	-	Pseudoreduced
Rel	-	Relative (Error)
Res	-	Reservoir
Si	-	Simpson
SSQ	-	Sum of squared (Error)
TP	-	Two-phase

References

[1] Aakre, H., Halvorsen, B., Werswick, B., & Mathiesen, V. (2014, September 24). Autonomous Inflow Control Valve for Heavy and Extra-Heavy Oil. Society of Petroleum Engineers.

[2] Alert Diver | The Physiology of Compressed-Gas Diving. *Alertdivercom*. 2017. Available at: http://www.alertdiver.com/Physiology_of_Compressed-Gas_Diving. Accessed June 8, 2017.

[3] Alsafran, E. M., & Kelkar, M. G. (2009, May 1). Predictions of Two-Phase Critical-Flow Boundary and Mass-Flow Rate Across Chokes. Society of Petroleum Engineers.

[4] Asheim, H., & Oudeman, P. (1997, March 1). Determination of Perforation Schemes To Control Production and Injection Profiles Along Horizontal Wells. Society of Petroleum Engineers.

[5] Bybee, K. (2008, March 1). Production Operations: Inflow-Control Devices. Society of Petroleum Engineers. doi:10.2118/0308-0081-JPT

[6] Corona, G et al. (2017, May 1). Testing of a Novel Autonomous ICD with Low-Viscosity Multiphase Fluids. Offshore Technology Conference.

[7] Denney, D. (2005, November 1). Success Factors in Troll Geosteering. Society of Petroleum Engineers.

[8] Haaland, A., Rundgren, G., & Johannessen, Ø. (2005, January 1). Completion Technology On Troll-Innovation And Simplicity. Offshore Technology Conference.

[9] Halvorsen, M et al. (2016). Enhanced Oil Recovery On Troll Field By Implementing Autonomous Inflow Control Device. SPE Bergen One Day Seminar.

[10] Halvorsen, M., Elseth, G., & Naevdal, O. M. (2012, January 1). Increased oil production at Troll by autonomous inflow control with RCP valves. Society of Petroleum Engineers

[11] Hatzignatiou, D. G., & Mohamed, F. (1994, January 1). Water And Gas Coning In Horizontal And Vertical Wells. Petroleum Society of Canada.

[12] Haug, R. (2012). Multiphase Flow Through Chokes: Evaluation of five models for prediction of mass flow rates. MSc. Thesis, Norwegian University of Science and Technology, Trondheim (June 2012).

[13] Hauge, J., & Horn, T. (2005, January 1). The Challenge Of Operating And Maintaining 115 Subsea Wells On The Troll Field. Offshore Technology Conference.

[14] Henriksen, K. H., Gule, E. I., & Augustine, J. R. (2006, January 1). Case Study: The Application of Inflow Control Devices in the Troll Field. Society of Petroleum Engineers.

[15] Madsen, T., & Abtahi, M. (2005, January 1). Handling The Oil Zone On Troll. Offshore Technology Conference.

[16] Mathiesen, V., Werswick, B., & Aakre, H. (2014, April 2). The Next Generation Inflow Control, the Next Step to Increase Oil Recovery on the Norwegian Continental Shelf. Society of Petroleum Engineers.

[17] Mathiesen, V., Werswick, B., Aakre, H., & Elseth, G. (2011, January 1). Autonomous Valve, A Game Changer Of Inflow Control In Horizontal Wells. Society of Petroleum Engineers.

[18] Mikkelsen, J. K., Norheim, T., & Sagatun, S. I. (2005, January 1). The Troll Story. Offshore Technology Conference.

[19] Nugraha, I et al. (2016, April 25). Optimizing Reservoir Performance through Utilization of Autonomous Inflow Control Valve – Lessons Learnt from the World's First Installation. Society of Petroleum Engineers.

[20] Prydz, R. (1993, January 1). Troll Oil Development Concept. Offshore Technology Conference.

[21] Richardson, J. M., & Shaw, A. H. (1982, March 1). Two-rate IPR Testinga Practical Production Tool. Petroleum Society of Canada.

[22] Sachdeva, R., Schmidt, Z., Brill, J. P., & Blais, R. M. (1986, January 1). Two-Phase Flow Through Chokes. Society of Petroleum Engineers.

[23] Schlumberger (2016). Eclipse 2016.2 Reference Manual.

[24] Stanko, M. (2016). Fluid behavior treatment in oil and gas production Systems. NTNU (2016)

[25] Sæten, S. (2015). Production Allocation of Oil and Gas: A case Study of the Skarv Field. MSc. Thesis, Norwegian University of Science and Technology, Trondheim (June 2015).

[26] White, F. (2010). Fluid mechanics. New York: McGraw-Hill.

[27] Whitson, C. H., Brule, M. R. (2000). Phase Behavior. Monograph Series, Richardson, Texas: Society of Petroleum Engineers Inc.

Appendix A: Overview of Attachments

Attachments to this Thesis is uploaded in a single (.ZIP)-file. It consists of the following files:

A.1: (Excel sheet "AICD_model_StatoilRCP.xlsm")

Macro-enabled excel file used to calculate AICD models for Dataset 1 (Statoil RCP valve).

- Sheet 1
  - Input data and solving for models.
- Sheet 2
  - Test data input. The data is transferred to other sheets by macro "Expand Data" in Sheet1.
- Sheets 3-4
  - Data handling and calculations.
- Sheets 5-8
  - Plots

A.2: (Excel sheet "AICD_model_Haliburton.xlsm")

Macro-enabled excel file used to calculate AICD models for Dataset 2 (Haliburton Fluidic Diode valve).

- Identical to A.2.

A.3: (Excel sheet "VFP_table_generation.xlsm")

Macro-enabled excel file used to tune the Statoil Hybrid model and generate VFP-files for Eclipse.

- Sheet 1
  - Input sheet for fluid and AICD properties
- Sheet 1.2
  - Black-Oil Table. Not made for inputting new table.
- Sheet 2.1-2.2
  - Data input for single and multiphase
- Sheet 3
  - Matching the respective models. Matching target can be chosen. Bottons start the solver and optimizes the models.
- Sheets 4.1-4.4
  - Plots of the optimized models
- Sheet 5
  - Sheet for creating and writing the VFP file. Variables are entered in the matrix, and button 'Create table' create the table in the spreadsheet. 'Write VFP-file' writes the table into a VFP file for Eclipse and saves to the filepath given.
- Sheet 6
  - Plot of the test data and the nodes in the VFP-table

A.4: (Excel sheet "Network_Analysis.xlsm")

Macro-enabled excel file used to analyze the Horizontal well Network.

- Sheet 1
  - Well input data (Figure 38).
    - Reservoir model is chosen in cell 'E19'.
    - GOR-Model chosen in 'E21'.
    - Turning AICDs on or off in 'B47'
    - Giving AICDs shut in option in 'B61
  - System solving (Figure 39)
    - Optimization target chosen in 'E36'
    - Drawdowns to solve in 'J9:J38'
    - Button 'Solve Network' starts the solver
  - Flow and pressure data
- Sheet 2.1
  - Black-Oil Table. Not made for inputting new table.
- Sheet 2.2
  - AICD model parameter input
- Sheet 2.3
  - Reservoir model input
- Sheet 2.4
  - GOR Model
- Sheets 3.1
  - Horizontal well calculations. Sections was shut in manually for AICVs here, by altering 1/0 in column 'W'
- Sheet 3.2
  - Vertical well calculations

A.5: (Eclipse VFP-file "VFPtable_primary.ECL")

VFP-file for Eclipse created with the Statoil Hybrid model.

A.6: (Eclipse VFP-file "VFPtable_multiphase.ECL")

VFP-file for Eclipse created with the only the multiphase tuning of the Statoil Hybrid model

A.7: (ZIP-file "BOPVT-Troll.ZIP")

Zip-file created by supervisor Curtis H. Whitson containing data for the Troll Black oil Table.

Common for all Excel files are:

- Red numbers are to be input by user
- Blue numbers are calculated by the spreadsheet
- Purple numbers are copied from other cells in the spreadsheet
- Green numbers are to be used in iterative processes by the spreadsheet
- Black numbers are calculated from the spreadsheet. Used in tables.

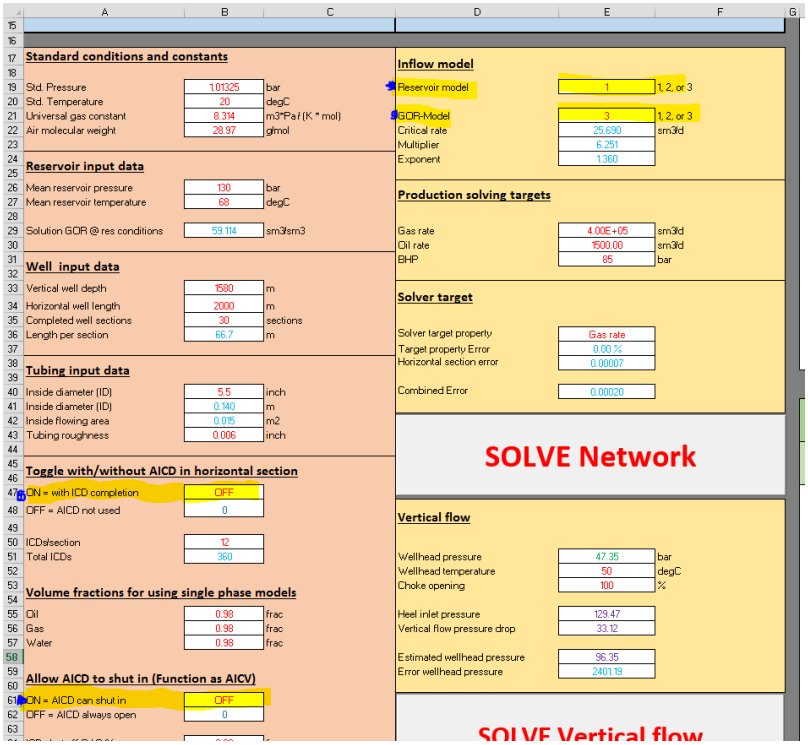

Figure 38: Screenshot of the production Network Analysis spreadsheet. Cells of interest in selecting reservoir and completion type are highlighted.

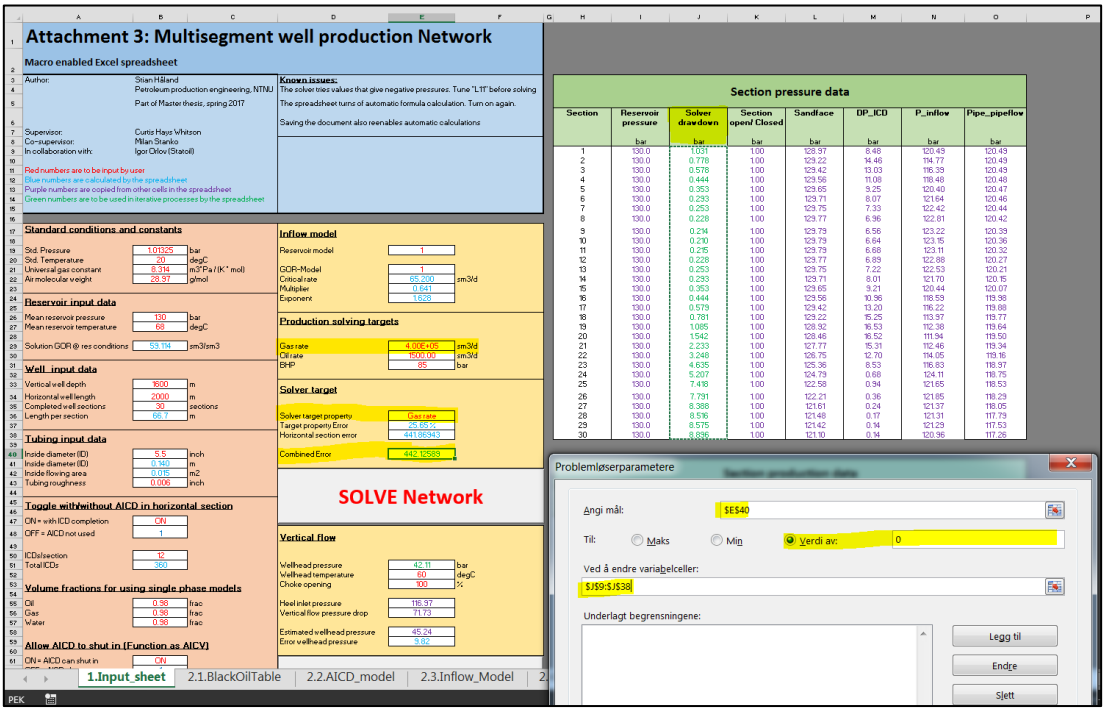

Figure 39: Screenshot of the production Network Analysis spreadsheet. Cells of interest in solving the system higthlighted.

Appendix B: AICD test datasets

B.1: Dataset 1: Statoil RCP Valve

Index	Inlet pressure	Outlet pressure	Measured volumetric flow rate	Volume fraction gas	Volume fraction oil	Volume fraction water
[#]	[Pa]	[Pa]	[m3/s]	[frac]	[frac]	[frac]
1	1.30E+07	1.29E+07	4.88E-05	0.250	0.375	0.375
2	1.30E+07	1.27E+07	7.85E-05	0.250	0.375	0.375
3	1.30E+07	1.25E+07	9.51E-05	0.250	0.375	0.375
4	1.30E+07	1.20E+07	1.29E-04	0.250	0.375	0.375
5	1.30E+07	1.15E+07	1.44E-04	0.250	0.375	0.375
6	1.30E+07	1.10E+07	1.61E-04	0.250	0.375	0.375
7	1.30E+07	1.00E+07	1.69E-04	0.250	0.375	0.375
8	1.30E+07	8.98E+06	1.74E-04	0.250	0.375	0.375
9	1.30E+07	1.29E+07	8.20E-05	0.700	0.150	0.150
10	1.30E+07	1.27E+07	1.09E-04	0.700	0.150	0.150
11	1.30E+07	1.25E+07	1.20E-04	0.700	0.150	0.150
12	1.30E+07	1.20E+07	1.46E-04	0.700	0.150	0.150
13	1.30E+07	1.15E+07	1.65E-04	0.700	0.150	0.150
14	1.30E+07	1.10E+07	1.69E-04	0.700	0.150	0.150
15	1.30E+07	1.00E+07	1.73E-04	0.700	0.150	0.150
16	1.30E+07	9.11E+06	1.96E-04	0.700	0.150	0.150
17	1.30E+07	1.29E+07	8.89E-05	0.870	0.065	0.065
18	1.30E+07	1.27E+07	1.12E-04	0.870	0.065	0.065
19	1.30E+07	1.25E+07	1.27E-04	0.870	0.065	0.065
20	1.30E+07	1.20E+07	1.59E-04	0.870	0.065	0.065
21	1.30E+07	1.15E+07	1.88E-04	0.870	0.065	0.065
22	1.30E+07	1.10E+07	1.90E-04	0.870	0.065	0.065
23	1.30E+07	9.00E+06	2.21E-04	0.870	0.065	0.065
24	1.30E+07	1.29E+07	1.02E-04	0.960	0.020	0.020
25	1.30E+07	1.27E+07	1.19E-04	0.960	0.020	0.020
26	1.30E+07	1.27E+07	1.27E-04	0.960	0.020	0.020
27	1.30E+07	1.25E+07	1.41E-04	0.960	0.020	0.020
28	1.30E+07	1.20E+07	1.62E-04	0.960	0.020	0.020
29	1.30E+07	1.20E+07	1.64E-04	0.960	0.020	0.020
30	1.30E+07	1.15E+07	1.86E-04	0.960	0.020	0.020
31	1.30E+07	1.10E+07	1.92E-04	0.960	0.020	0.020
32	1.30E+07	9.02E+06	2.26E-04	0.960	0.020	0.020
33	1.30E+07	1.27E+07	8.38E-05	0.250	0.750	0.000
34	1.30E+07	1.27E+07	1.02E-04	0.250	0.750	0.000
35	1.30E+07	1.27E+07	1.06E-04	0.250	0.750	0.000
36	1.30E+07	1.20E+07	1.39E-04	0.250	0.750	0.000
37	1.30E+07	1.10E+07	1.82E-04	0.250	0.750	0.000
38	1.30E+07	1.00E+07	1.96E-04	0.250	0.750	0.000
39	1.30E+07	1.27E+07	1.11E-04	0.700	0.300	0.000
40	1.30E+07	1.20E+07	1.56E-04	0.700	0.300	0.000
41	1.30E+07	1.10E+07	1.89E-04	0.700	0.300	0.000

42	1.30E+07	9.99E+06	1.98E-04	0.700	0.300	0.000
43	1.30E+07	1.27E+07	1.27E-04	0.870	0.130	0.000
44	1.30E+07	1.20E+07	1.61E-04	0.870	0.130	0.000
45	1.30E+07	1.10E+07	1.84E-04	0.870	0.130	0.000
46	1.30E+07	9.99E+06	1.93E-04	0.870	0.130	0.000
47	1.30E+07	1.27E+07	1.35E-04	0.960	0.040	0.000
48	1.30E+07	1.20E+07	1.61E-04	0.960	0.040	0.000
49	1.30E+07	1.10E+07	1.73E-04	0.960	0.040	0.000
50	1.30E+07	1.00E+07	1.93E-04	0.960	0.040	0.000
51	1.30E+07	1.29E+07	5.56E-05	1.000	0.000	0.000
52	1.30E+07	1.29E+07	5.83E-05	1.000	0.000	0.000
53	1.30E+07	1.29E+07	6.67E-05	1.000	0.000	0.000
54	1.30E+07	1.29E+07	7.22E-05	1.000	0.000	0.000
55	1.30E+07	1.29E+07	7.50E-05	1.000	0.000	0.000
56	1.30E+07	1.29E+07	8.33E-05	1.000	0.000	0.000
57	1.30E+07	1.29E+07	8.61E-05	1.000	0.000	0.000
58	1.30E+07	1.29E+07	9.17E-05	1.000	0.000	0.000
59	1.30E+07	1.29E+07	9.44E-05	1.000	0.000	0.000
60	1.30E+07	1.28E+07	1.00E-04	1.000	0.000	0.000
61	1.30E+07	1.28E+07	1.03E-04	1.000	0.000	0.000
62	1.30E+07	1.28E+07	1.06E-04	1.000	0.000	0.000
63	1.30E+07	1.28E+07	1.08E-04	1.000	0.000	0.000
64	1.30E+07	1.28E+07	1.11E-04	1.000	0.000	0.000
65	1.30E+07	1.28E+07	1.17E-04	1.000	0.000	0.000
66	1.30E+07	1.27E+07	1.28E-04	1.000	0.000	0.000
67	1.30E+07	1.27E+07	1.31E-04	1.000	0.000	0.000
68	1.30E+07	1.27E+07	1.33E-04	1.000	0.000	0.000
69	1.30E+07	1.27E+07	1.39E-04	1.000	0.000	0.000
70	1.30E+07	1.27E+07	1.42E-04	1.000	0.000	0.000
71	1.30E+07	1.27E+07	1.44E-04	1.000	0.000	0.000
72	1.30E+07	1.26E+07	1.56E-04	1.000	0.000	0.000
73	1.30E+07	1.26E+07	1.58E-04	1.000	0.000	0.000
74	1.30E+07	1.26E+07	1.64E-04	1.000	0.000	0.000
75	1.30E+07	1.26E+07	1.67E-04	1.000	0.000	0.000
76	1.30E+07	1.26E+07	1.69E-04	1.000	0.000	0.000
77	1.30E+07	1.26E+07	1.72E-04	1.000	0.000	0.000
78	1.30E+07	1.25E+07	1.81E-04	1.000	0.000	0.000
79	1.30E+07	1.25E+07	1.83E-04	1.000	0.000	0.000
80	1.30E+07	1.25E+07	1.86E-04	1.000	0.000	0.000
81	1.30E+07	1.24E+07	1.92E-04	1.000	0.000	0.000
82	1.30E+07	1.24E+07	1.94E-04	1.000	0.000	0.000
83	1.30E+07	1.24E+07	1.97E-04	1.000	0.000	0.000
84	1.30E+07	1.23E+07	2.08E-04	1.000	0.000	0.000
85	1.30E+07	1.23E+07	2.11E-04	1.000	0.000	0.000
86	1.30E+07	1.22E+07	2.14E-04	1.000	0.000	0.000
87	1.30E+07	1.22E+07	2.17E-04	1.000	0.000	0.000
88	1.30E+07	1.22E+07	2.19E-04	1.000	0.000	0.000
89	1.30E+07	1.21E+07	2.25E-04	1.000	0.000	0.000

90	1.30E+07	1.21E+07	2.28E-04	1.000	0.000	0.000
91	1.30E+07	1.21E+07	2.31E-04	1.000	0.000	0.000
92	1.30E+07	1.20E+07	2.33E-04	1.000	0.000	0.000
93	1.30E+07	1.20E+07	2.36E-04	1.000	0.000	0.000
94	1.30E+07	1.19E+07	2.44E-04	1.000	0.000	0.000
95	1.30E+07	1.19E+07	2.47E-04	1.000	0.000	0.000
96	1.30E+07	1.18E+07	2.50E-04	1.000	0.000	0.000
97	1.30E+07	1.18E+07	2.53E-04	1.000	0.000	0.000
98	1.30E+07	1.18E+07	2.56E-04	1.000	0.000	0.000
99	1.30E+07	1.18E+07	2.58E-04	1.000	0.000	0.000
100	1.30E+07	1.17E+07	2.64E-04	1.000	0.000	0.000
101	1.30E+07	1.17E+07	2.67E-04	1.000	0.000	0.000
102	1.30E+07	1.16E+07	2.69E-04	1.000	0.000	0.000
103	1.30E+07	1.16E+07	2.72E-04	1.000	0.000	0.000
104	1.30E+07	1.16E+07	2.75E-04	1.000	0.000	0.000
105	1.30E+07	1.15E+07	2.78E-04	1.000	0.000	0.000
106	1.30E+07	1.15E+07	2.81E-04	1.000	0.000	0.000
107	1.30E+07	1.15E+07	2.83E-04	1.000	0.000	0.000
108	1.30E+07	1.14E+07	2.85E-04	1.000	0.000	0.000
109	1.30E+07	1.13E+07	2.89E-04	1.000	0.000	0.000
110	1.30E+07	1.13E+07	2.90E-04	1.000	0.000	0.000
111	1.30E+07	1.12E+07	2.92E-04	1.000	0.000	0.000
112	1.30E+07	1.12E+07	2.93E-04	1.000	0.000	0.000
113	1.30E+07	1.11E+07	2.97E-04	1.000	0.000	0.000
114	1.30E+07	1.10E+07	2.99E-04	1.000	0.000	0.000
115	1.30E+07	1.09E+07	3.00E-04	1.000	0.000	0.000
116	1.30E+07	1.02E+07	3.04E-04	1.000	0.000	0.000
117	1.30E+07	9.90E+06	3.06E-04	1.000	0.000	0.000
118	1.30E+07	9.00E+06	3.06E-04	1.000	0.000	0.000
119	1.30E+07	1.29E+07	3.50E-05	0.000	1.000	0.000
120	1.30E+07	1.29E+07	4.00E-05	0.000	1.000	0.000
121	1.30E+07	1.29E+07	4.50E-05	0.000	1.000	0.000
122	1.30E+07	1.28E+07	5.00E-05	0.000	1.000	0.000
123	1.30E+07	1.28E+07	5.50E-05	0.000	1.000	0.000
124	1.30E+07	1.28E+07	6.00E-05	0.000	1.000	0.000
125	1.30E+07	1.28E+07	6.50E-05	0.000	1.000	0.000
126	1.30E+07	1.27E+07	7.00E-05	0.000	1.000	0.000
127	1.30E+07	1.27E+07	7.50E-05	0.000	1.000	0.000
128	1.30E+07	1.26E+07	8.00E-05	0.000	1.000	0.000
129	1.30E+07	1.26E+07	8.50E-05	0.000	1.000	0.000
130	1.30E+07	1.26E+07	9.00E-05	0.000	1.000	0.000
131	1.30E+07	1.25E+07	9.50E-05	0.000	1.000	0.000
132	1.30E+07	1.24E+07	1.00E-04	0.000	1.000	0.000
133	1.30E+07	1.23E+07	1.05E-04	0.000	1.000	0.000
134	1.30E+07	1.22E+07	1.10E-04	0.000	1.000	0.000
135	1.30E+07	1.22E+07	1.15E-04	0.000	1.000	0.000
136	1.30E+07	1.21E+07	1.20E-04	0.000	1.000	0.000
137	1.30E+07	1.20E+07	1.25E-04	0.000	1.000	0.000

138	1.30E+07	1.19E+07	1.30E-04	0.000	1.000	0.000
139	1.30E+07	1.18E+07	1.35E-04	0.000	1.000	0.000
140	1.30E+07	1.17E+07	1.40E-04	0.000	1.000	0.000
141	1.30E+07	1.17E+07	1.45E-04	0.000	1.000	0.000
142	1.30E+07	1.16E+07	1.50E-04	0.000	1.000	0.000
143	1.30E+07	1.15E+07	1.55E-04	0.000	1.000	0.000
144	1.30E+07	1.15E+07	1.60E-04	0.000	1.000	0.000
145	1.30E+07	1.14E+07	1.65E-04	0.000	1.000	0.000
146	1.30E+07	1.13E+07	1.70E-04	0.000	1.000	0.000
147	1.30E+07	1.11E+07	1.75E-04	0.000	1.000	0.000
148	1.30E+07	1.10E+07	1.80E-04	0.000	1.000	0.000
149	1.30E+07	1.09E+07	1.85E-04	0.000	1.000	0.000
150	1.30E+07	1.08E+07	1.90E-04	0.000	1.000	0.000
151	1.30E+07	1.07E+07	1.95E-04	0.000	1.000	0.000
152	1.30E+07	1.06E+07	2.00E-04	0.000	1.000	0.000
153	1.30E+07	1.05E+07	2.05E-04	0.000	1.000	0.000
154	1.30E+07	1.04E+07	2.10E-04	0.000	1.000	0.000
155	1.30E+07	1.03E+07	2.15E-04	0.000	1.000	0.000
156	1.30E+07	1.02E+07	2.20E-04	0.000	1.000	0.000
157	1.30E+07	1.01E+07	2.25E-04	0.000	1.000	0.000
158	1.30E+07	9.95E+06	2.30E-04	0.000	1.000	0.000
159	1.30E+07	9.81E+06	2.35E-04	0.000	1.000	0.000
160	1.30E+07	9.70E+06	2.40E-04	0.000	1.000	0.000
161	1.30E+07	9.55E+06	2.45E-04	0.000	1.000	0.000
162	1.30E+07	9.41E+06	2.50E-04	0.000	1.000	0.000
163	1.30E+07	9.28E+06	2.55E-04	0.000	1.000	0.000
164	1.30E+07	9.15E+06	2.60E-04	0.000	1.000	0.000
165	1.30E+07	9.05E+06	2.65E-04	0.000	1.000	0.000
166	1.30E+07	1.29E+07	3.00E-05	0.000	0.000	1.000
167	1.30E+07	1.29E+07	3.50E-05	0.000	0.000	1.000
168	1.30E+07	1.28E+07	4.00E-05	0.000	0.000	1.000
169	1.30E+07	1.28E+07	4.50E-05	0.000	0.000	1.000
170	1.30E+07	1.28E+07	5.00E-05	0.000	0.000	1.000
171	1.30E+07	1.27E+07	5.50E-05	0.000	0.000	1.000
172	1.30E+07	1.27E+07	6.00E-05	0.000	0.000	1.000
173	1.30E+07	1.26E+07	6.50E-05	0.000	0.000	1.000
174	1.30E+07	1.25E+07	7.00E-05	0.000	0.000	1.000
175	1.30E+07	1.25E+07	7.50E-05	0.000	0.000	1.000
176	1.30E+07	1.24E+07	8.00E-05	0.000	0.000	1.000
177	1.30E+07	1.23E+07	8.50E-05	0.000	0.000	1.000
178	1.30E+07	1.22E+07	9.00E-05	0.000	0.000	1.000
179	1.30E+07	1.21E+07	9.50E-05	0.000	0.000	1.000
180	1.30E+07	1.20E+07	1.00E-04	0.000	0.000	1.000
181	1.30E+07	1.18E+07	1.05E-04	0.000	0.000	1.000
182	1.30E+07	1.17E+07	1.10E-04	0.000	0.000	1.000
183	1.30E+07	1.15E+07	1.15E-04	0.000	0.000	1.000
184	1.30E+07	1.14E+07	1.20E-04	0.000	0.000	1.000
185	1.30E+07	1.12E+07	1.25E-04	0.000	0.000	1.000

186	1.30E+07	1.10E+07	1.30E-04	0.000	0.000	1.000
187	1.30E+07	1.08E+07	1.35E-04	0.000	0.000	1.000
188	1.30E+07	1.06E+07	1.40E-04	0.000	0.000	1.000
189	1.30E+07	1.03E+07	1.45E-04	0.000	0.000	1.000
190	1.30E+07	1.01E+07	1.50E-04	0.000	0.000	1.000
191	1.30E+07	9.83E+06	1.55E-04	0.000	0.000	1.000
192	1.30E+07	9.59E+06	1.60E-04	0.000	0.000	1.000
193	1.30E+07	9.33E+06	1.65E-04	0.000	0.000	1.000
194	1.30E+07	9.07E+06	1.70E-04	0.000	0.000	1.000

Table 24: complete dataset for Statoil RCP Valve, converted to volumetric flow

B.2: Dataset 2: Haliburton Fluidic Diode Valve

Index [#]	Inlet pressure [Pa]	Outlet pressure [Pa]	Measured volumetric flow rate [m3/s]	Volume fraction gas [frac]	Volume fraction oil [frac]	Volume fraction water [frac]
1	1.30E+07	1.27E+07	1.289E-04	0.256	0.744	0.000
2	1.30E+07	1.23E+07	1.962E-04	0.256	0.744	0.000
3	1.30E+07	1.20E+07	2.360E-04	0.256	0.744	0.000
4	1.30E+07	1.16E+07	2.652E-04	0.256	0.744	0.000
5	1.30E+07	1.10E+07	3.221E-04	0.256	0.744	0.000
6	1.30E+07	1.26E+07	1.486E-04	0.498	0.502	0.000
7	1.30E+07	1.23E+07	2.146E-04	0.498	0.502	0.000
8	1.30E+07	1.19E+07	2.599E-04	0.498	0.502	0.000
9	1.30E+07	1.16E+07	2.956E-04	0.498	0.502	0.000
10	1.30E+07	1.10E+07	3.509E-04	0.498	0.502	0.000
11	1.30E+07	1.26E+07	1.709E-04	0.752	0.248	0.000
12	1.30E+07	1.23E+07	2.468E-04	0.752	0.248	0.000
13	1.30E+07	1.19E+07	3.038E-04	0.752	0.248	0.000
14	1.30E+07	1.16E+07	3.391E-04	0.752	0.248	0.000
15	1.30E+07	1.10E+07	4.108E-04	0.752	0.248	0.000
16	1.30E+07	1.27E+07	1.161E-04	0.000	0.494	0.506
17	1.30E+07	1.23E+07	1.615E-04	0.000	0.494	0.506
18	1.30E+07	1.20E+07	1.975E-04	0.000	0.494	0.506
19	1.30E+07	1.15E+07	2.183E-04	0.000	0.494	0.506
20	1.30E+07	1.10E+07	2.366E-04	0.000	0.494	0.506
21	1.30E+07	1.26E+07	1.148E-04	0.000	0.254	0.746
22	1.30E+07	1.20E+07	1.830E-04	0.000	0.254	0.746
23	1.30E+07	1.19E+07	1.918E-04	0.000	0.254	0.746
24	1.30E+07	1.15E+07	2.076E-04	0.000	0.254	0.746
25	1.30E+07	1.10E+07	2.252E-04	0.000	0.254	0.746
26	1.30E+07	1.27E+07	1.893E-04	1.000	0.000	0.000
27	1.30E+07	1.23E+07	3.142E-04	1.000	0.000	0.000
28	1.30E+07	1.20E+07	3.382E-04	1.000	0.000	0.000
29	1.30E+07	1.16E+07	3.785E-04	1.000	0.000	0.000
30	1.30E+07	1.10E+07	4.303E-04	1.000	0.000	0.000
31	1.30E+07	1.27E+07	1.211E-04	0.000	1.000	0.000
32	1.30E+07	1.23E+07	1.729E-04	0.000	1.000	0.000
33	1.30E+07	1.20E+07	2.095E-04	0.000	1.000	0.000
34	1.30E+07	1.16E+07	2.461E-04	0.000	1.000	0.000
35	1.30E+07	1.09E+07	2.864E-04	0.000	1.000	0.000
36	1.30E+07	1.26E+07	1.066E-04	0.000	0.000	1.000
37	1.30E+07	1.22E+07	1.508E-04	0.000	0.000	1.000
38	1.30E+07	1.20E+07	1.767E-04	0.000	0.000	1.000
39	1.30E+07	1.15E+07	2.032E-04	0.000	0.000	1.000
40	1.30E+07	1.11E+07	2.095E-04	0.000	0.000	1.000
41	1.30E+07	1.08E+07	2.170E-04	0.000	0.000	1.000

Table 25: Complete dataset for the Haliburton Fluidic Diode Valve, converted to volumetric flow

Appendix C: AICD Model results

C.1: Dataset 1: Statoil RCP Valve

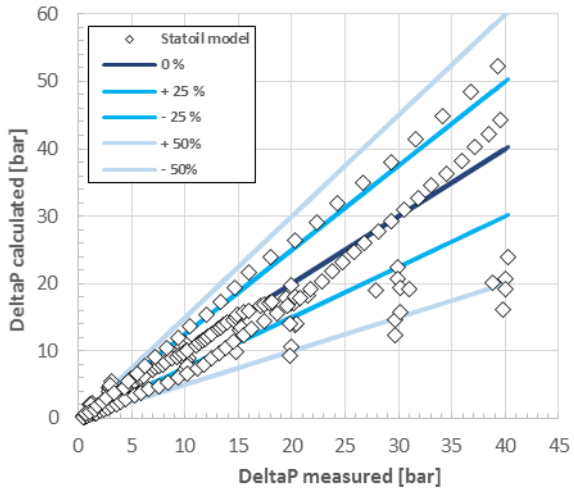

(a) Statoil model: Error distribution

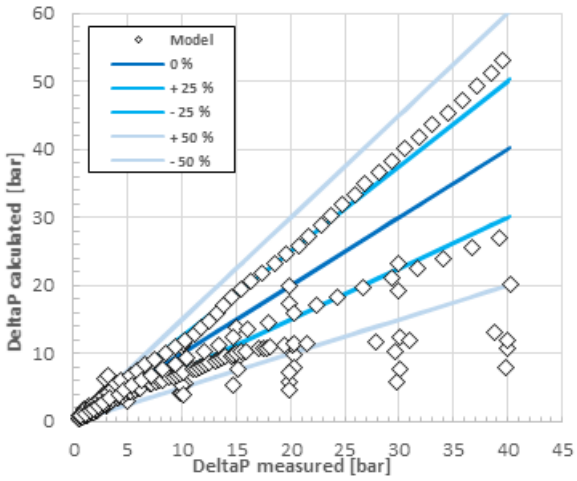

(b) Bernoulli model (Homogenous): Error distribution

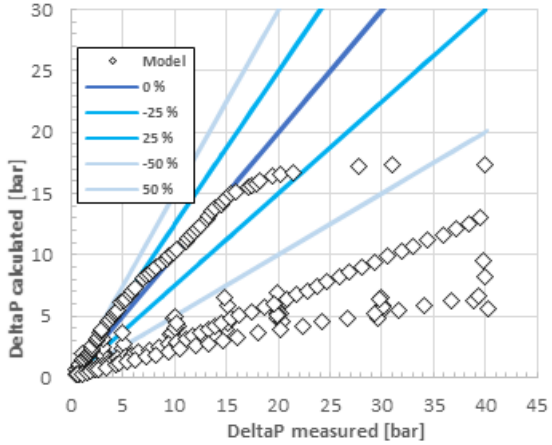

(c) Bernoulli model (Simpson): Error distribution

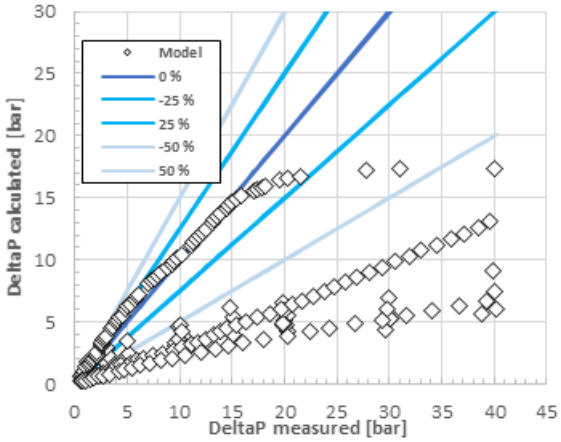

(d) Bernoulli model (Chisholm): Error distribution

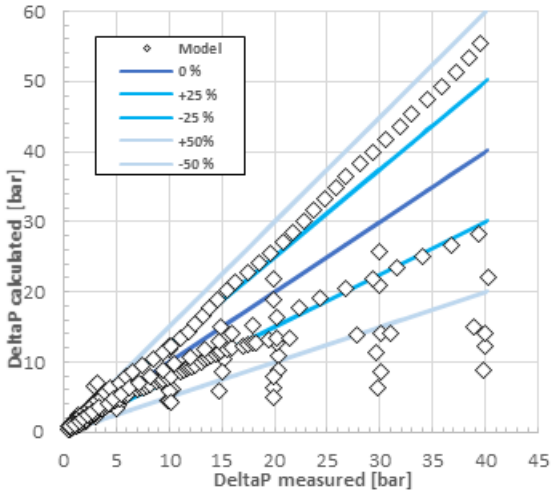

(e) Sachdeva model: Error distribution

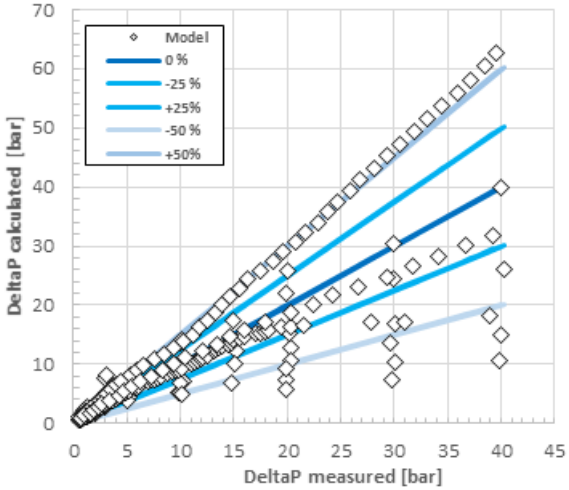

(f) Asheim model: Error distribution

Figure 40: Error distribution plots for all models, Dataset 1

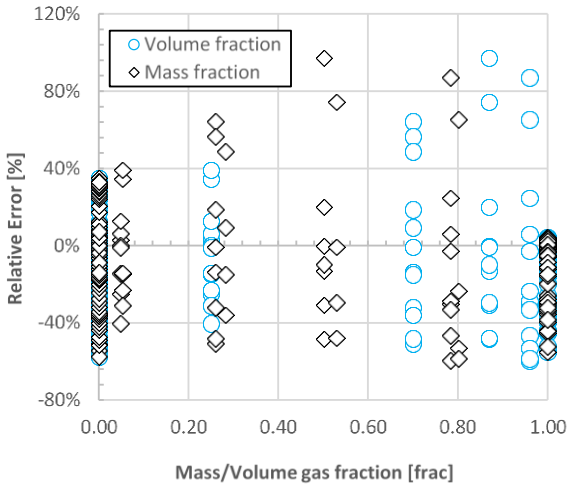

(a) Statoil model: Error vs gas mass/volume fraction

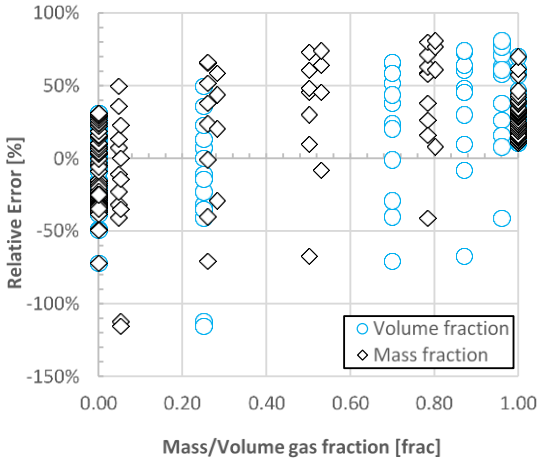

(b) Bernoulli model (Homogenous): Error vs mass/volume gas fraction

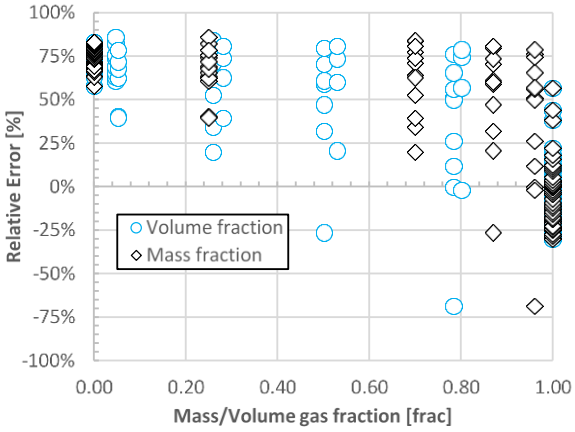

(c) Bernoulli model (Simpson): Error vs mass/volume gas fraction

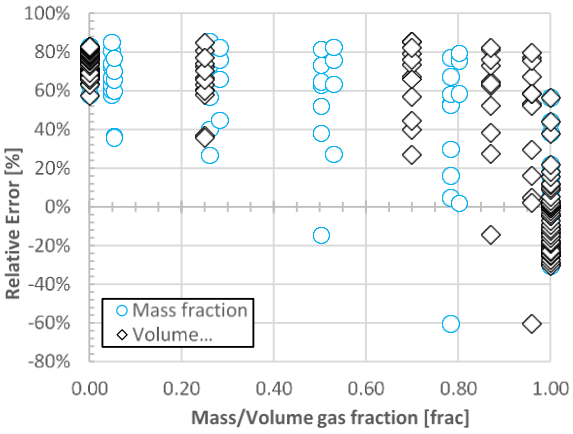

(d) Bernoulli model (Chisholm): Error vs mass/volume gas fraction

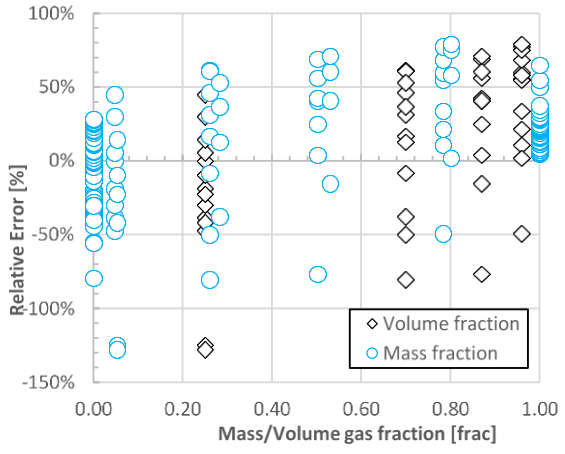

(e) Sachdeva model: Error vs mass/volume gas fraction

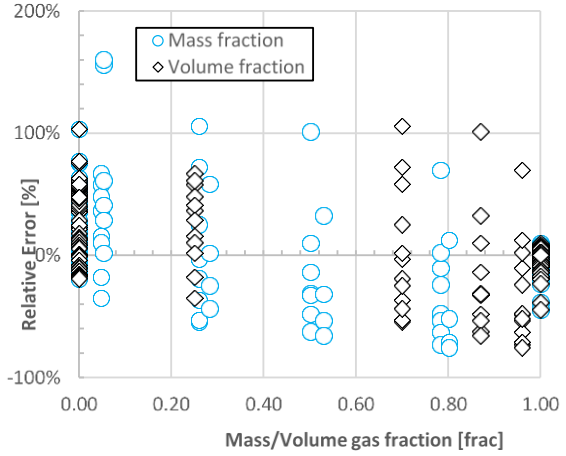

(f) Asheim model: Error vs mass/volume fraction

Figure 41: Error vs gas fraction for all models, dataset 1

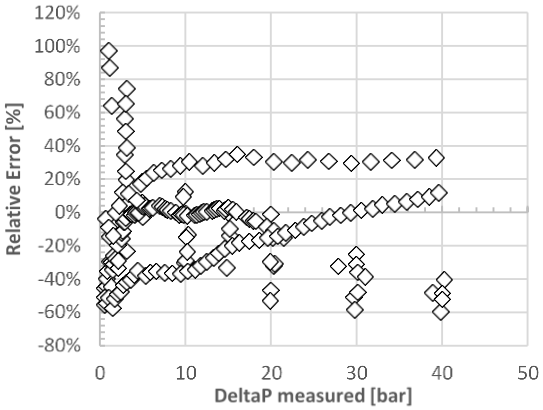

(a) Statoil model: Error vs deltaP

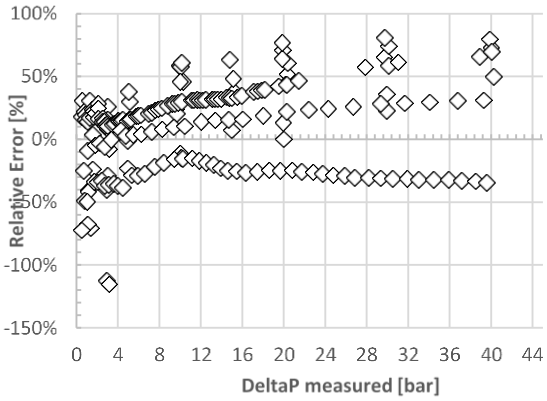

(b) Bernoulli model (Homogenous): Error vs deltaP

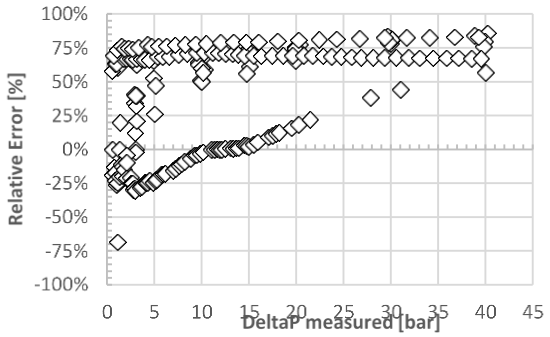

(c) Bernoulli model (Simpson): Error vs deltaP

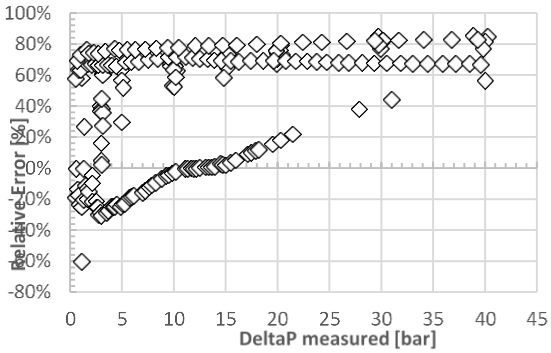

(d) Bernoulli model (Chisholm): Error vs deltaP

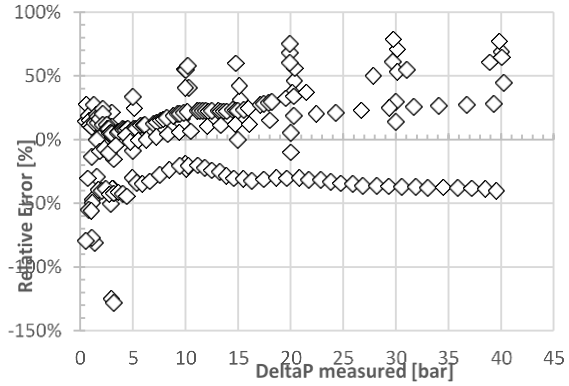

(e) Sachdeva model: Error vs deltaP

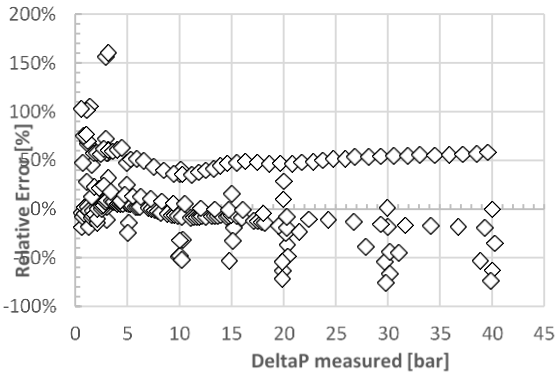

(f) Asheim model: Error vs deltaP

Figure 42: Error vs deltaP plots for all models, dataset 1

C.2: Dataset 2: Haliburtin Fluidic Diode Valve

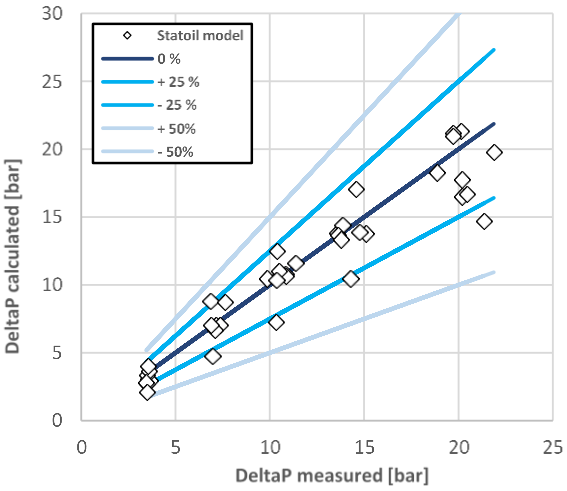

(a) Statoil model: Error distribution

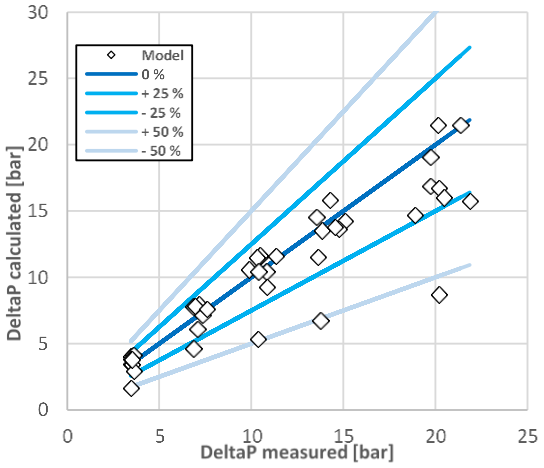

(b) Bernoulli model (Homogenous): Error distribution

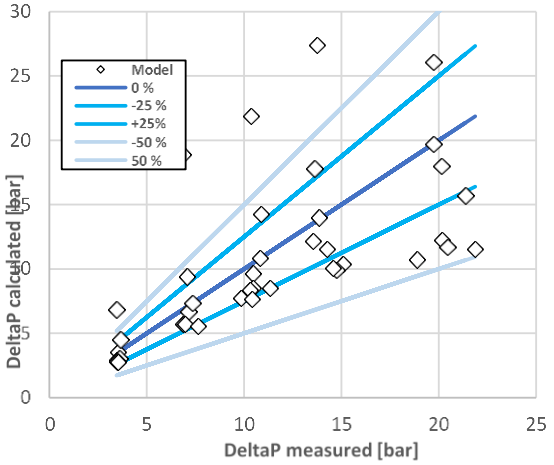

(c) Bernoulli model (Simpson): Error distribution

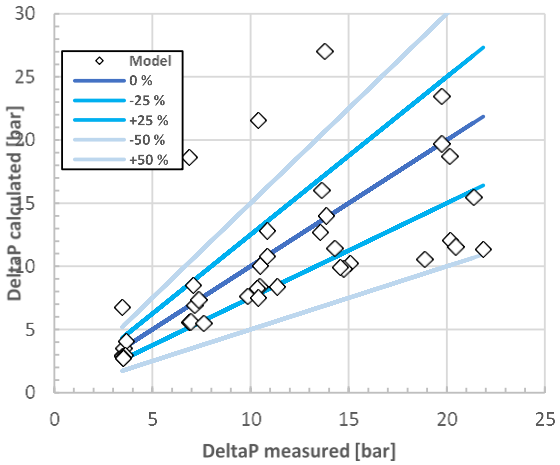

(d) Bernoulli model (Chisholm): Error distribution

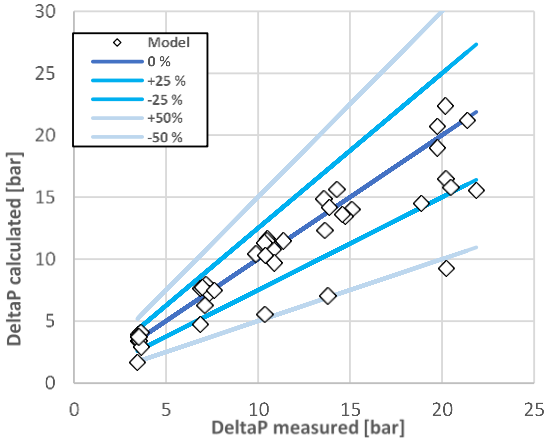

(e) Sachdeva model: Error distribution

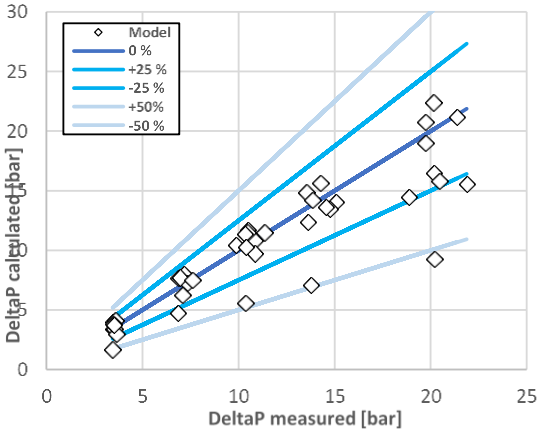

(f) Asheim model: Error distribution

Figure 43: Error distribution plot for all models, dataset 2

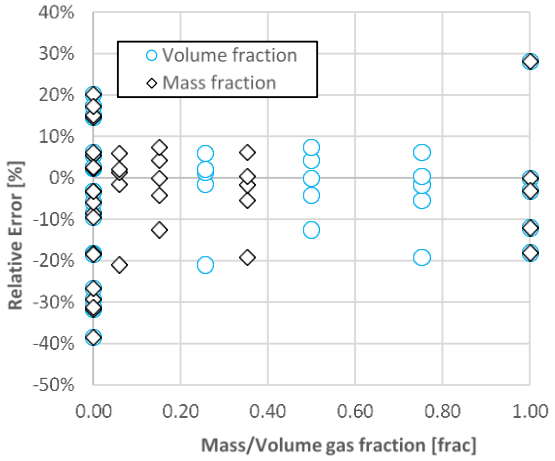

(a) Statoil model: Error vs gas mass/volume fraction

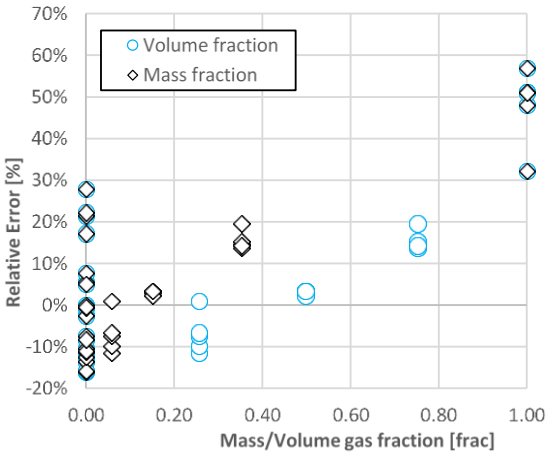

(b) Bernoulli model (Homogenous): Error vs mass/volume gas fraction

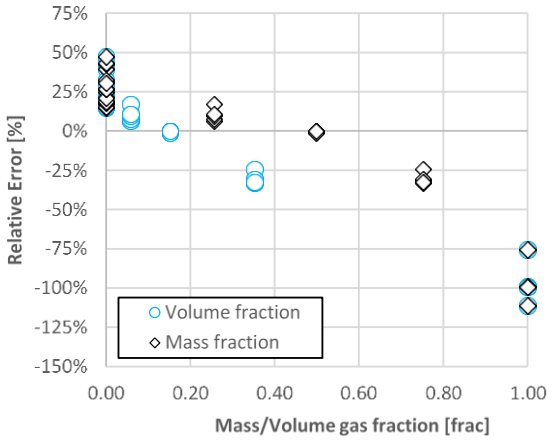

(c) Bernoulli model (Simpson): Error vs mass/volume gas fraction

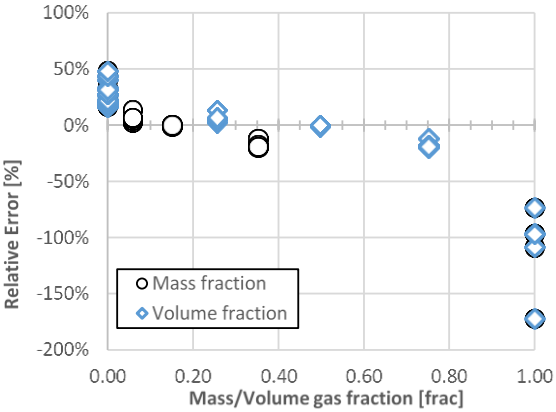

(d) Bernoulli model (Chisholm): Error vs mass/volume gas fraction

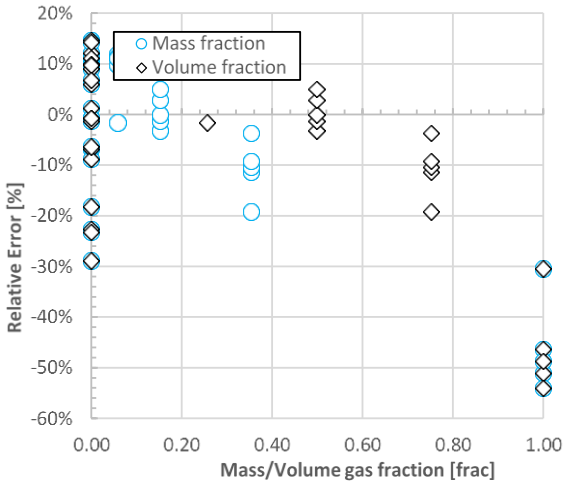

(e) Sachdeva model: Error vs mass/volume gas fraction

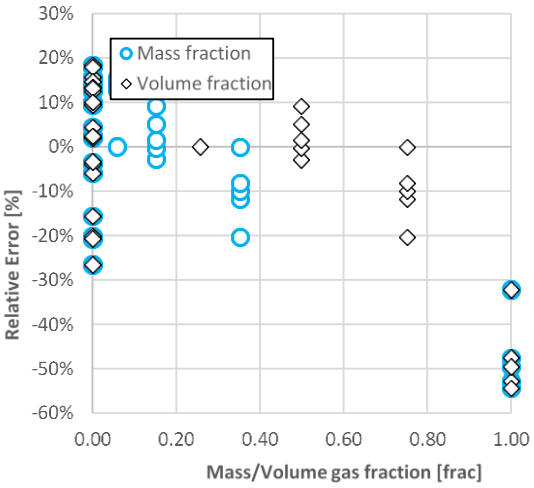

(f) Asheim model: Error vs mass/volume fraction

Figure 44: Error gas fraction plot for all models, dataset 2

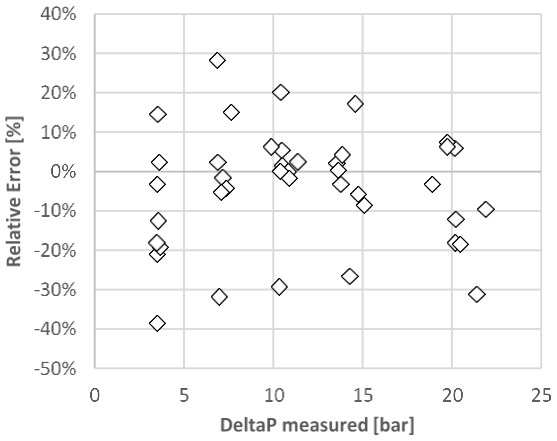

(a) Statoil model: Error vs deltaP

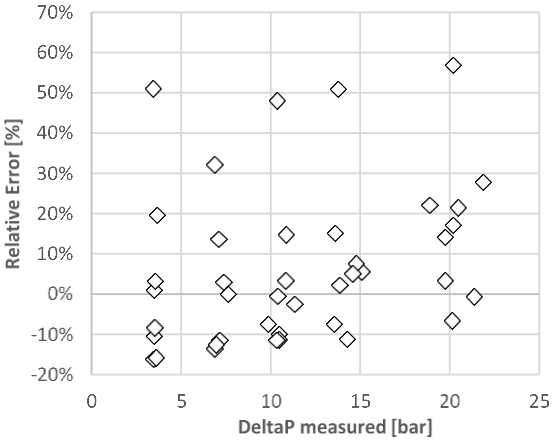

(b) Bernoulli model (Homogenous): Error vs deltaP

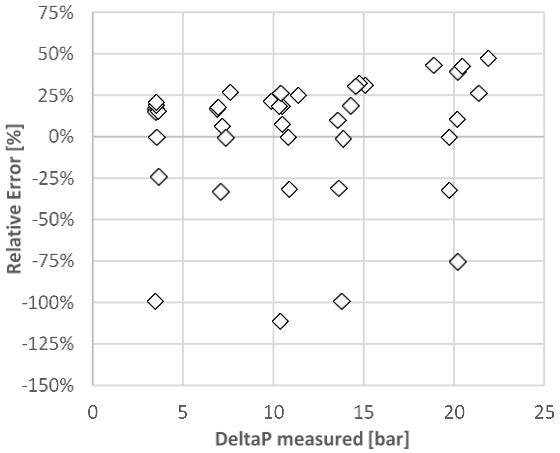

(c) Bernoulli model (Simpson): Error vs deltaP

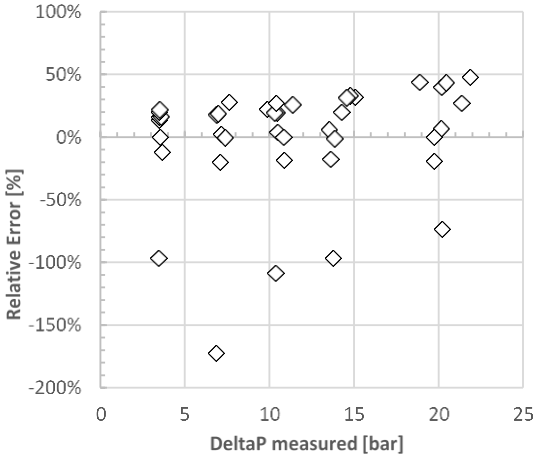

(d) Bernoulli model (Chisholm): Error vs deltaP

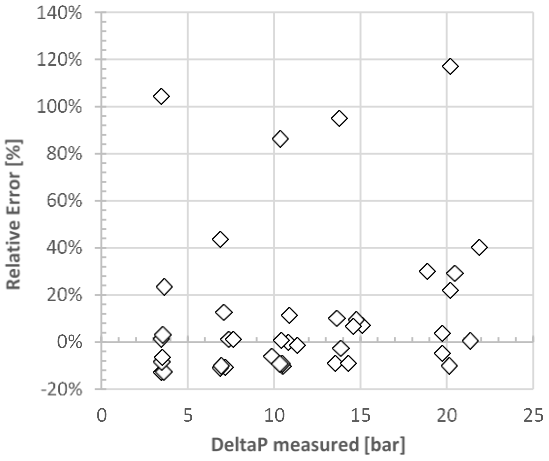

(e) Sachdeva model: Error vs deltaP

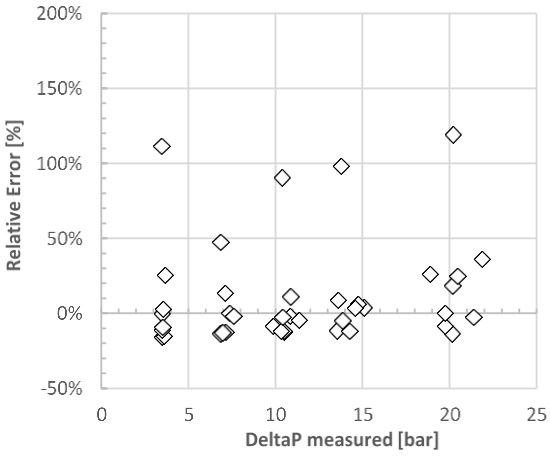

(f) Asheim model: Error vs deltaP

Figure 45: Error vs DeltaP for all models, dataset 2

Appendix D: Extracted GOR-Model data

Curve	Oil rate sm3/d	GOR from figure sm3/sm3	GOR from model sm3/sm3	SSQ Error
1	0.000	58.840	59.114	0.075
1	30.000	58.840	59.114	0.075
1	65.000	58.840	59.114	0.075
1	65.200	58.840	59.114	0.075
1	75.450	74.870	80.542	32.169
1	80.300	97.660	99.373	2.934
1	87.490	134.300	135.003	0.494
1	91.800	165.940	160.307	31.736
1	97.010	197.610	194.508	9.621
1	101.860	225.320	229.691	19.105
2	0.000	58.840	59.114	0.075
2	20.000	58.840	59.114	0.075
2	41.000	58.840	59.114	0.075
2	41.500	58.840	59.114	0.075
2	44.010	70.110	72.703	6.725
2	45.810	83.950	89.780	33.989
2	48.320	113.570	120.304	45.352
2	50.300	149.090	148.923	0.028
2	53.710	210.260	206.153	16.871
2	56.590	266.500	261.361	26.405
2	59.100	318.780	314.076	22.129
2	61.800	368.110	375.183	50.022
3	0.458	58.840	59.114	0.075
3	25.000	58.840	59.114	0.075
3	25.690	58.840	59.114	0.075
3	29.280	130.800	127.890	8.471
3	30.720	170.250	167.916	5.446
3	32.870	229.420	235.651	38.821
3	35.390	320.130	324.890	22.655
3	37.190	402.930	394.122	77.585
3	39.340	481.810	482.061	0.063
3	40.960	549.830	551.751	3.690

Table 26: Extracted data from Statoil's GOR-Model

Appendix E: Network Analysis Results

E.1: Optimized drawdown for all sections

Section	CASE 1 NO ICD /1	CASE 2 NO ICD/2	CASE 3 NO ICD /3	CASE 4 AICD/1	CASE 5 AICD/2	CASE 6 AICD/3	CASE 7 AICV/1	CASE 8 AICV/2	CASE 9 AICV/3
1	0.217	0.163	0.122	0.535	0.331	0.217	0.549	0.338	0.223
2	0.218	0.161	0.123	0.535	0.331	0.217	0.549	0.338	0.223
3	0.218	0.161	0.123	0.535	0.331	0.217	0.549	0.338	0.223
4	0.219	0.162	0.123	0.535	0.331	0.217	0.549	0.338	0.223
5	0.220	0.163	0.123	0.535	0.331	0.218	0.549	0.338	0.223
6	0.221	0.164	0.124	0.535	0.331	0.218	0.549	0.338	0.223
7	0.223	0.165	0.125	0.535	0.331	0.218	0.549	0.339	0.223
8	0.226	0.167	0.126	0.535	0.331	0.218	0.549	0.339	0.223
9	0.230	0.169	0.127	0.535	0.331	0.218	0.549	0.339	0.223
10	0.234	0.172	0.129	0.536	0.331	0.218	0.550	0.339	0.223
11	0.240	0.175	0.130	0.536	0.332	0.218	0.550	0.339	0.223
12	0.246	0.179	0.133	0.536	0.332	0.218	0.550	0.339	0.223
13	0.254	0.183	0.136	0.536	0.332	0.218	0.550	0.339	0.223
14	0.263	0.189	0.139	0.537	0.332	0.218	0.550	0.339	0.223
15	0.274	0.195	0.142	0.537	0.332	0.218	0.551	0.339	0.223
16	0.286	0.202	0.146	0.537	0.332	0.218	0.551	0.339	0.223
17	0.300	0.210	0.151	0.538	0.333	0.218	0.551	0.340	0.224
18	0.316	0.219	0.155	0.538	0.333	0.219	0.552	0.340	0.224
19	0.335	0.228	0.160	0.539	0.333	0.219	0.552	0.340	0.224
20	0.356	0.239	0.169	0.540	0.333	0.219	0.553	0.340	0.224
21	0.381	0.247	0.177	0.540	0.334	0.219	0.553	0.341	0.224
22	0.410	0.257	0.187	0.541	0.334	0.219	0.554	0.341	0.224
23	0.442	0.269	0.198	0.542	0.334	0.220	0.555	0.341	0.225
24	0.480	0.303	0.211	0.543	0.335	0.220	0.556	0.342	0.225
25	0.523	0.325	0.226	0.544	0.335	0.220	0.556	0.342	0.225
26	0.575	0.359	0.245	0.544	0.336	0.221	0.557	0.342	0.225
27	0.638	0.398	0.270	0.546	0.336	0.221	0.558	0.343	0.226
28	0.718	0.447	0.301	0.547	0.337	0.221	0.000	0.000	0.000
29	0.823	0.505	0.342	0.548	0.337	0.222	0.000	0.000	0.000
30	0.977	0.581	0.414	0.549	0.338	0.222	0.000	0.000	0.000

Table 27: Solved drawdown pressures [bar] for cases 1-9 (Reservoir 1)

Section	CASE 10 NO ICD /1	CASE 11 NO ICD /2	CASE 12 NO ICD /3	CASE 13 AICD/1	CASE 14 AICD/2	CASE 15 AICD/3	CASE 16 AICV/1	CASE 17 AICV/2	CASE 18 AICV/3
1	0.220	0.142	0.097	1.087	0.671	0.441	1.112	0.683	0.450
2	0.218	0.143	0.097	0.789	0.487	0.320	0.807	0.496	0.326
3	0.218	0.144	0.097	0.592	0.365	0.240	0.605	0.372	0.245
4	0.218	0.145	0.096	0.460	0.284	0.186	0.471	0.289	0.190
5	0.218	0.147	0.106	0.371	0.229	0.151	0.380	0.233	0.153
6	0.219	0.141	0.098	0.311	0.192	0.126	0.318	0.195	0.129
7	0.199	0.138	0.089	0.271	0.167	0.110	0.277	0.170	0.112
8	0.223	0.138	0.097	0.246	0.152	0.100	0.252	0.154	0.102
9	0.237	0.141	0.094	0.232	0.143	0.094	0.238	0.000	0.000
10	0.257	0.155	0.100	0.227	0.140	0.092	0.233	0.000	0.000
11	0.283	0.164	0.101	0.232	0.143	0.094	0.238	0.000	0.000
12	0.309	0.185	0.109	0.246	0.152	0.100	0.252	0.154	0.102
13	0.344	0.210	0.163	0.272	0.168	0.110	0.278	0.170	0.112
14	0.400	0.251	0.173	0.312	0.192	0.126	0.319	0.196	0.129
15	0.474	0.291	0.192	0.372	0.230	0.151	0.380	0.233	0.154
16	0.584	0.360	0.241	0.462	0.285	0.187	0.472	0.289	0.190
17	0.715	0.437	0.296	0.594	0.366	0.241	0.607	0.372	0.245
18	0.866	0.531	0.365	0.793	0.489	0.321	0.809	0.497	0.327
19	1.041	0.643	0.449	1.093	0.674	0.443	1.116	0.686	0.451
20	1.243	0.772	0.537	1.552	0.958	0.630	1.586	0.974	0.641
21	1.454	0.906	0.629	2.254	1.393	0.915	2.304	1.416	0.932
22	1.672	1.042	0.727	3.309	2.048	1.345	3.385	2.084	1.371
23	1.899	1.182	0.828	4.828	2.994	1.966	4.945	3.050	2.008
24	2.131	1.326	0.931	6.840	4.254	2.790	7.031	4.342	2.861
25	2.369	1.472	1.035	9.152	5.731	3.750	9.470	5.862	3.863
26	2.611	1.620	1.141	11.379	7.062	4.670	11.828	7.353	4.855
27	2.856	1.770	1.248	13.134	8.103	5.378	13.801	8.568	5.660
28	3.105	1.922	1.356	14.311	8.866	5.866	15.059	9.400	6.202
29	3.358	2.076	1.465	15.010	9.403	6.079	15.870	9.882	6.538
30	3.614	2.232	1.576	15.446	9.615	6.383	16.399	10.190	6.727

Table 28: Solved drawdown pressures [bar] for cases 10-18 (Reservoir 2)

Section	CASE 19 NO ICD /1	CASE 20 NO ICD /2	CASE 21 NO ICD /3	CASE 22 AICD/1	CASE 23 AICD/2	CASE 24 AICD/3	CASE 25 AICV/1	CASE 26 AICV/2	CASE 27 AICV/3
1	0.0822	0.05028	0.04030	8.814	5.474	3.593	9.284	5.728	3.779
2	0.0823	0.05167	0.04093	8.818	5.474	3.593	9.284	5.728	3.778
3	0.0910	0.06199	0.03474	0.094	0.058	0.038	0.000	0.000	0.000
4	0.0900	0.04833	0.03432	0.094	0.058	0.038	0.000	0.000	0.000
5	0.0854	0.05299	0.04172	8.817	5.474	3.594	9.284	5.728	3.779
6	0.0879	0.05418	0.04233	8.815	5.475	3.594	9.284	5.728	3.779
7	0.0903	0.05539	0.04295	8.820	5.475	3.595	9.286	5.729	3.780
8	0.0928	0.05660	0.04358	8.825	5.477	3.595	9.285	5.729	3.780
9	0.0953	0.05782	0.04421	8.825	5.479	3.596	9.286	5.729	3.780
10	0.0978	0.05904	0.04485	8.821	5.479	3.597	9.287	5.730	3.780
11	0.1004	0.06028	0.04549	8.824	5.480	3.598	9.288	5.731	3.781
12	0.1029	0.06153	0.04614	8.830	5.482	3.599	9.290	5.731	3.781
13	0.1055	0.06278	0.04679	8.833	5.484	3.601	9.292	5.732	3.781
14	0.1081	0.06404	0.04745	8.840	5.487	3.603	9.294	5.734	3.782
15	0.1107	0.06531	0.04811	8.843	5.490	3.604	9.297	5.735	3.783
16	0.1133	0.06659	0.04878	8.852	5.493	3.607	9.300	5.737	3.785
17	0.1160	0.06787	0.04945	8.860	5.502	3.609	9.308	5.739	3.786
18	0.1187	0.06917	0.05013	8.860	5.501	3.612	9.309	5.741	3.788
19	0.1214	0.07046	0.05081	8.869	5.508	3.615	9.313	5.743	3.789
20	0.1242	0.07177	0.05150	8.884	5.510	3.619	9.319	5.746	3.791
21	0.1269	0.07308	0.05219	8.895	5.516	3.622	9.323	5.749	3.793
22	0.1297	0.07440	0.05289	8.906	5.521	3.626	9.333	5.752	3.795
23	0.1453	0.07713	0.05375	0.094	0.058	0.038	0.000	0.000	0.000
24	0.1466	0.08443	0.06227	0.095	0.058	0.038	0.000	0.000	0.000
25	0.1706	0.11013	0.07809	0.095	0.058	0.038	0.000	0.000	0.000
26	0.2799	0.17666	0.12539	8.964	5.551	3.646	9.361	5.767	3.805
27	0.3731	0.24045	0.18007	8.979	5.559	3.651	9.369	5.771	3.808
28	0.4668	0.30458	0.23493	8.998	5.568	3.657	9.379	5.775	3.811
29	0.5611	0.36911	0.29004	9.019	5.577	3.664	9.388	5.780	3.814
30	0.6562	0.43409	0.34548	9.036	5.587	3.670	9.397	5.785	3.817

Table 29: Solved drawdown pressures [bar] for cases 19-27 (Reservoir 3)

Section	CASE 28 NO ICD	CASE 29 AICD	CASE 30 AICV
1	0.0368	8.7000	9.32502
2	0.0356	8.7005	9.32544
3	0.0378	0.0401	0.05281
4	0.0380	0.0401	0.05281
5	0.0371	8.7011	9.32414
6	0.0383	8.7013	9.32439
7	0.0395	8.7024	9.32523
8	0.0408	8.7026	9.32241
9	0.0420	8.7036	9.32532
10	0.0432	8.7118	9.32607
11	0.0445	8.7150	9.32785
12	0.0457	8.7165	9.33023
13	0.0470	8.7200	9.33242
14	0.0483	8.7253	9.33586
15	0.0495	8.7312	9.33766
16	0.0508	8.7380	9.34181
17	0.0521	8.7453	9.34744
18	0.0534	8.7533	9.34916
19	0.0547	8.7600	9.35514
20	0.0560	8.7717	9.35864
21	0.0573	8.7834	9.36730
22	0.0575	8.7948	9.37167
23	0.0585	0.0403	0.05907
24	0.0611	0.0403	0.06082
25	0.0746	0.0404	0.05869
26	0.1397	8.8511	9.40000
27	0.1938	8.8675	9.41000
28	0.2483	8.8848	9.41984
29	0.3030	8.9027	9.42745
30	0.3576	8.9219	9.43577

Table 30: Solved drawdown pressures for cases 28-30

E.2: Inflow distribution for all sections

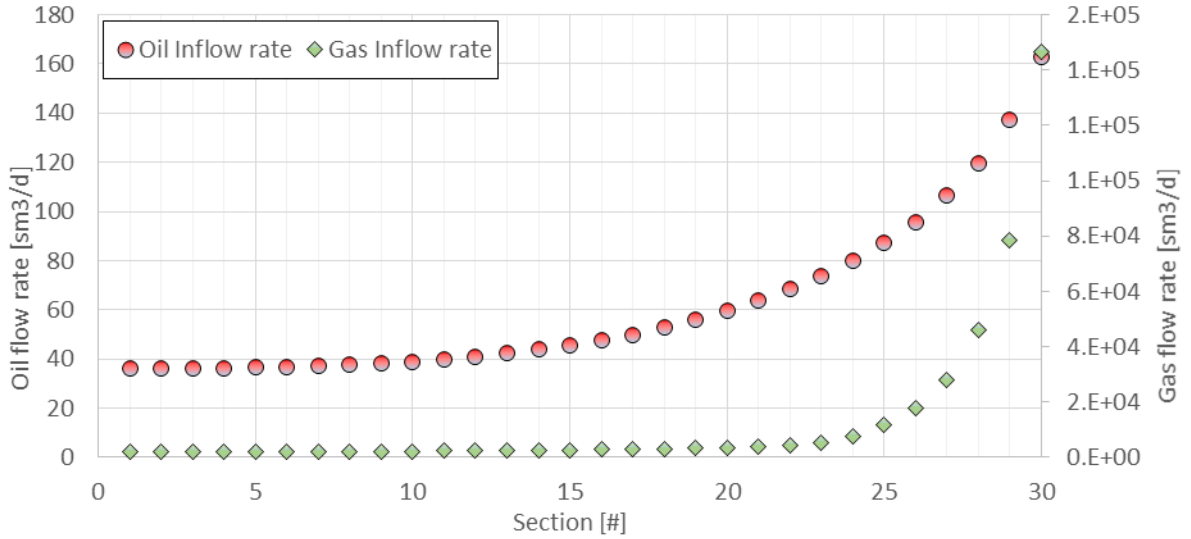

(a) Case 1

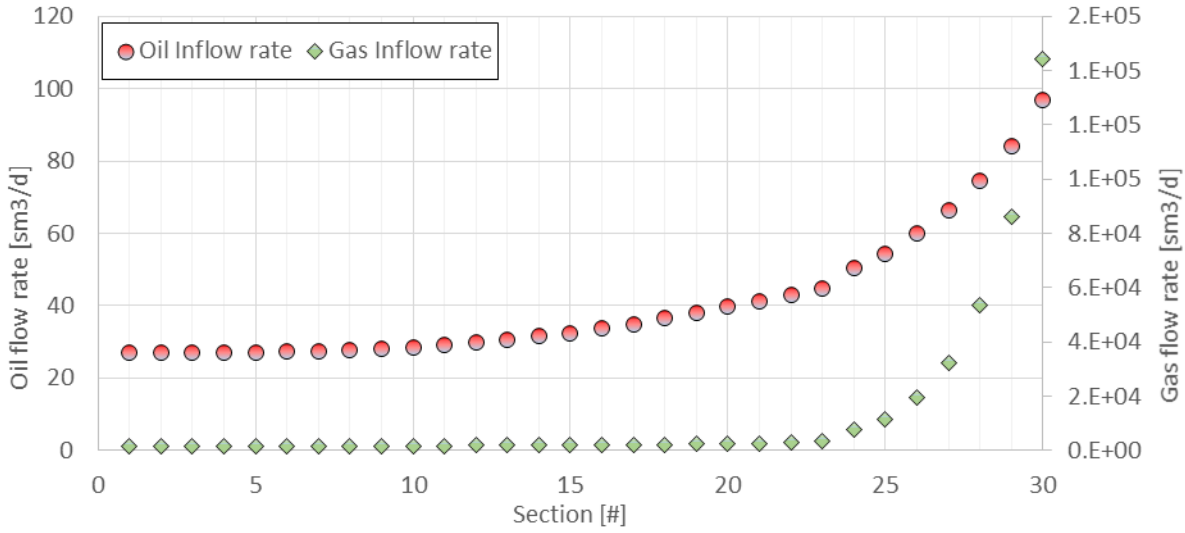

(b) Case 2

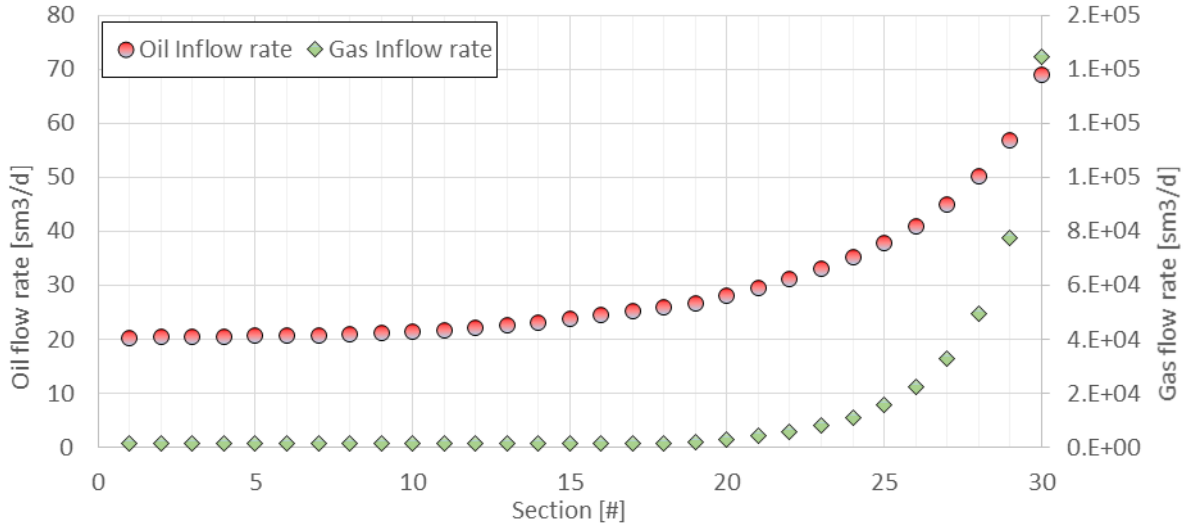

(c) Case 3

Figure 46: Inflow distribution for cases 1-3. Reservoir 1, Open Hole, GORM 1-3.

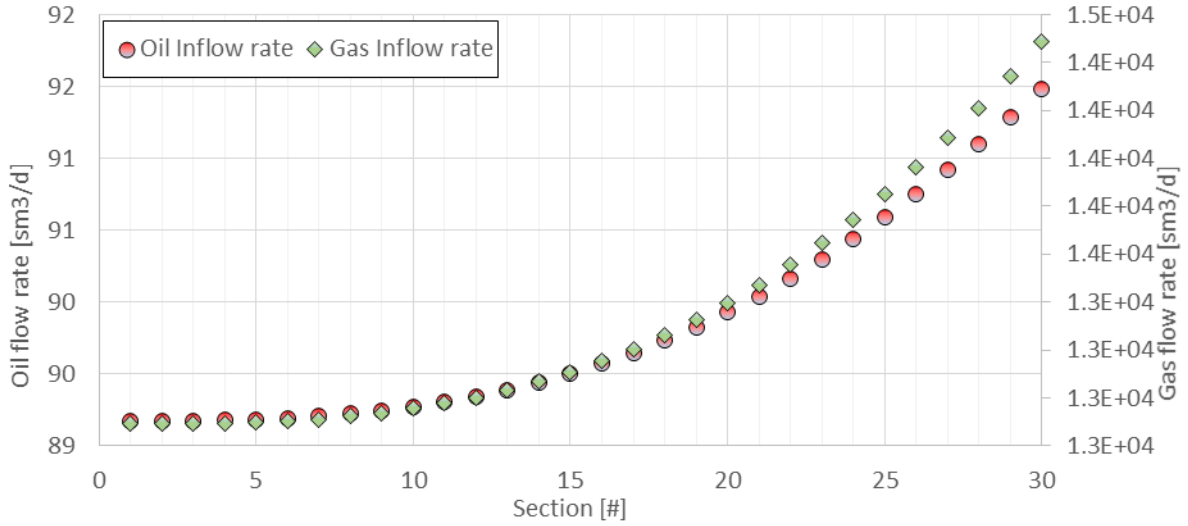

(a) Case 4

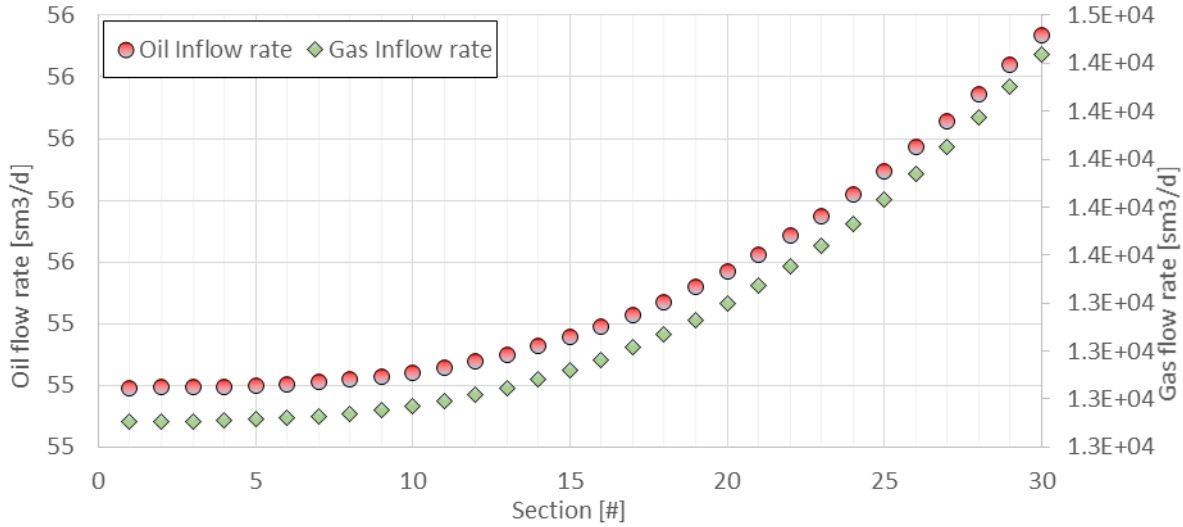

(b) Case 5

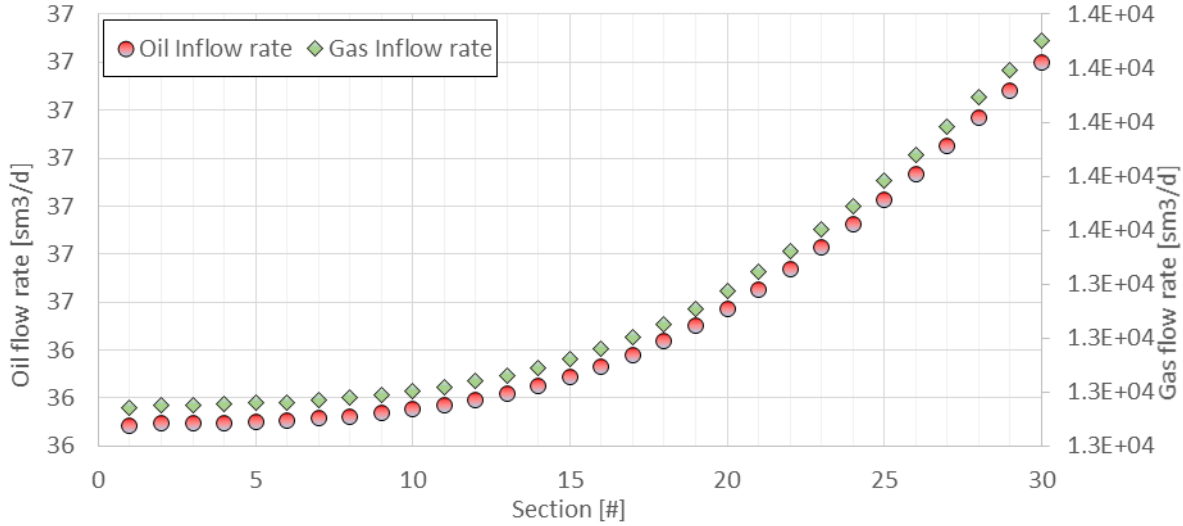

(c) Case 6

Figure 47: Inflow distribution for cases 4-6. Reservoir 1, AICD, GORM 1-3.

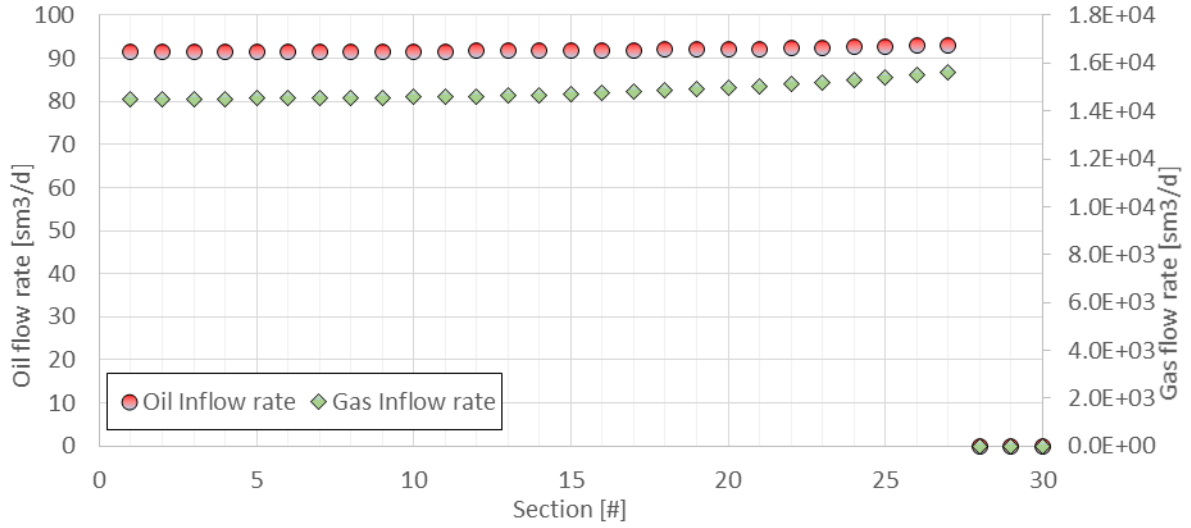

(a) Case 7

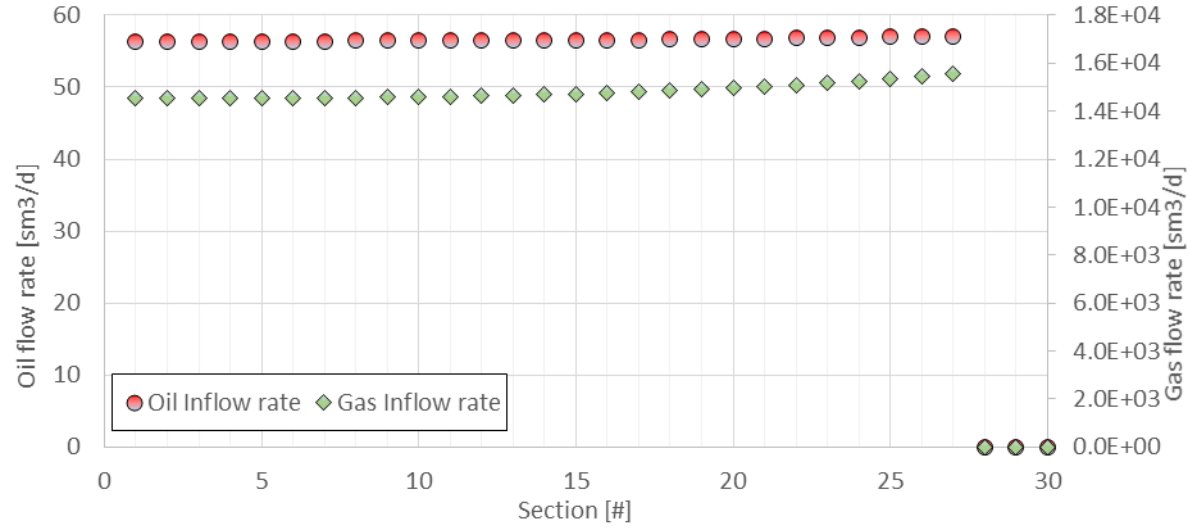

(b) Case 8

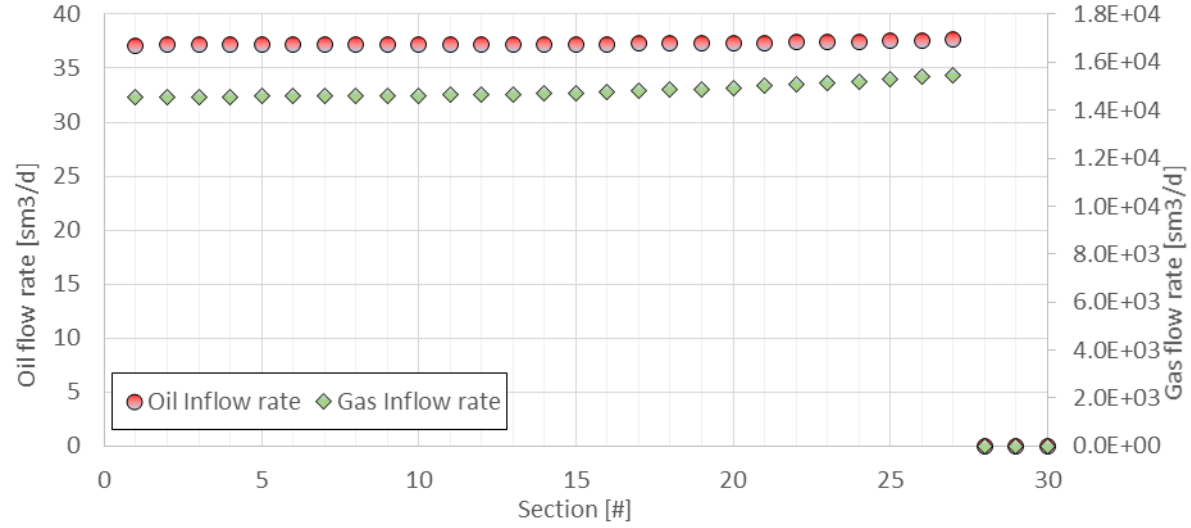

(c) Case 9

Figure 48: Inflow distribution for cases 7-9. Reservoir 1, AICV, GORM 1-3.

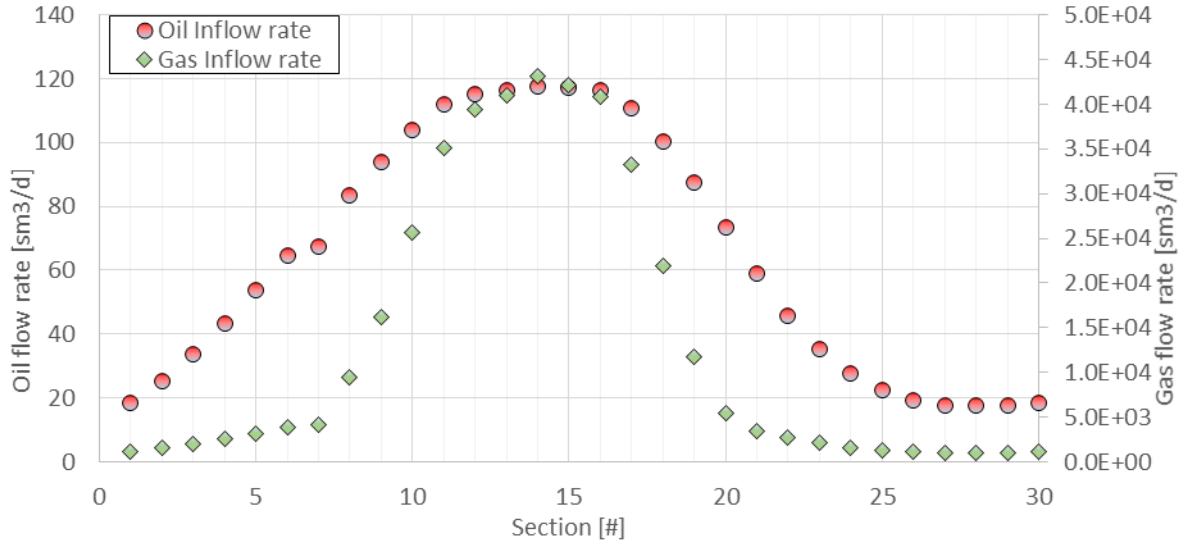

(a) Case 10

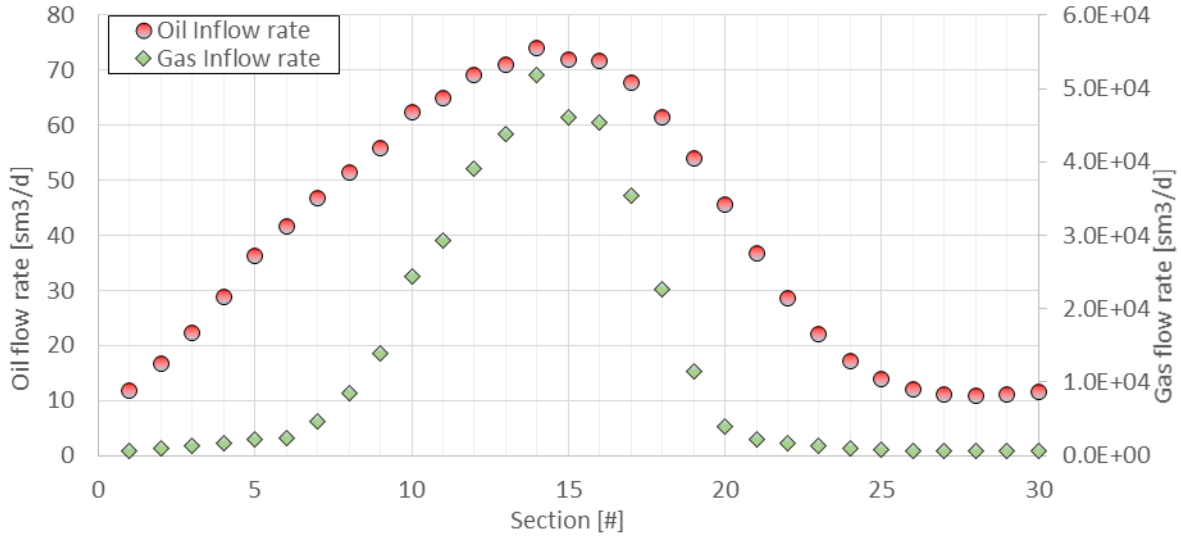

(b) Case 11

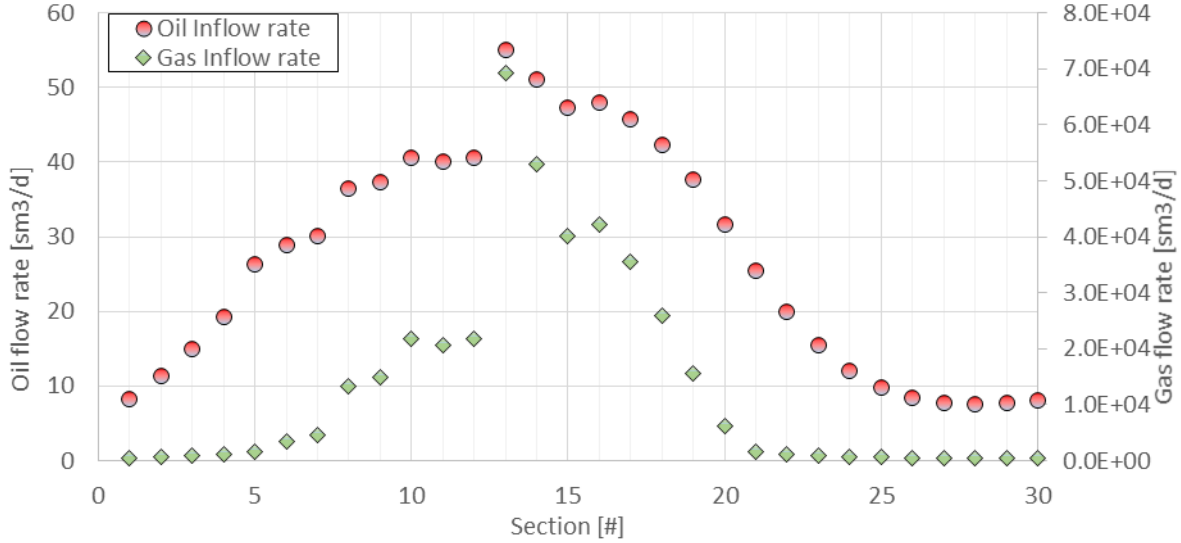

(c) Case 12

Figure 49: Inflow distribution for cases 10-12. Reservoir 2, Open Hole, GORM 1-3.

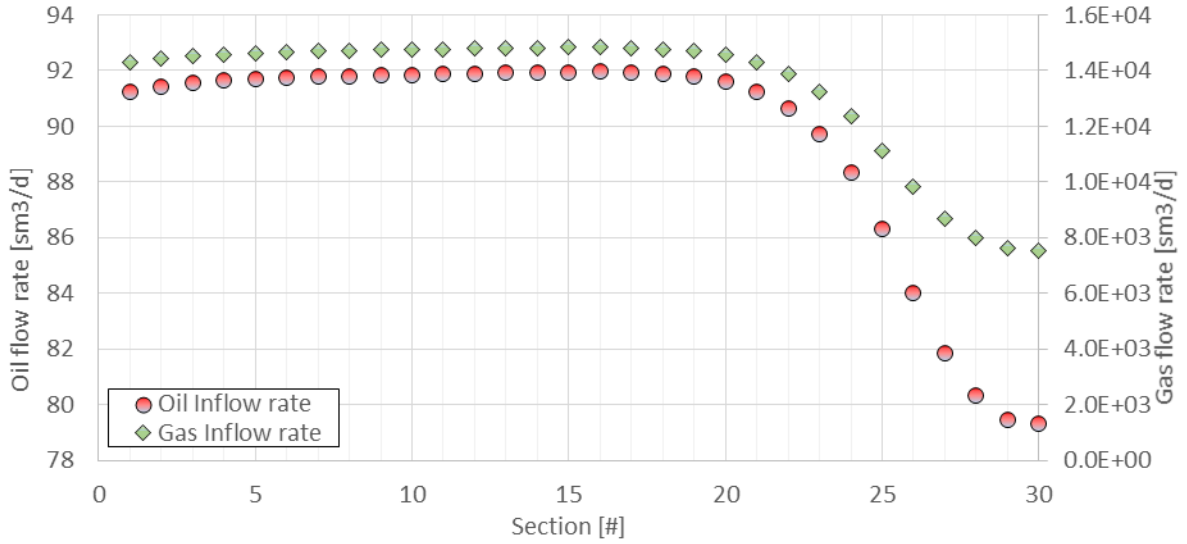

(a) Case 13

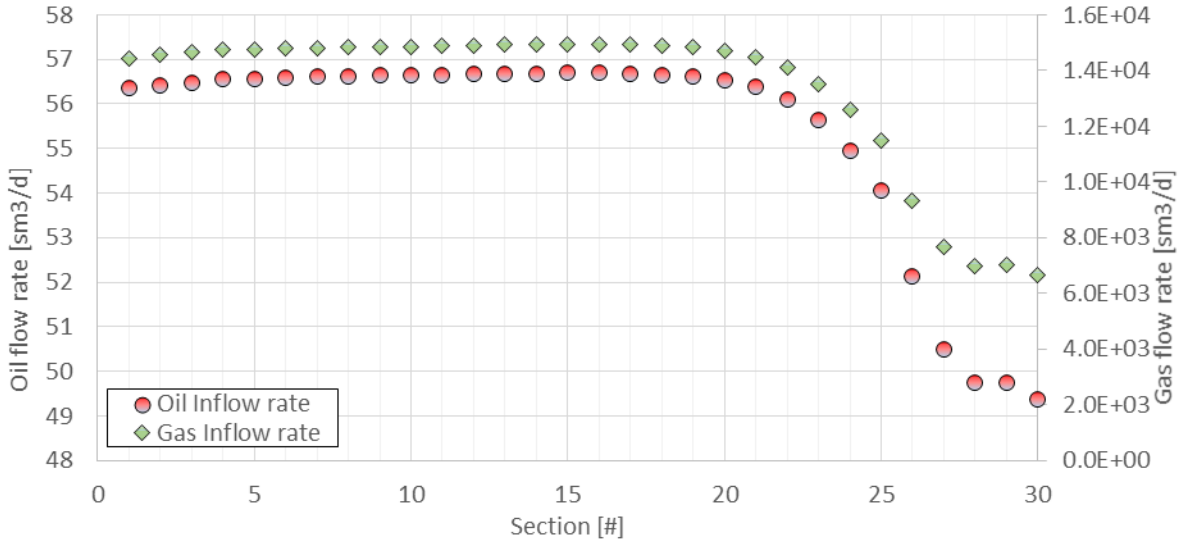

(b) Case 14

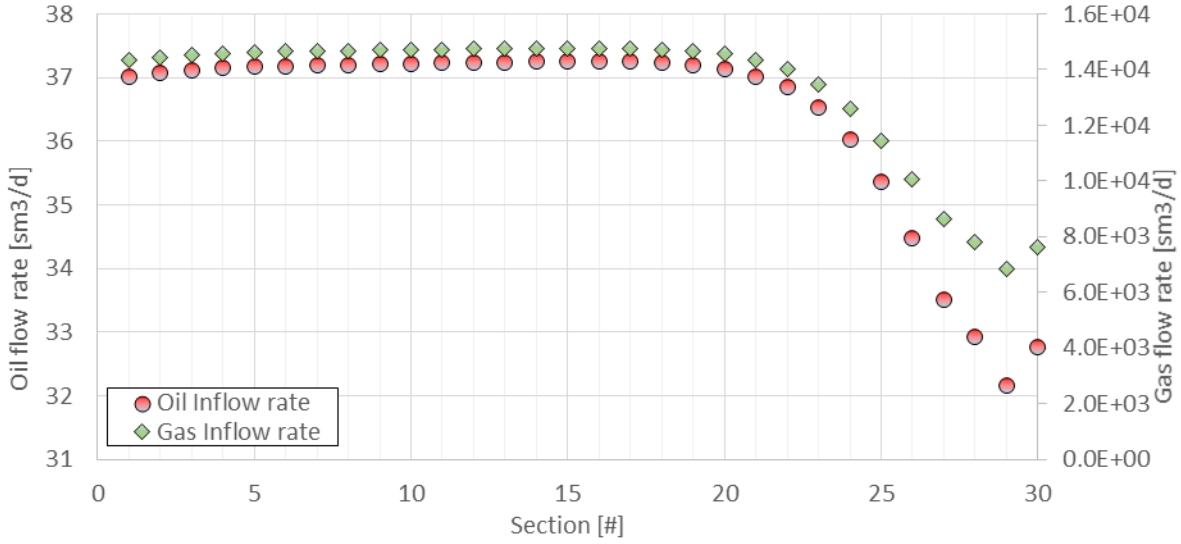

(c) Case 15

Figure 50: Inflow distribution for cases 13-15. Reservoir 2, AICD, GORM 1-3.

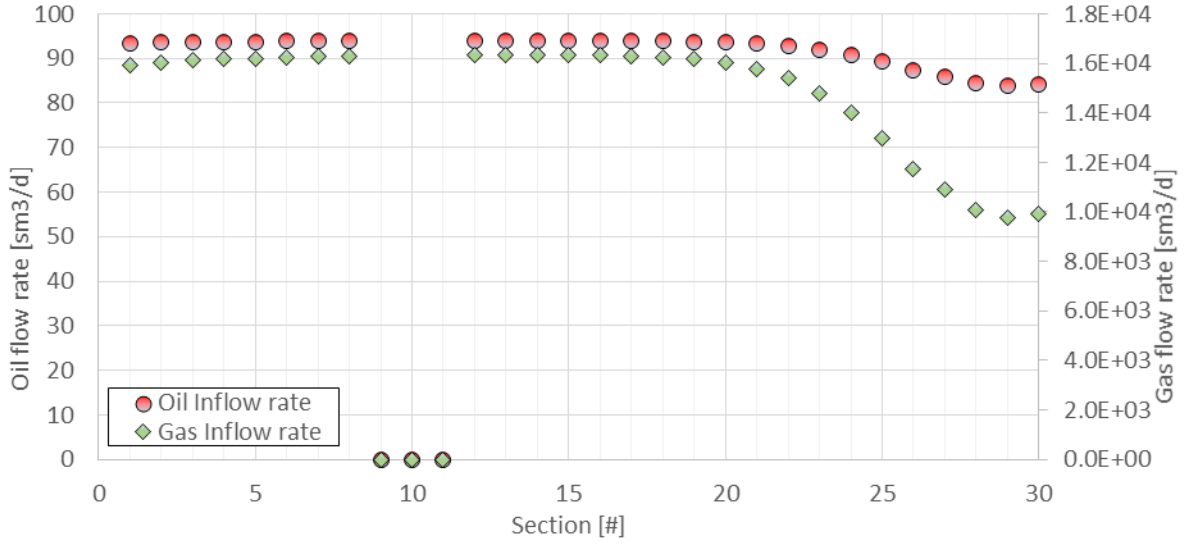

(a) Case 16

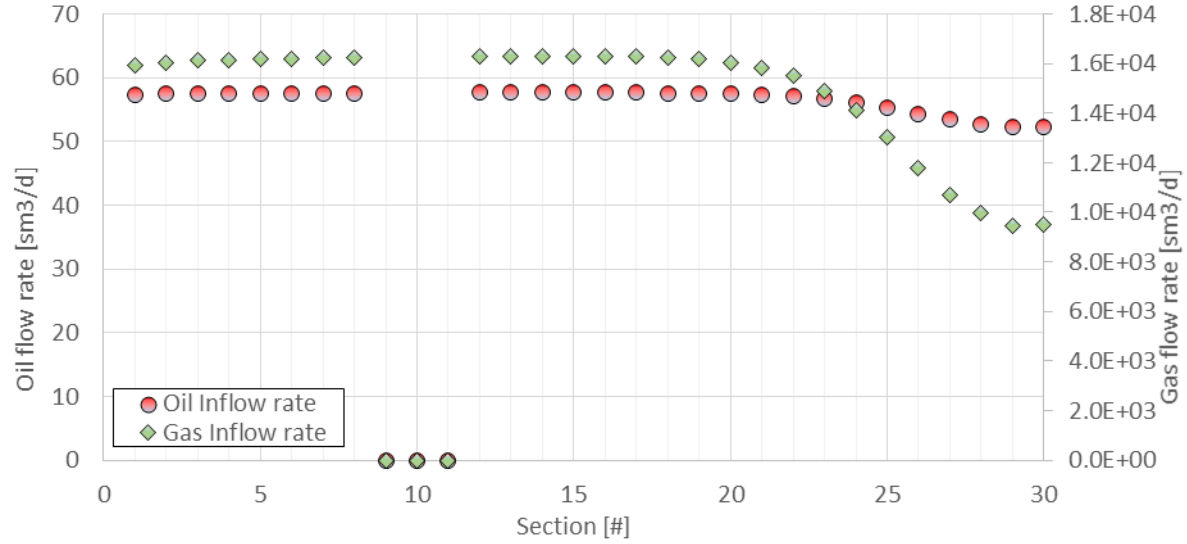

(b) Case 17

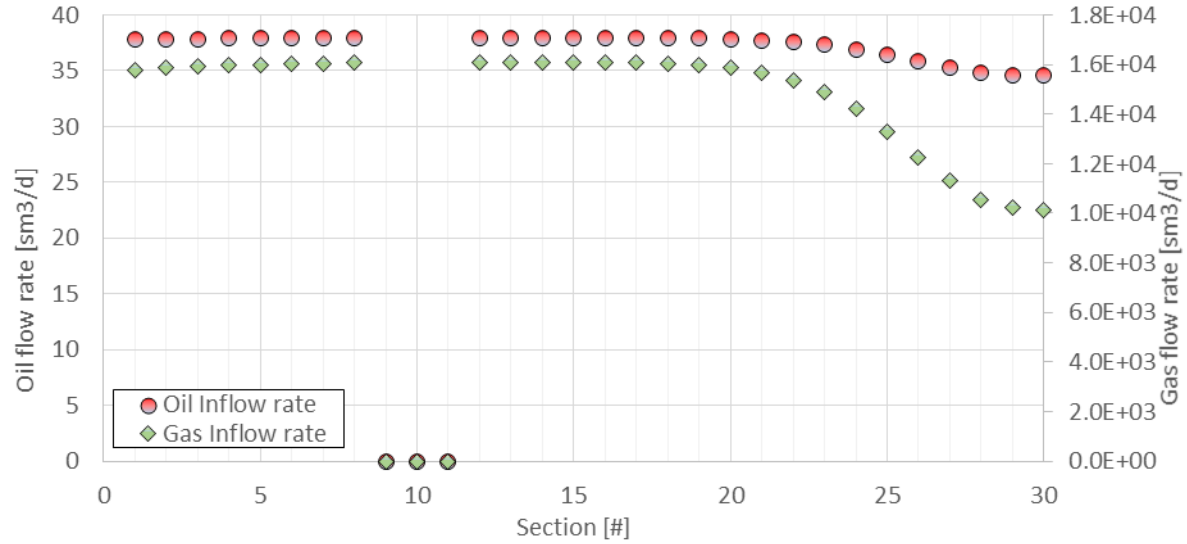

(c) Case 18

Figure 51: Inflow distribution for cases 16-18. Reservoir 2, AICV, GORM 1-3.

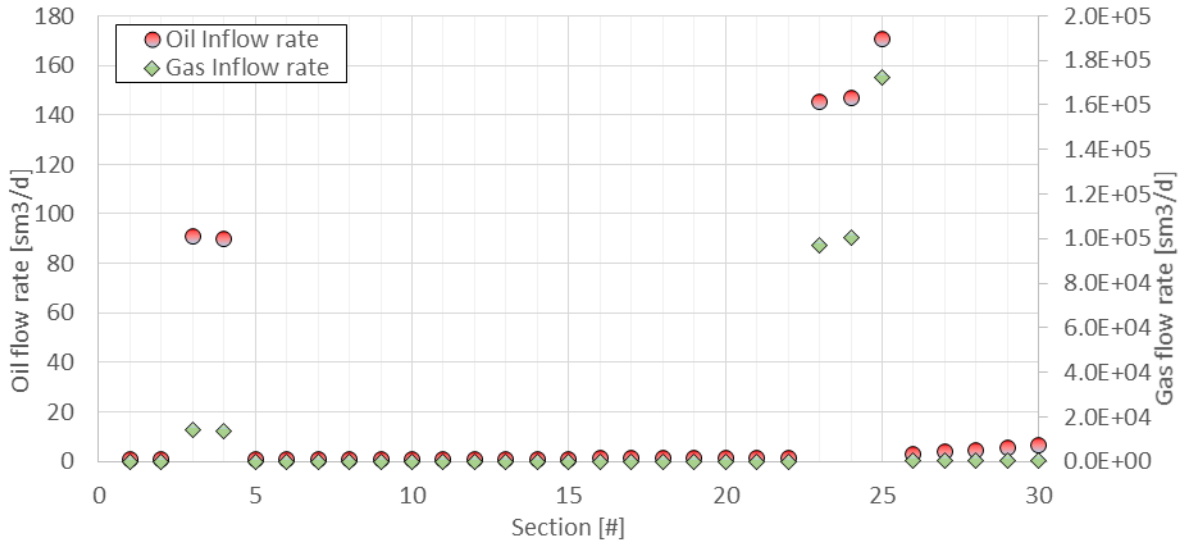

(a) Case 19

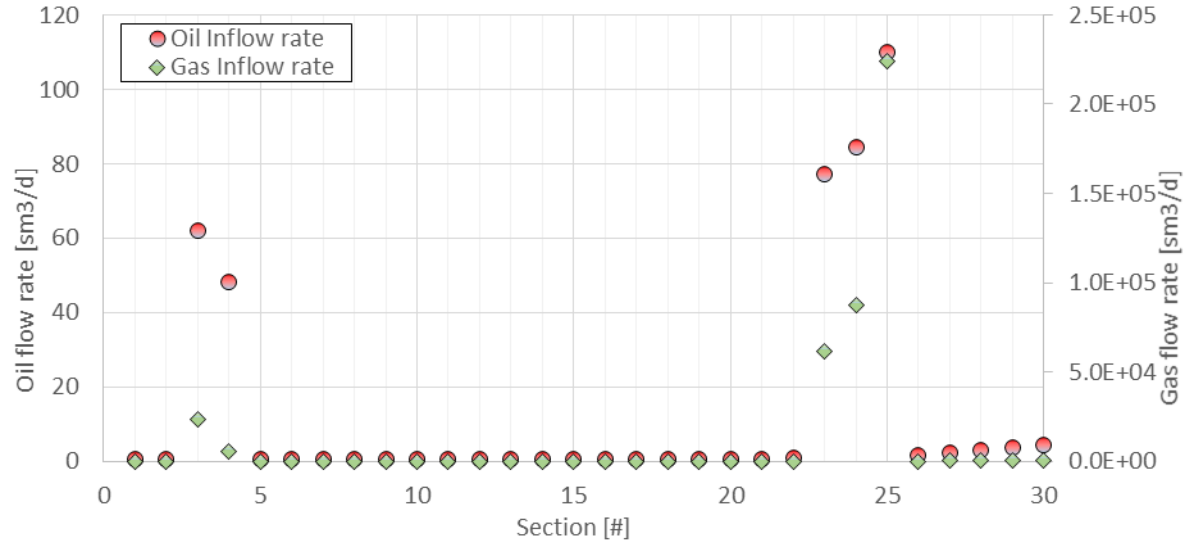

(b) Case 20

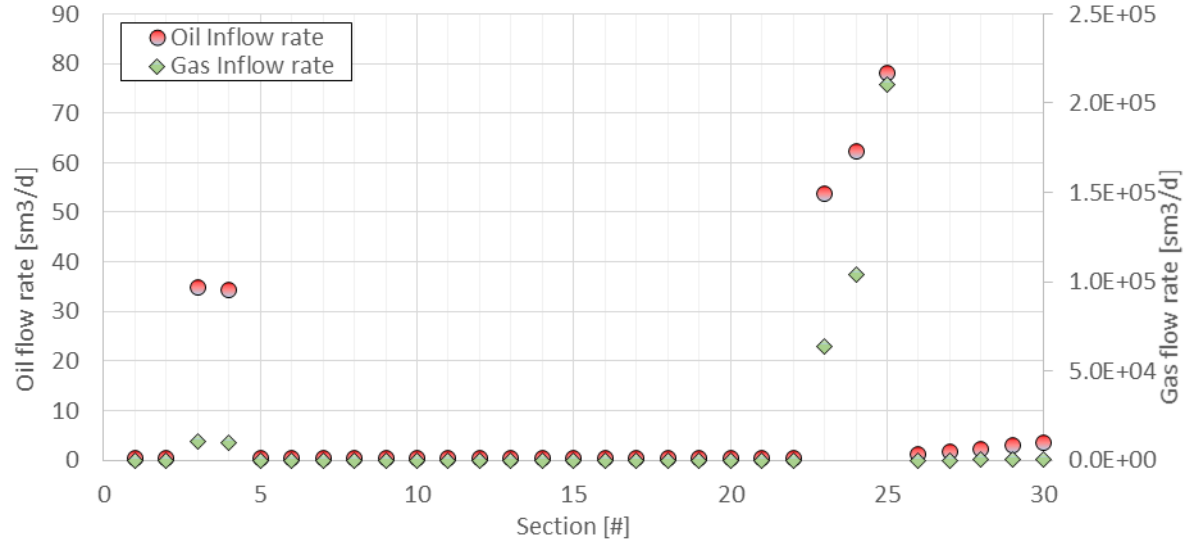

(c) Case 21

Figure 52: Inflow distribution for cases 19-21. Reservoir 3, Open Hole, GORM 1-3.

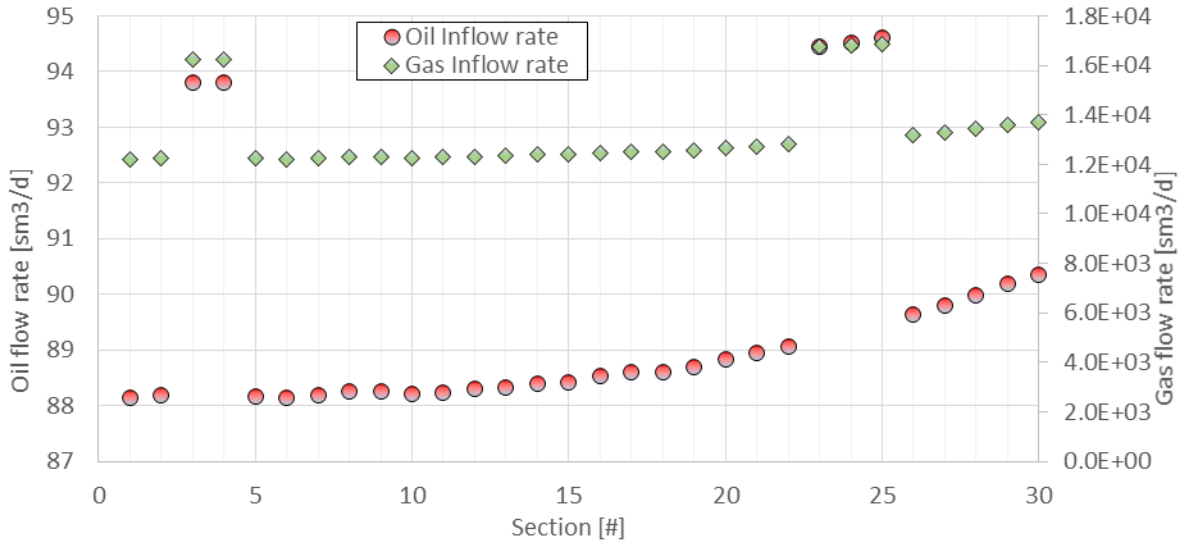

(a) Case 22

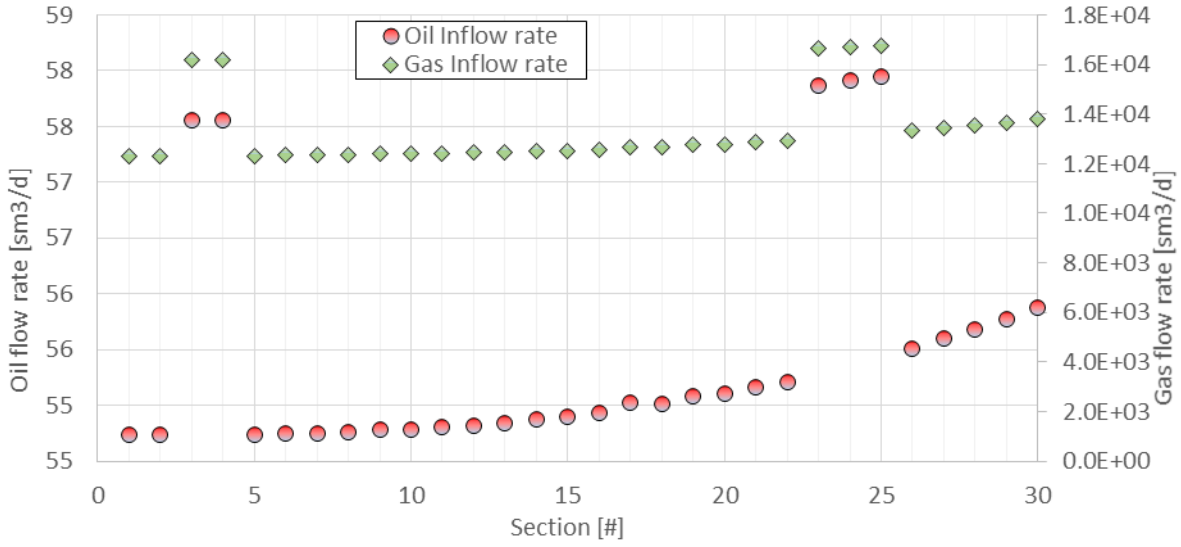

(b) Case 23

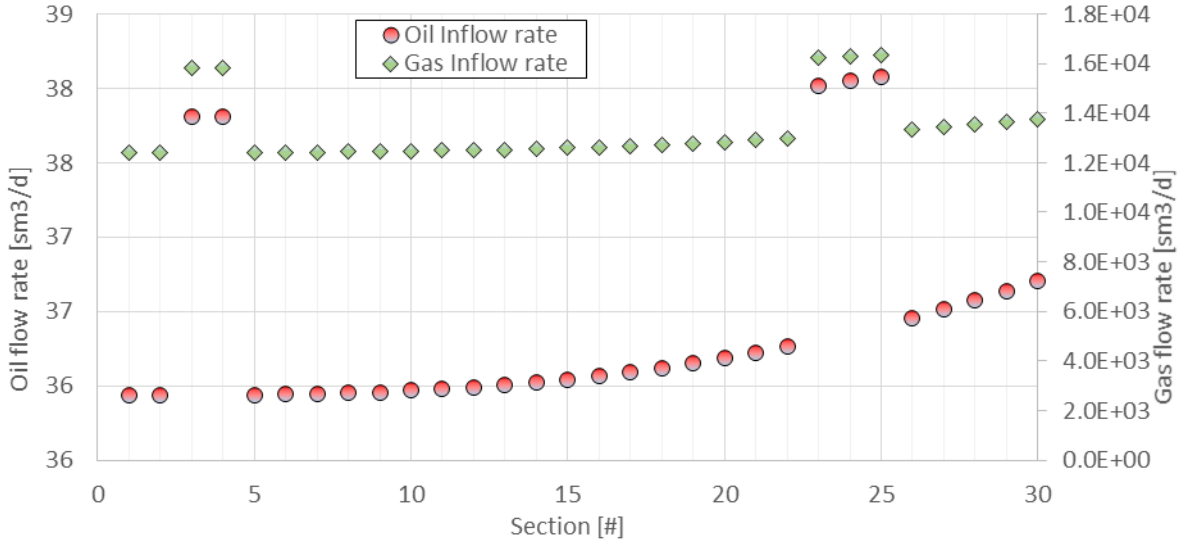

(c) Case 24

Figure 53: Inflow distribution for cases 22-24. Reservoir 3, AICD, GORM 1-3.

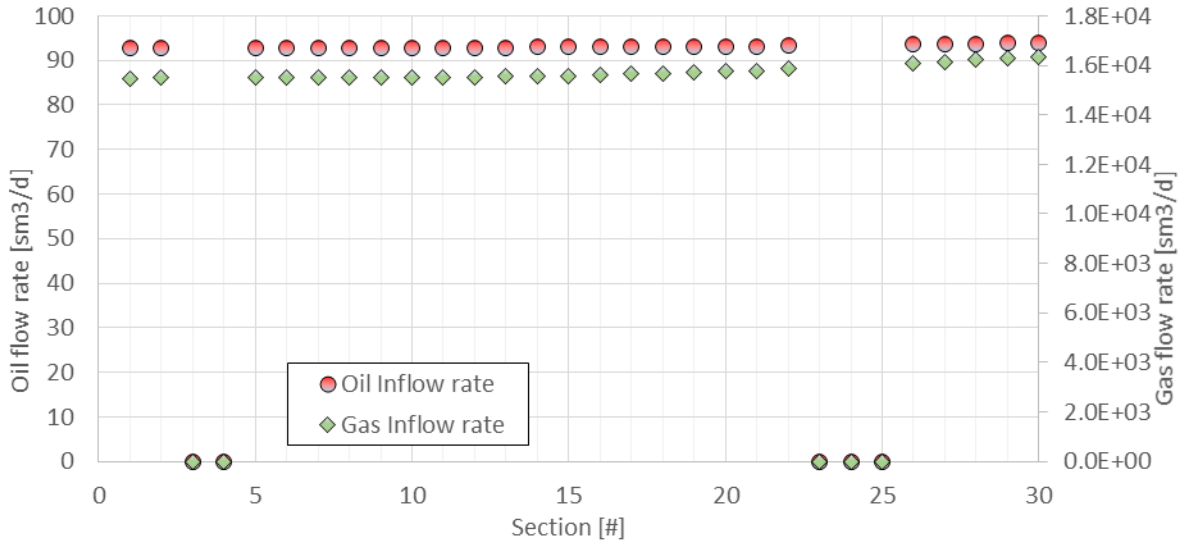

(a) Case 25

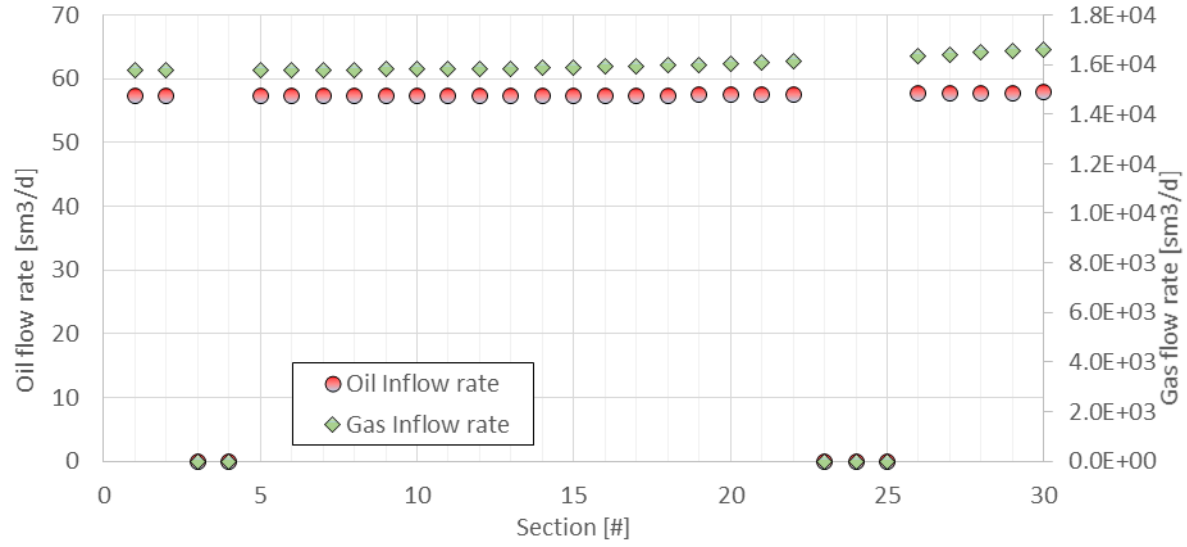

(b) Case 26

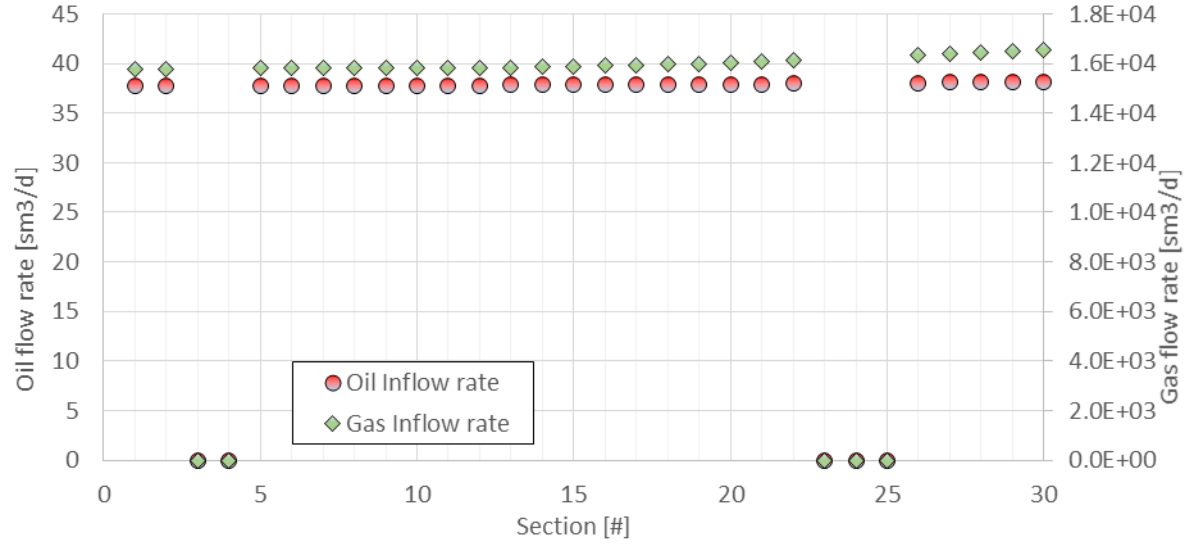

(c) Case 27

Figure 54: Inflow distribution for cases 10-12. Reservoir 3, AICV, GORM 1-3.

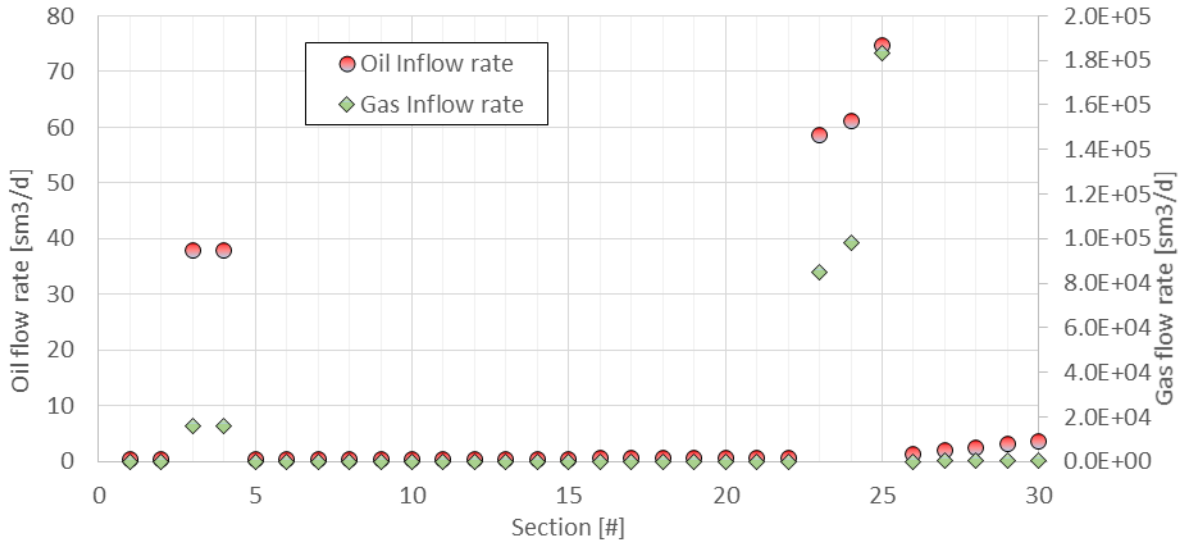

(a) Case 28

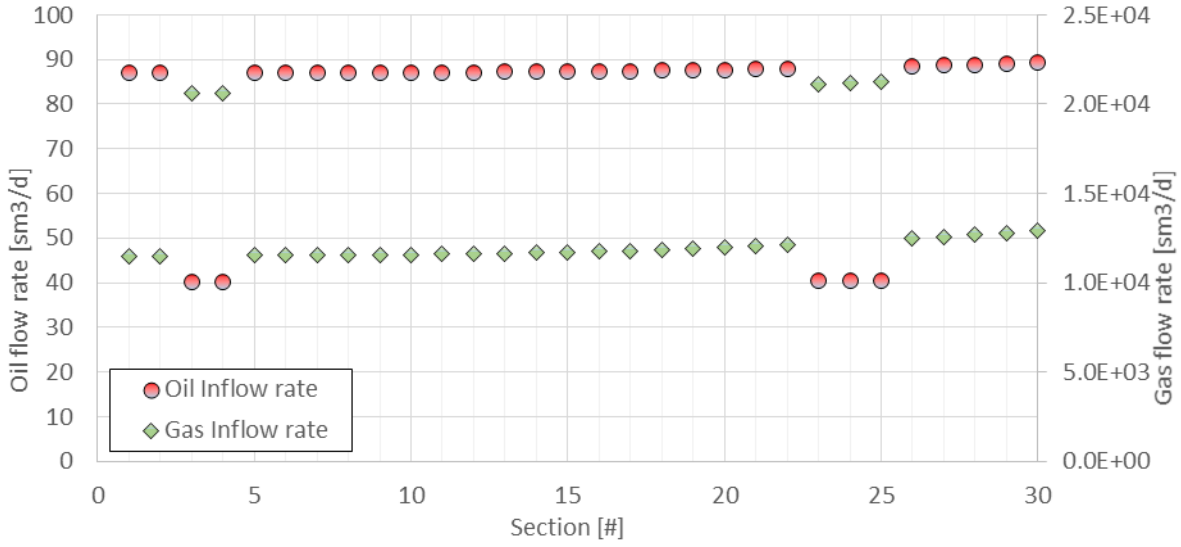

(b) Case 29

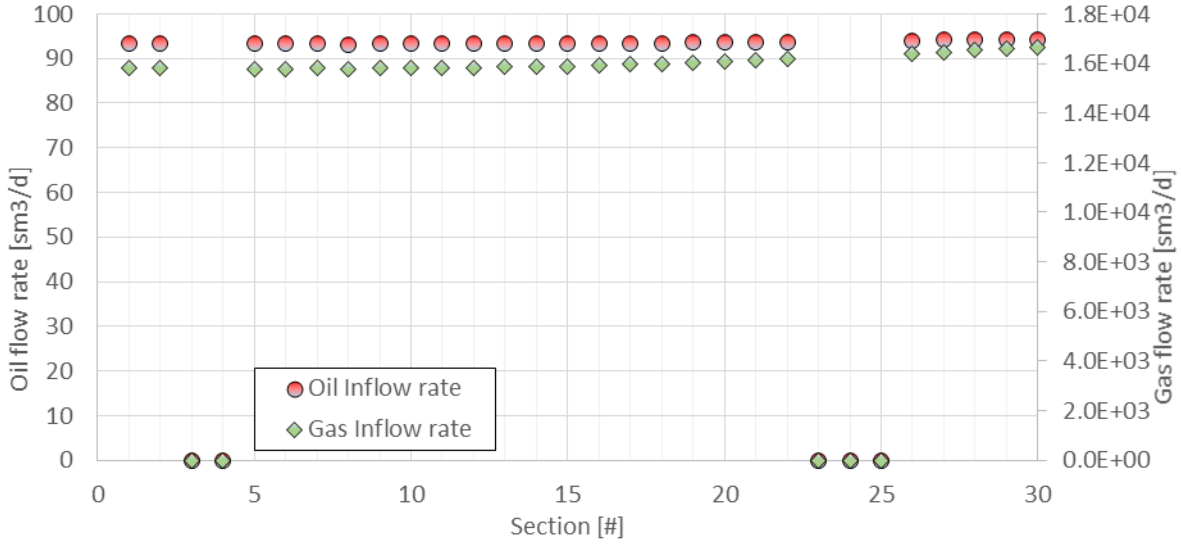

(c) Case 30

Figure 55: Inflow distribution for cases 28-30. Reservoir 3 with varying GORM. Open Hole, AICD and AICV.

E.3: Pressure distribution for all sections

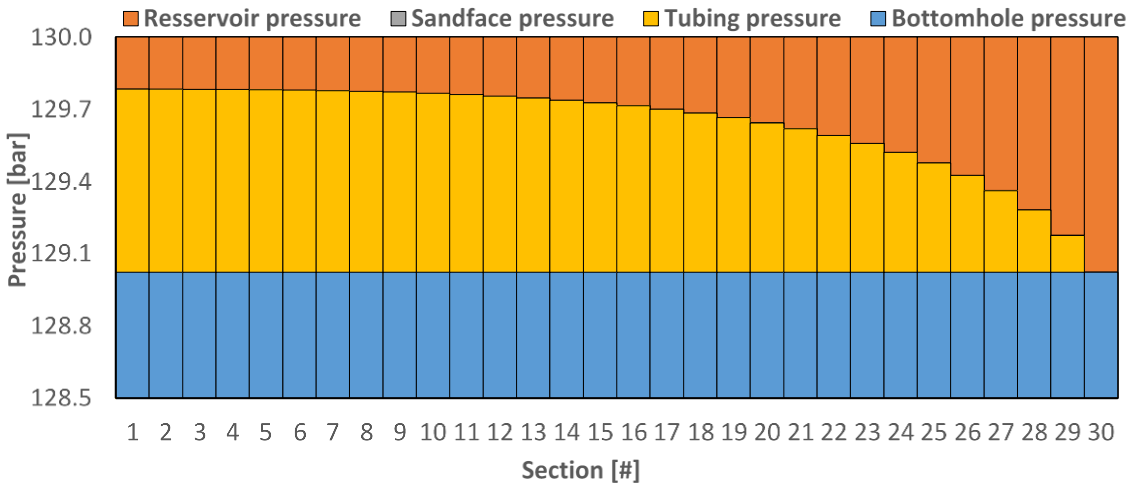

(a) Case 1

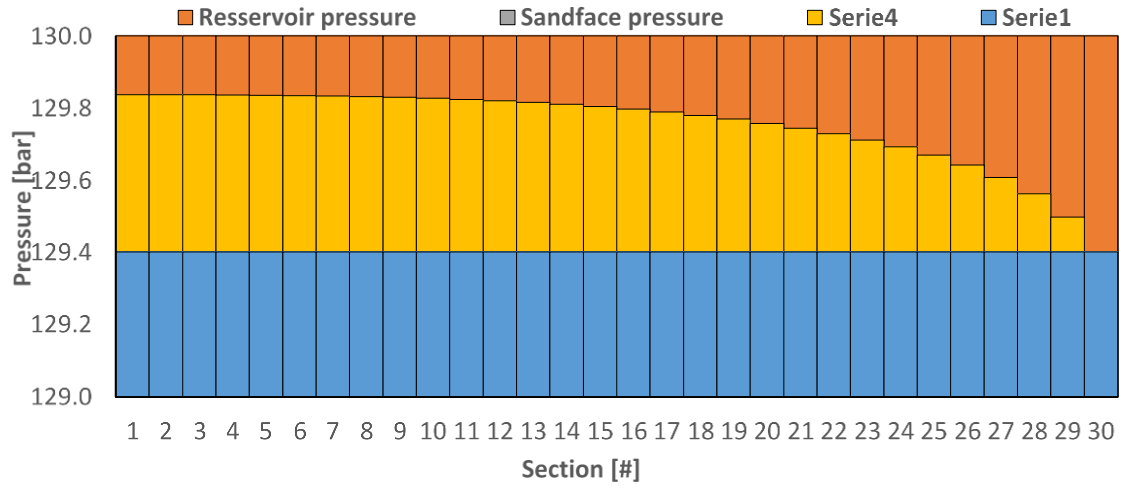

(b) Case 2

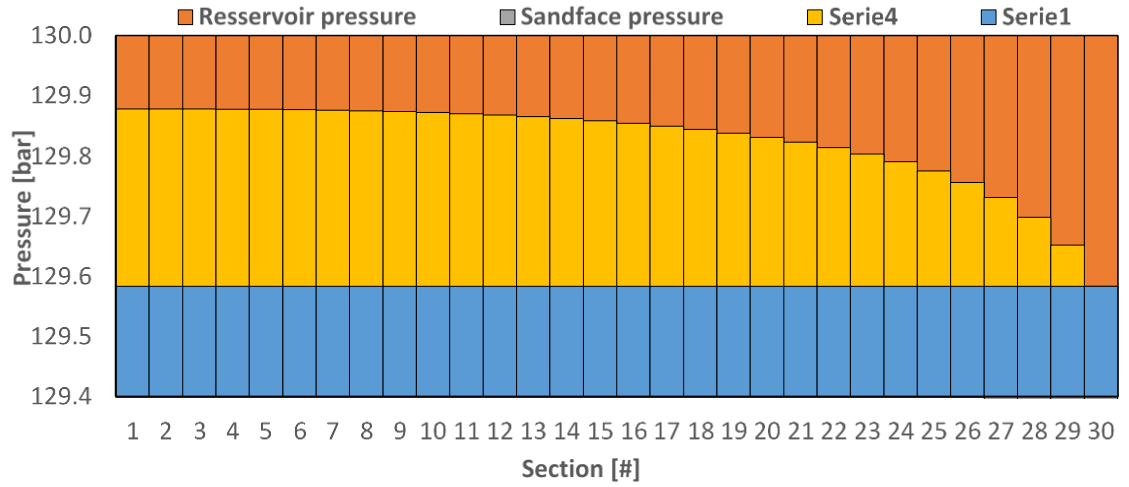

(c) Case 3

Figure 56: Pressure distribution for cases 1-3. Reservoir 1, Open Hole, GORM 1-3.

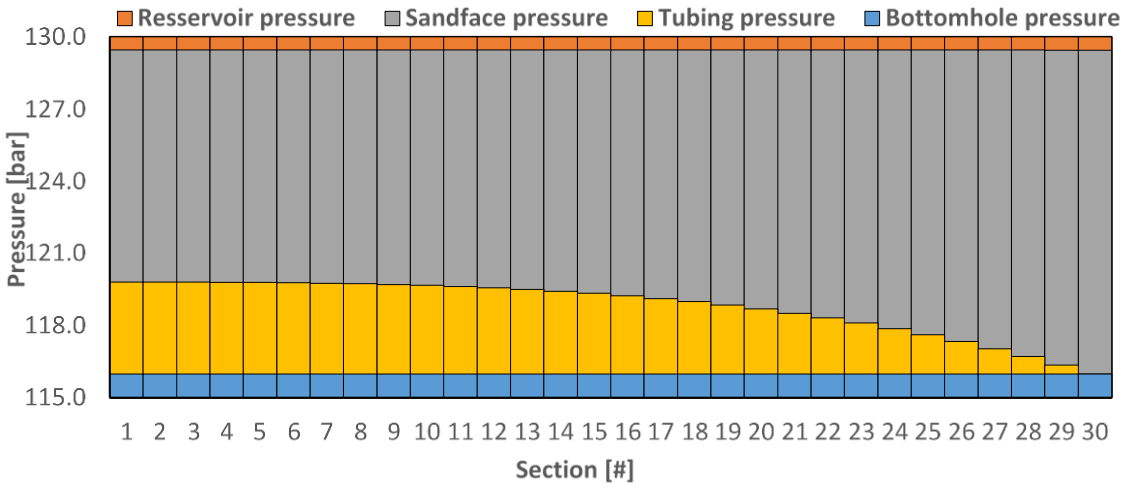

(a) Case 4

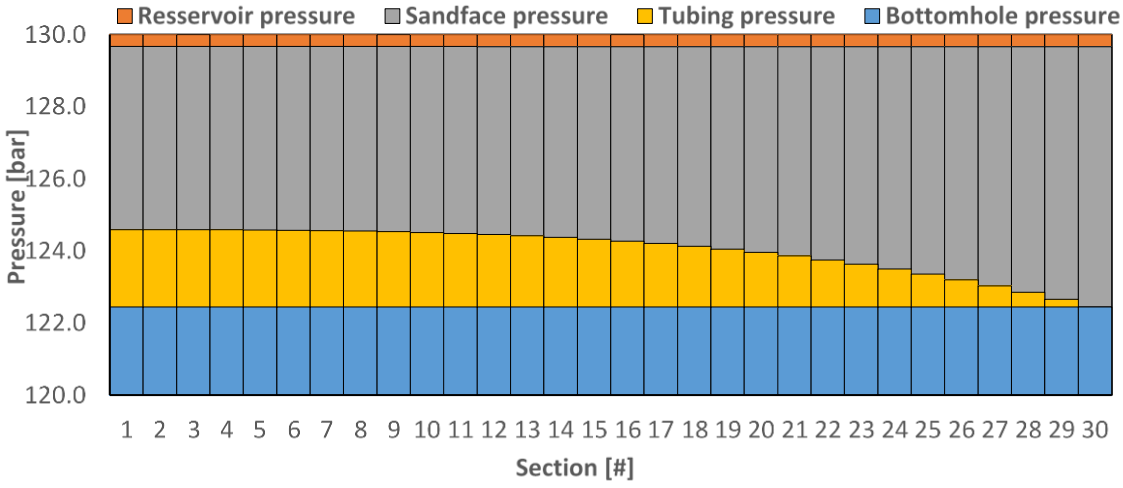

(b) Case 5

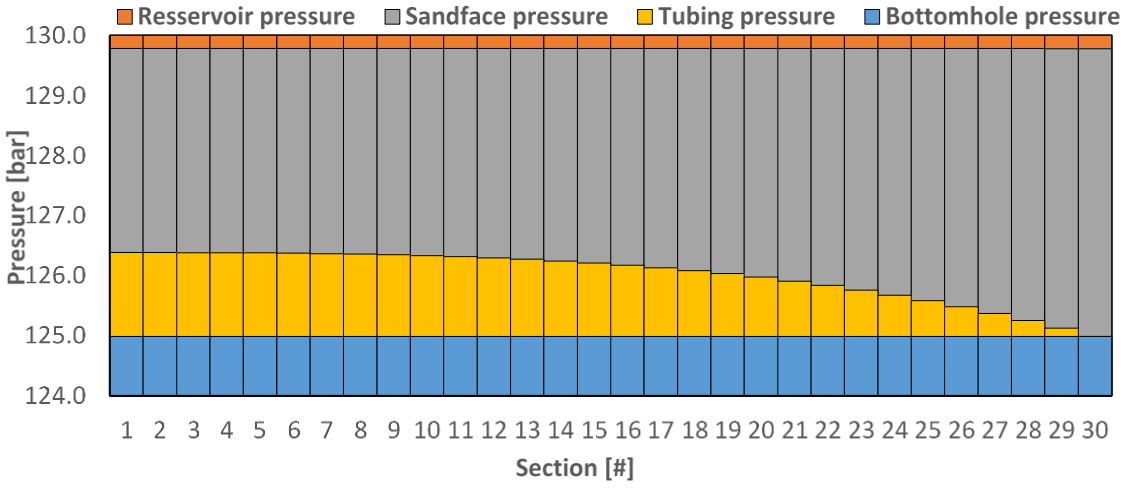

(c) Case 6

Figure 57: Pressure distribution for cases 4-6. Reservoir 1, AICD, GORM 1-3.

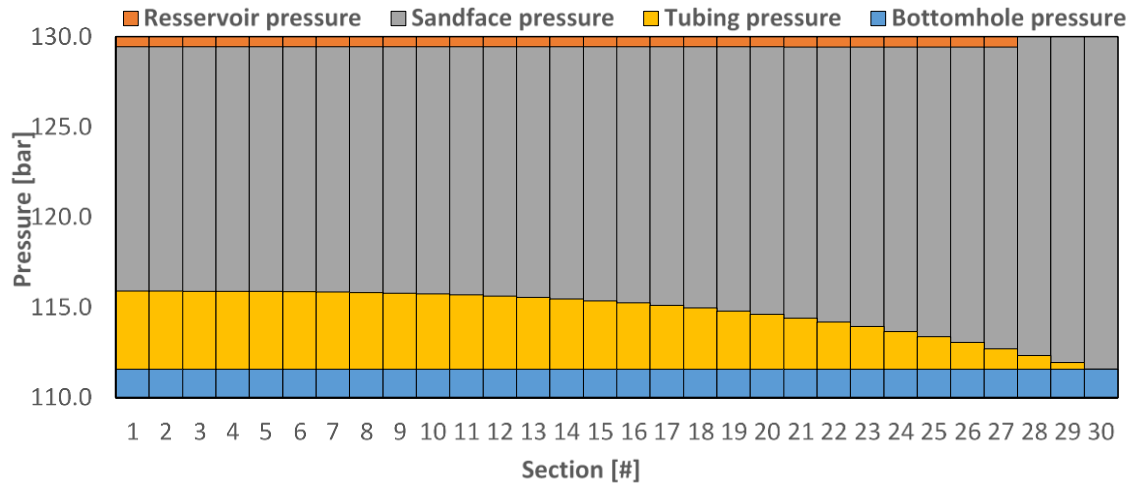

(a) Case 7

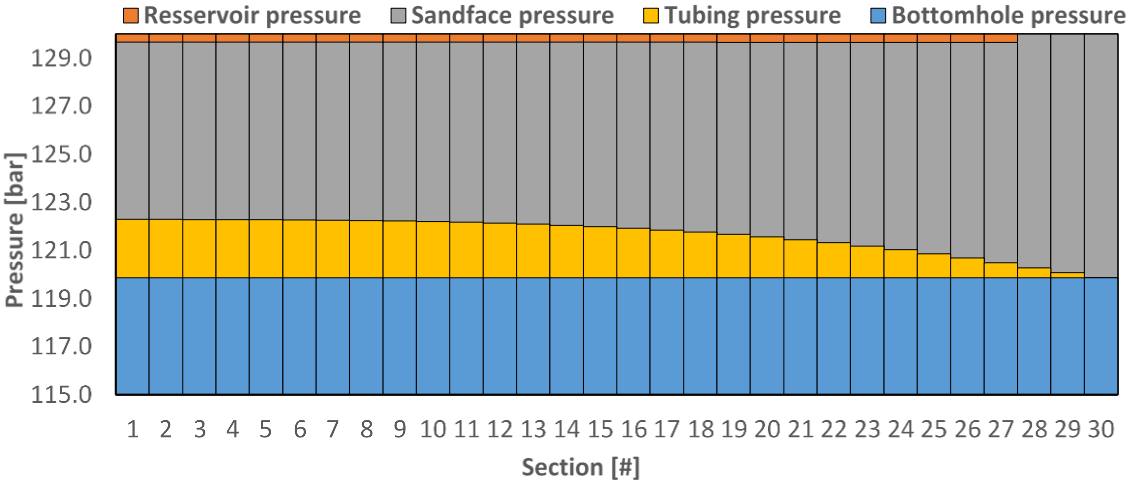

(b) Case 8

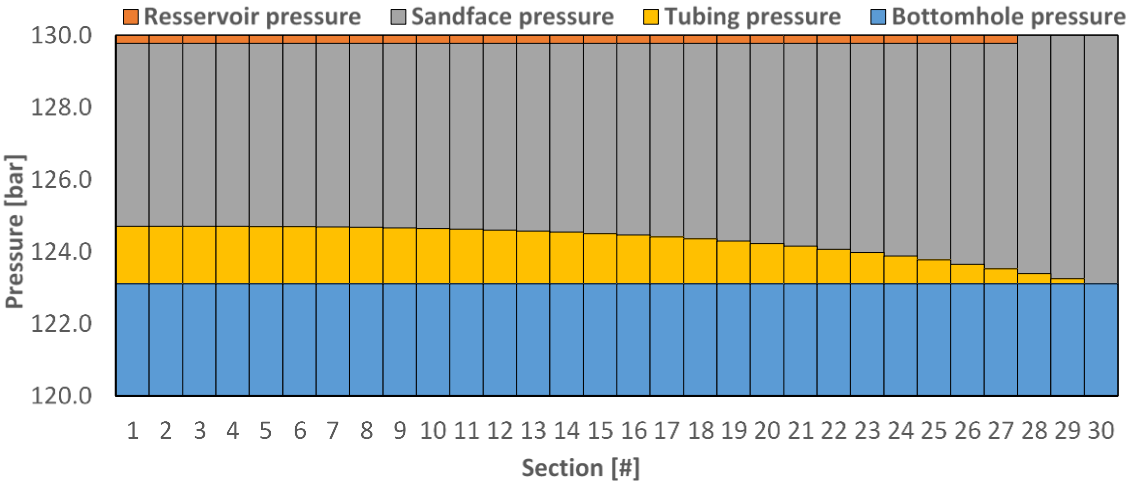

(c) Case 9

Figure 58: Pressure distribution for cases 7-9. Reservoir 1, AICV, GORM 1-3.

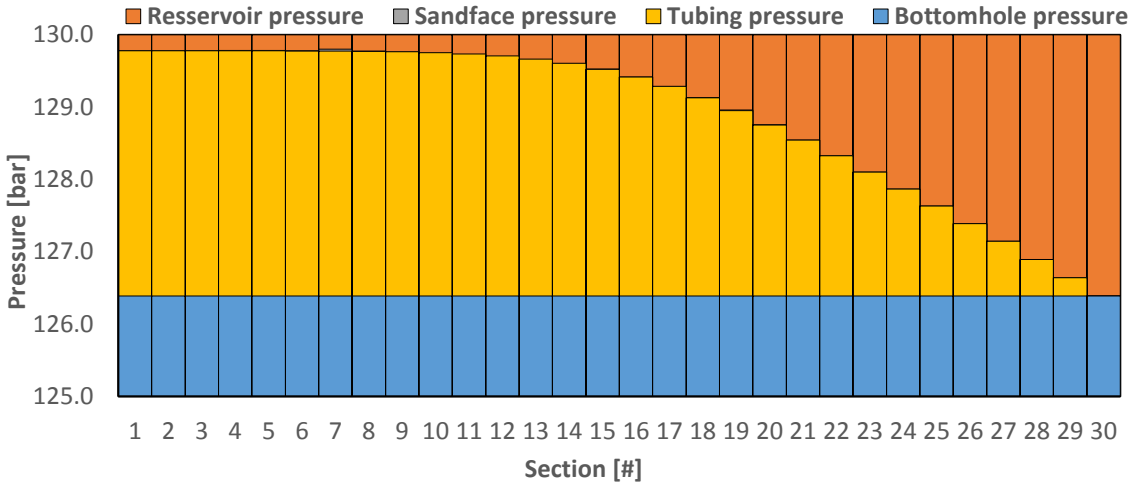

(a) Case 10

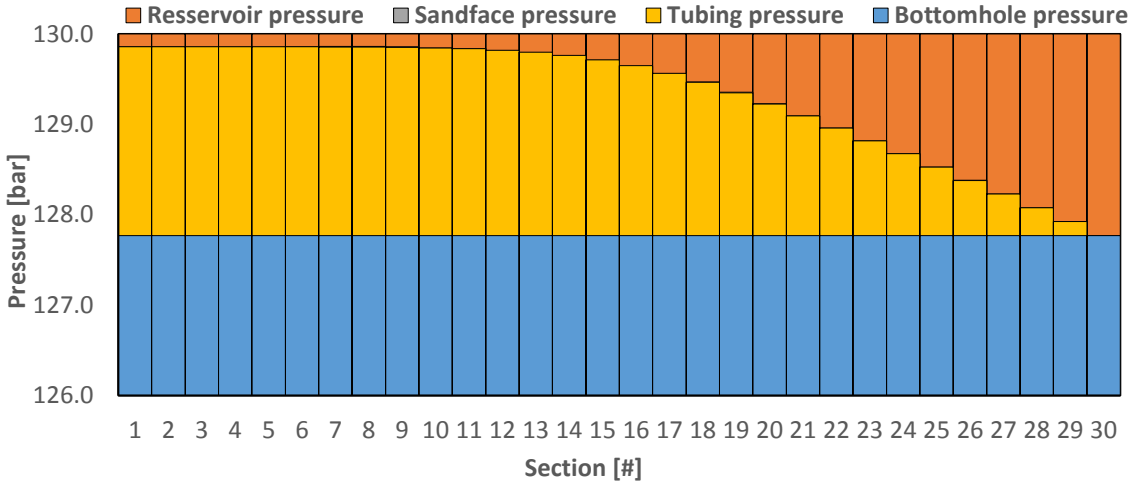

(b) Case 11

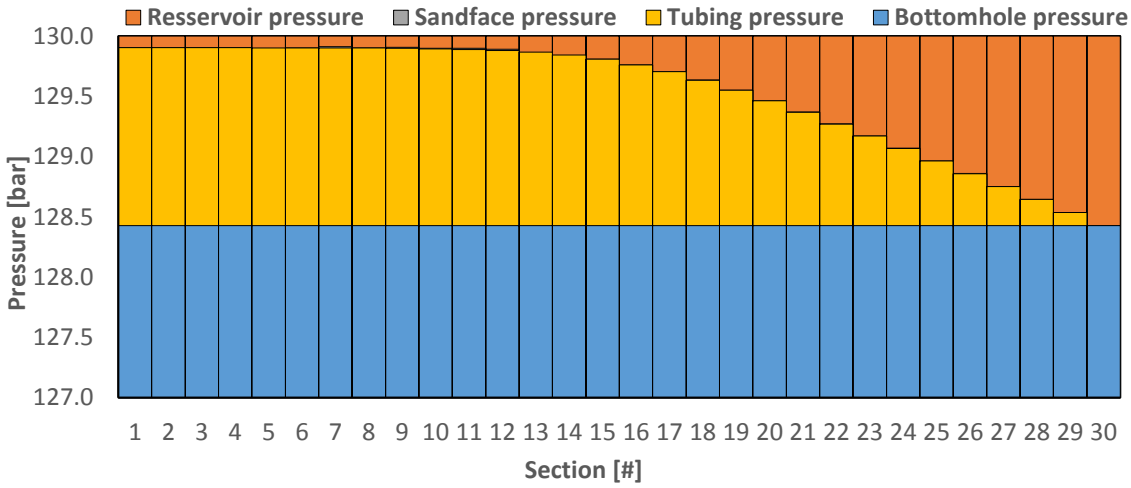

(b) Case 12

Figure 59: Pressure distribution for cases 10-12. Reservoir 2, Open Hole, GORM 1-3.

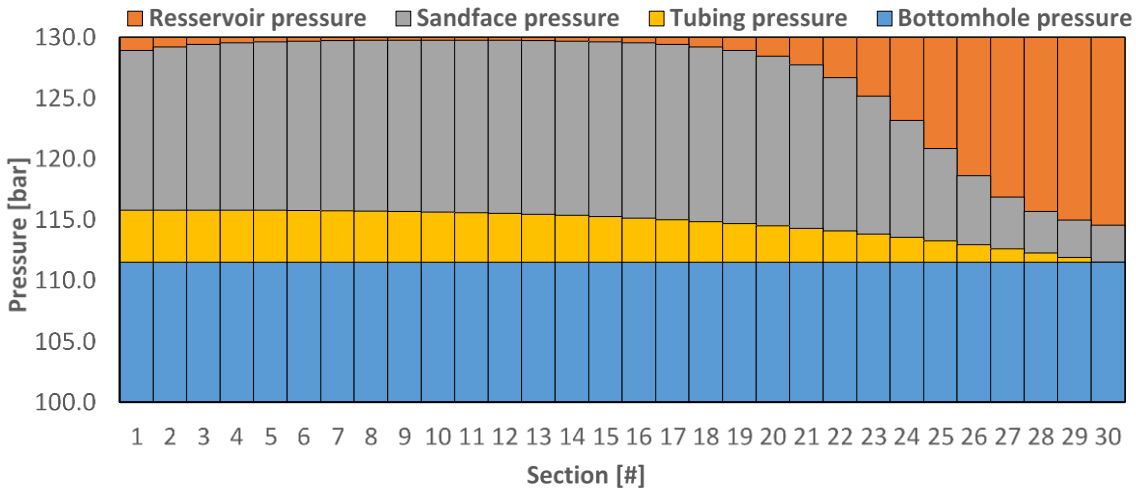

(a) Case 13

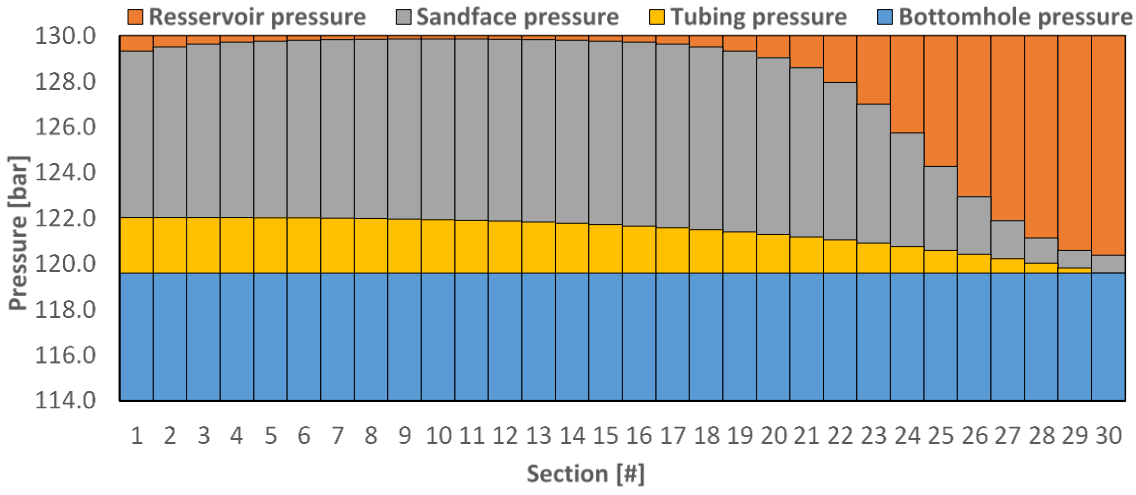

(b) Case 14

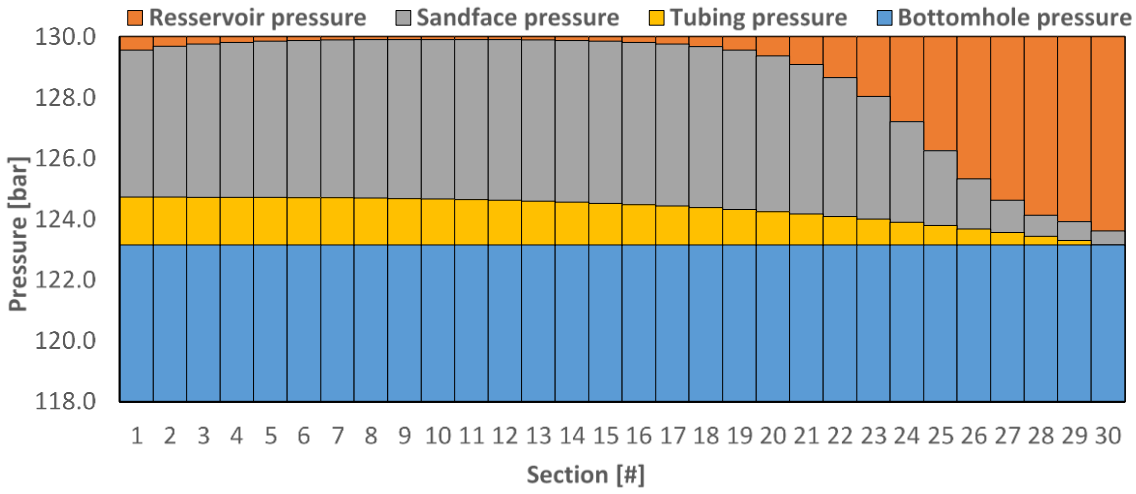

(c) Case 15

Figure 60: Pressure distribution for cases 13-15. Reservoir 2, AICD , GORM 1-3

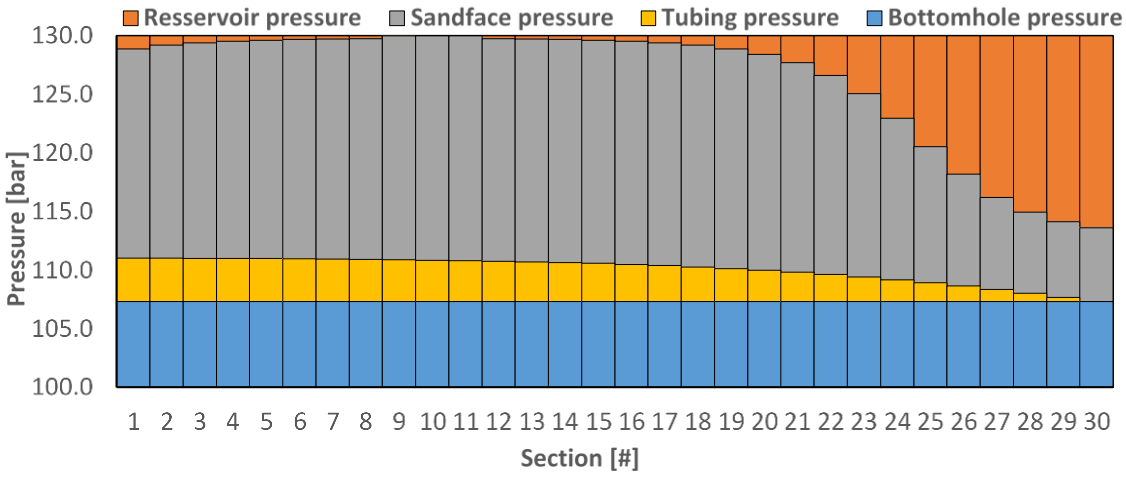

(a) Case 16

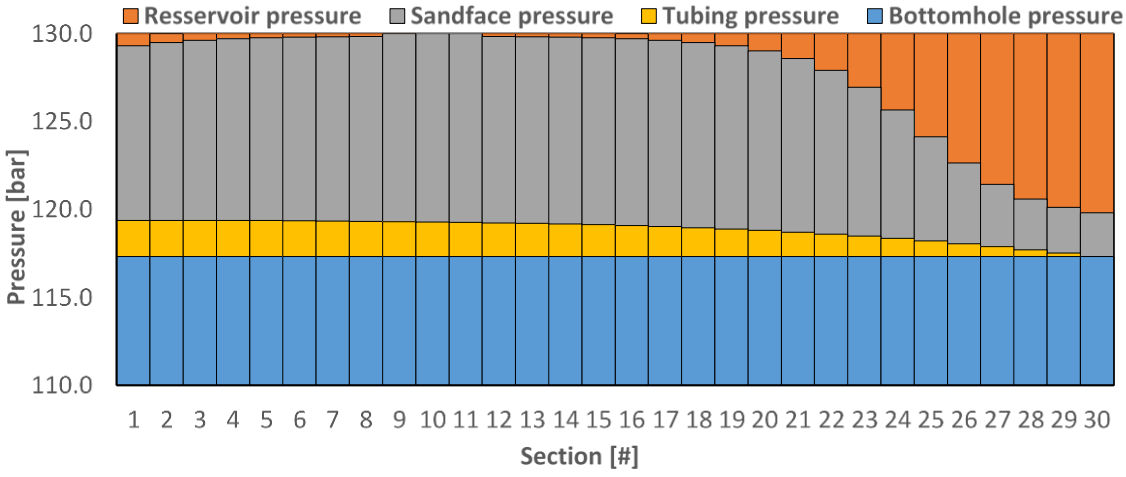

(b) Case 17

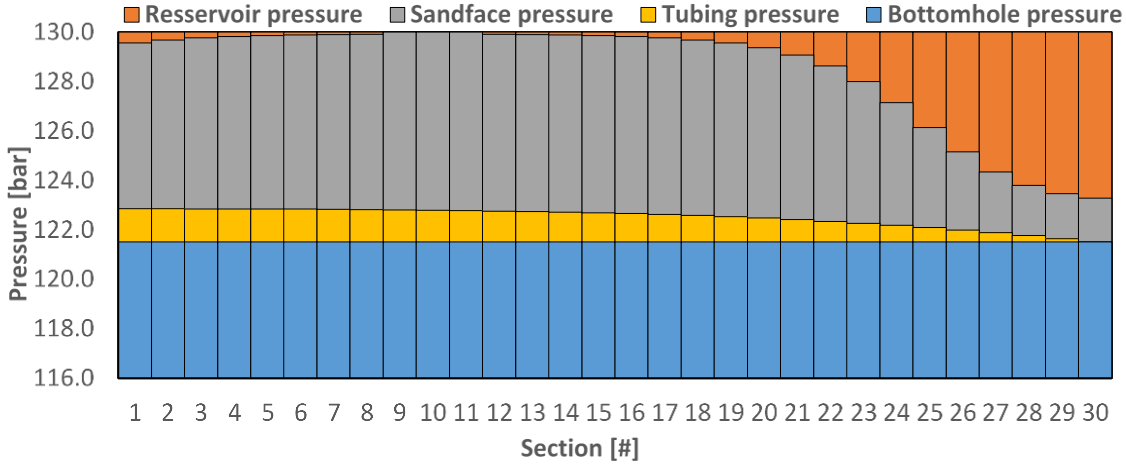

(c) Case 18

Figure 61: Pressure distribution for cases 16-18. Reservoir 2, AICV, GORM 1-3.

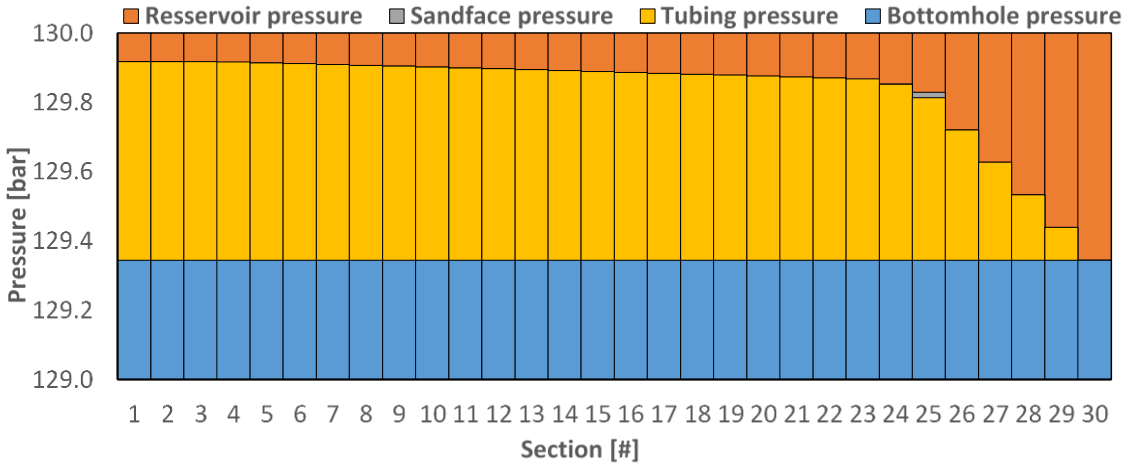

(a) Case 19

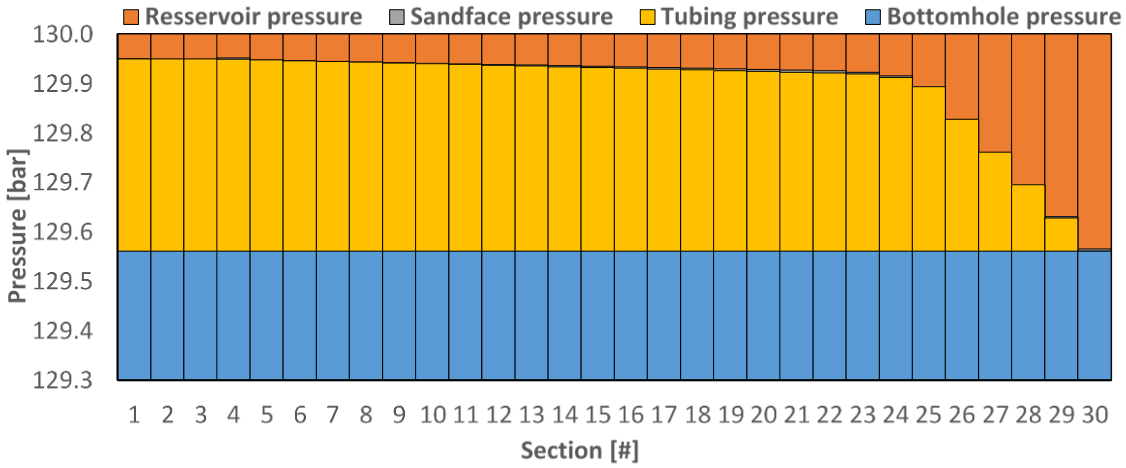

(b) Case 20

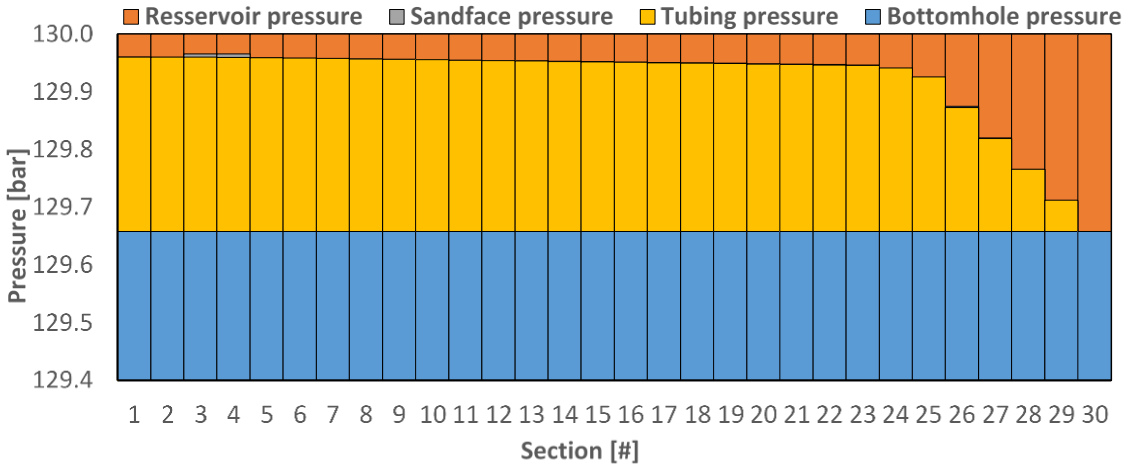

(c) Case 21

Figure 62: Pressure distribution for cases 19-21. Reservoir 3, Open Hole, GORM 1-3.

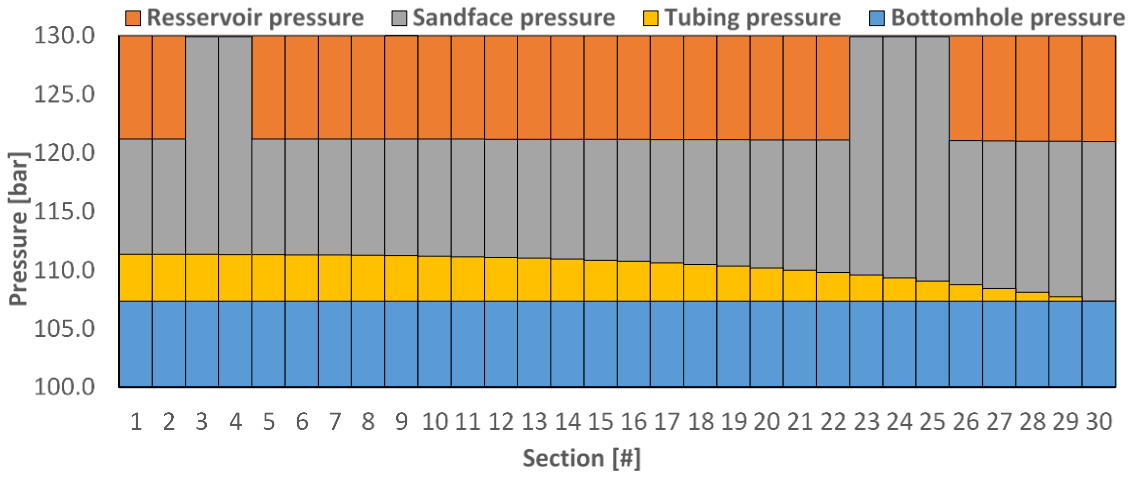

(a) Case 22

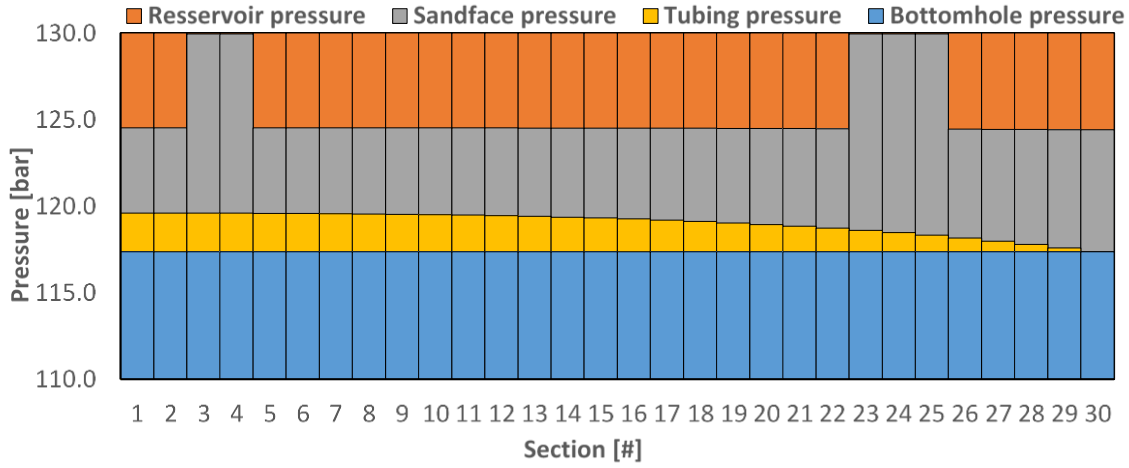

(b) Case 23

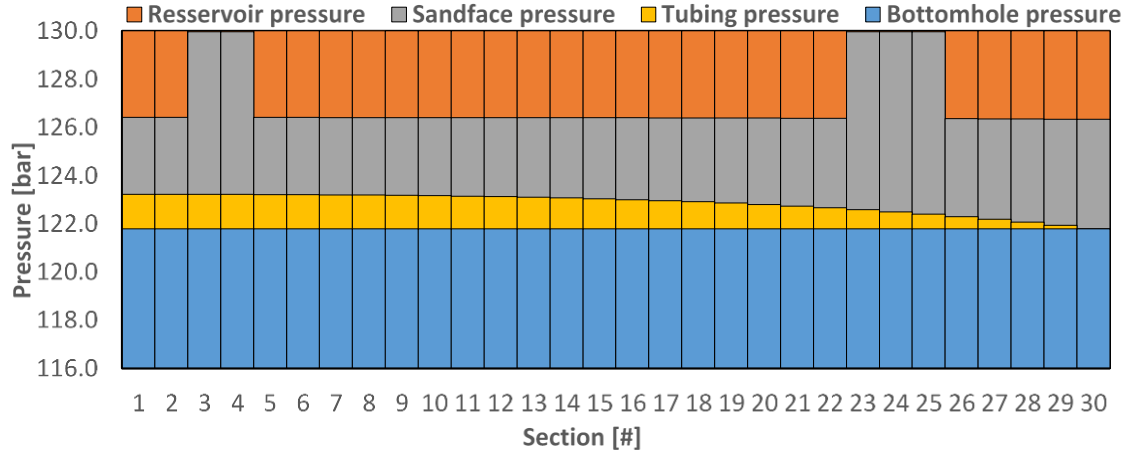

(c) Case 24

Figure 63: Pressure distribution for cases 22-24. Reservoir 3, AICD, GORM 1-3.

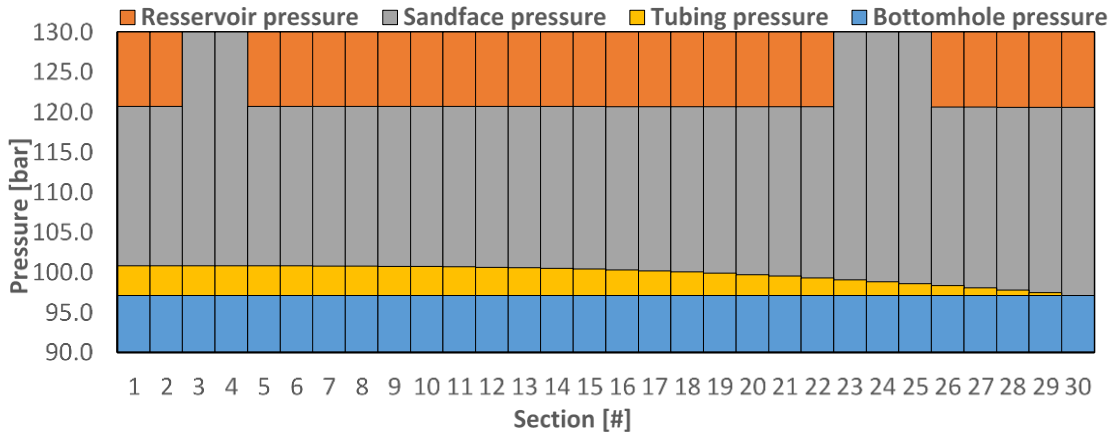

(a) Case 25

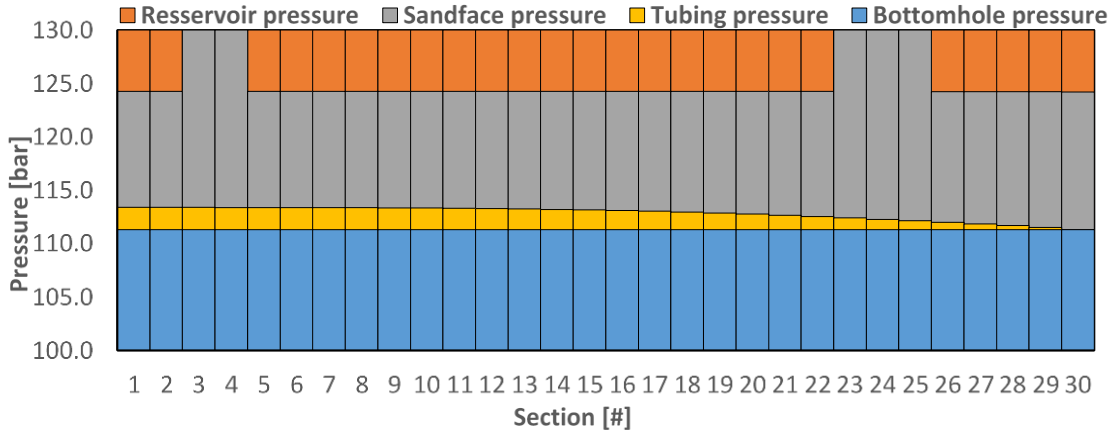

(b) Case 26

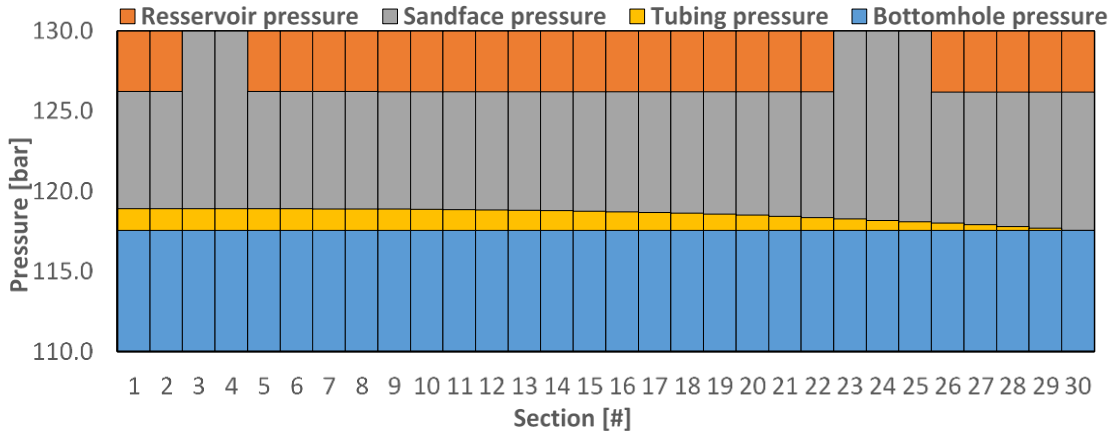

(c) Case 27

Figure 64: Pressure distribution for cases 25-27. Reservoir 3, AICV, GORM 1-3.

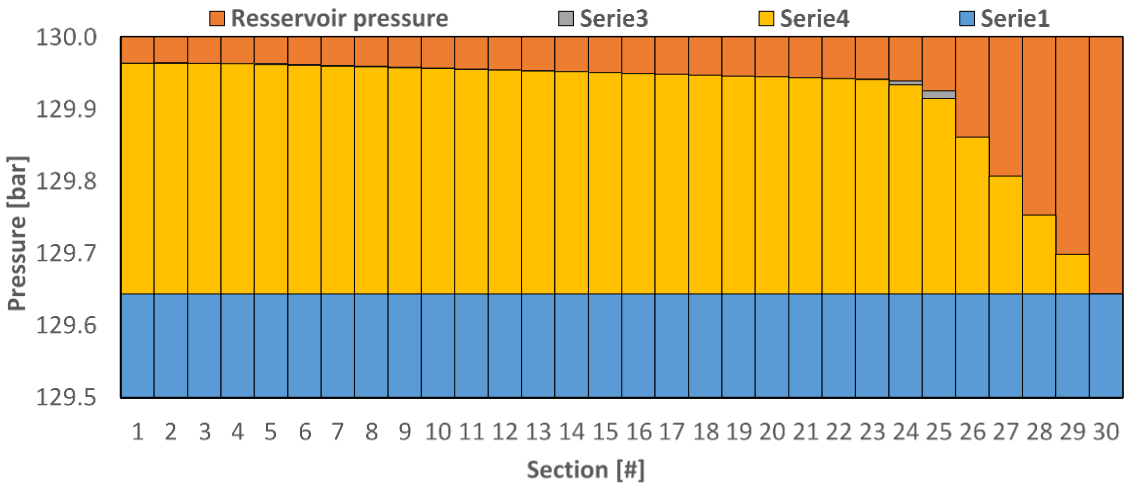

(a) Case 28

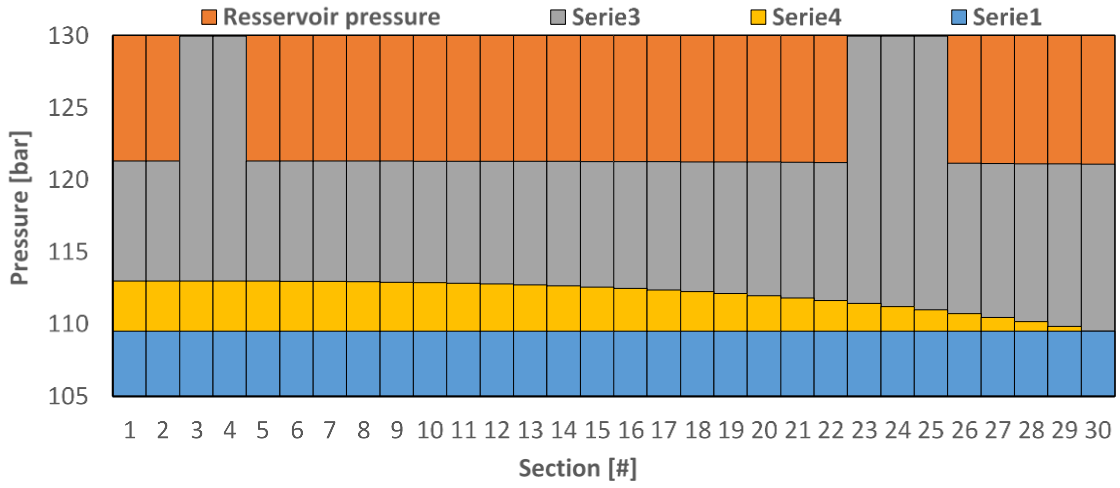

(b) Case 29

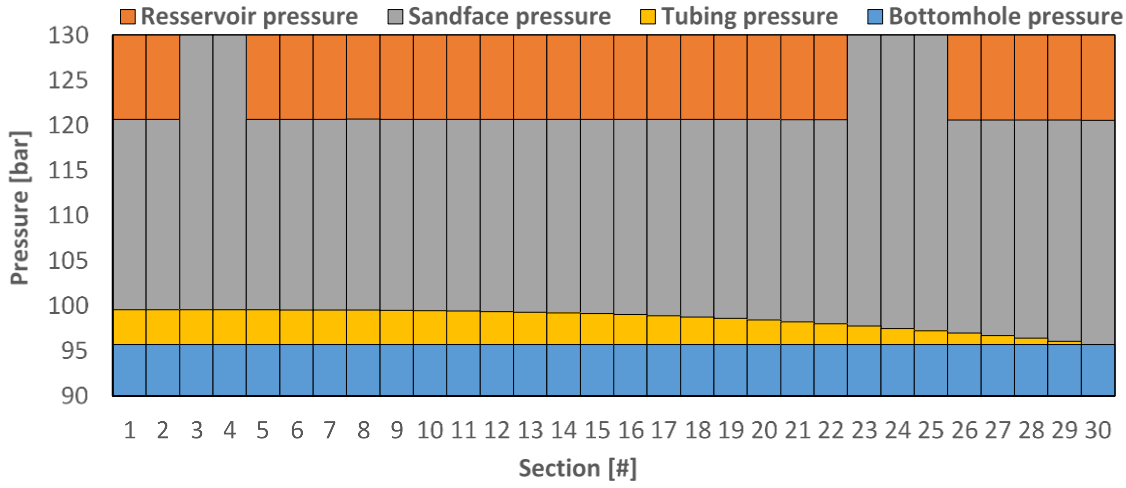

(c) Case 30

Figure 65: Pressure distribution for cases 28-30. Reservoir 3, GORM 1 for low PI sections. GORM 3 for high PI sections. Open Hole, AICD and AICV completion.

Appendix F: VBA-code Overview

This appendix contains all VBA codes used in the attached Excel spreadsheets. The codes can be categorized into:

- Equations
    - Simple macros with algebraic equations.
- Models
    - More complex equations. Might include iterative processes.
- Procedures
    - Macros used in the spreadsheets. Includes writing data to cells in the spreadsheets, running the SOLVER to optimize a model, write tables and write VFP-file for Eclipse.

Repeated or very similar codes are only listed once. Codes are structured in chapters for each of the Excel-files.

F.1: AICD modelling spreadsheets

F.1.1: Multiphase properties

Simpson slip factor

```
Function slip_simpson(rho_liq, rho_gas)
slip_simpson = (rho_liq / rho_gas) ^ (1 / 6)
End Function
```

Chisholm slip factor

```
Function slip_chisholm(rho_liq, rho_gas, x_gas, x_liq)
X = x_liq / x_gas * (rho_gas / rho_liq) ^ (0.5)
slip_chisholm = (rho_liq / rho_gas) ^ (0.25)

    If X > 1 Then
       slip_chisholm = (1 + x_gas * ((rho_liq /
rho_gas) - 1)) ^ (0.5)
    End If
End Function
```

Two phase density

```
Function TP_density(x_gas, x_liq, rho_gas, rho_liq,
slip_factor)

TP_density = (((x_gas / rho_gas) + slip_factor * (x_liq
/ rho_liq)) / (x_gas + slip_factor * x_liq)) ^ (-1)

End Function
```

Homogenous density

```
Function H_density(x_gas, x_liq, rho_gas, rho_liq)
H_density = ((x_gas / rho_gas) + (x_liq / rho_liq)) ^
(-1)
End Function
```

Adiabatic density

```
Function adiabatic_density(rho1, Y, k)
adiabatic_density = ((Y ^ (-1 / k)) / rho1) ^ (-1)
End Function
```

Polytropic density

```
Function polytropic_density(rho_gas1, P1, P2, n)
polytropic_density = ((1 / rho_gas1) * (P1 / P2) ^ (1 /
n)) ^ (-1)
End Function
```

Polytropic exponent

```
Function polytropic_exponent(x_gas, x_liq, Cv_gas,
Cv_liq, k)
polytropic_exponent = (x_gas * k * Cv_gas + x_liq *
Cv_liq) / (x_gas * Cv_gas + x_liq * Cv_liq)
End Function
```

Sutton pseudocritical temperature

```
Function Tpc_sutton_degC(Y)
'Pseudocritical temperature. Sutton Correlation
'Input gas specific gravity

Tpc_sutton_degC = (169.2 + 349.5 * Y - 74 * Y ^ 2 -
491.67) * 5 / 9
'outputs degC unit

End Function
```

Sutton pseudocritical pressure

```
Function Ppc_sutton_bara(Y)
'Pseudocritical pressure. Sutton Correlation
'Input gas specific gravity
Ppc_sutton_bara = (756.8 - 131 * Y - 3.6 * Y ^ 2) *
0.0689475728
'outputs bara unit

End Function
```

Hall-Yarborough Z-factor

```
Function Z_Hall_Yarb(P, T, Ppc, Tpc)
'Hall-Yarborough Z-factor correlation
'Input units degC and bara

Dim Ppr As Double
Dim Tpr As Double
Dim A As Double
Dim b As Double
Dim Y As Double
Dim f_Y As Double
Dim d_F_Y As Double
Dim Z As Double
Dim Z_New As Double
Dim Error As Double

'Calculating pseudoreduced properites
Ppr = P / Ppc
'Temperature needs to be in absolute scale
Tpr = (T + 273.15) / (Tpc + 273.15)

b = 1 / Tpr
A = 0.06125 * b * Exp(-1.2 * (1 - b) ^ 2)

'Setting up for iteration
Error = 1
Z = 0
Y = 0.001

'Iterating to find Z
Do While Error > 0.0001

f_Y = -A * Ppr + (Y + Y ^ 2 + Y ^ 3 - Y ^ 4) / ((1 - Y)
^ 3) - (14.76 * b - 9.76 * b ^ 2 + 4.58 * b ^ 3) * Y ^
2 + (90.7 * b - 242.2 * b ^ 2 + 42.4 * b ^ 3) * Y ^
(2.18 + 2.82 * b)
d_F_Y = (1 + 4 * Y + 4 * Y ^ 2 - 4 * Y ^ 3 + Y ^ 4) /
((1 - Y) ^ 4) - (29.52 * b - 19.52 * b ^ 2 + 9.16 * b ^
3) * Y + (2.18 + 2.82 * b) * (90.7 * b - 242.2 * b ^ 2
+ 42.4 * b ^ 3) * Y ^ (1.18 + 2.82 * b)
Y = Y - f_Y / d_F_Y
Z_New = A * Ppr / Y

Error = Abs(Z - Z_New)
Z = Z_New

Loop

Z_Hall_Yarb = Z

End Function
```

F.1.2: Multiphase models

Simpson Two-phase multiplier

```
Function phi_2phase_simpson(x_gas, slip_factor)

phi_2phase_simpson = (1 + x_gas * (slip_factor - 1)) *
(1 + x_gas * ((slip_factor ^ 5) - 1))

End Function
```

Chisholm Two-phase multiplier

```
Function phi_2phase_chisholm(x_gas, x_liq, rho_gas,
rho_liq, slip_factor)

b = ((1 / slip_factor) * (rho_liq / rho_gas) +
slip_factor - 2) / ((rho_liq / rho_gas) - 1)

phi_2phase_chisholm = 1 + ((rho_liq / rho_gas) - 1) *
(b * x_gas * x_liq + x_gas ^ 2)

End Function
```

Bernoulli model for deltaP

```
Function Berboulli_DP_model(Cd, A1, A2, P1, phi_TP,
rho_mix, m)

Berboulli_DP_model = P1 - phi_TP / (2 * rho_mix) * (m /
(Cd * A2)) ^ 2 * (1 - (Cd * A2 / A1) ^ 2)

End Function
```

Bernoulli model for Mass rate

```
Function Berboulli_massrate_model(Cd, A1, A2, P1, P2,
phi_TP, rho_mix)

Berboulli_massrate_model = Cd * A2 * (((2 * rho_mix *
(P1 - P2)) / phi_TP) / (1 - (Cd * A2 / A1) ^ 2)) ^
(0.5)

End Function
```

Sachdeva model critical flow rate

```
Function sachdeva_critical_flow_ratio(k_adi, n_poly,
rho_gas1, rho_gas2, rho_liq, x_gas, x_liq, y_iteration)


A = k_adi / (k_adi + 1)
b = k_adi / (k_adi - 1)
B1 = (k_adi - 1) / k_adi
c = x_liq * (1 - y_iteration) * rho_gas1 / (x_gas *
rho_liq)
d = n_poly / 2
e = n_poly * x_liq * rho_gas2 / (x_gas * rho_liq)
f = x_liq * rho_gas2 / (x_gas * rho_liq)


Y = ((A + c) / (B1 + d + e + d * f ^ 2)) ^ b

sachdeva_critical_flow_ratio = Y

End Function
```

Sachdeva model for mass rate

```
Function sachdeva_model(A2, Cd, P1, x_liq, x_gas, Y, k,
rho_gas1, rho_gas2, rho_liq, rho_mix2)
'Sachdeva model for massrate

sachdeva_model = A2 * Cd * (2 * P1 * rho_mix2 *
rho_mix2 * ((x_liq * (1 - Y)) / (rho_liq) + ((k *
x_gas) / (k - 1)) * ((1 / rho_gas1) - (Y / rho_gas2))))
^ (0.5)

End Function
```

Statoil Model

```
Function Statoil_ICD(rho_cal, my_cal, rho_mix, my_mix,
a_icd, X, Y, q_oil, q_gas, q_water)

q_tot = q_oil + q_gas + q_water
```

Sachdeva model for deltaP

```
Function Sachdeva_DP_model(A2, A, b, Cd, P1, m, k,
q_gas, q_oil, q_water, rho_gas1, rho_oil, rho_water,
my_gas, my_oil, my_water)
'Sachdeva model for DeltaP. Iterative process included

m_gas = q_gas * rho_gas1
m_oil = q_oil * rho_oil
m_water = q_water * rho_water
m_tot = m_gas + m_oil + m_water

x_gas = m_gas / m_tot
x_oil = m_oil / m_tot
x_water = m_water / m_tot
x_liq = x_water + x_oil

rho_liq = rho_oil
If q_water > 0 Then
rho_liq = (q_oil * rho_oil + q_water * rho_water) /
(q_oil + q_water)
End If

rho_mix1 = ((x_gas / rho_gas1) + (x_liq / rho_liq)) ^
(-1)
my_mix = (q_gas * my_gas + q_oil * my_oil + q_water *
my_water) / (q_gas + q_oil + q_water)


P2 = P1 * 0.99
d_P2 = 1000
error_P2 = 1

Do While error_P2 > 0.001

Y = P2 / P1
DP = P1 - P2
rho_gas2 = ((Y ^ (-1 / k)) / rho_gas1) ^ (-1)
rho_mix2 = ((x_gas / rho_gas2) + (x_liq / rho_liq)) ^
(-1)

f_DP = (A2 * Cd) ^ 2 * (2 * P1 * rho_mix2 * rho_mix2 *
((x_liq * (1 - Y)) / (rho_liq) + ((k * x_gas) / (k -
1)) * ((1 / rho_gas1) - (Y / rho_gas2)))) - m ^ 2

'########

P2_dummy = P2 + d_P2

Y = P2_dummy / P1
rho_gas2 = ((Y ^ (-1 / k)) / rho_gas1) ^ (-1)
rho_mix2 = ((x_gas / rho_gas2) + (x_liq / rho_liq)) ^
(-1)
df_DP = (A2 * Cd) ^ 2 * (2 * P1 * rho_mix2 * rho_mix2 *
((x_liq * (1 - Y)) / (rho_liq) + ((k * x_gas) / (k -
1)) * ((1 / rho_gas1) - (Y / rho_gas2)))) - m ^ 2

'########

If (df_DP - f_DP) = 0 Then
Exit Do
End If

P2_new = P2 - d_P2 * f_DP / (df_DP - f_DP)
```

```
Statoil_ICD = ((rho_mix ^ 2) / rho_cal) * (my_cal /
my_mix) ^ Y * a_icd * q_tot ^ X

End Function
```

Asheims model

```
Function Asheim_model(Cd, A2, rho_liq, x_gas, x_liq,
P1, P2, Z, R, T, m)

A = Cd * A2 * rho_liq * P2
b = x_gas * rho_liq * Z * R * T / m + x_liq * P2
c = 2 * (x_gas * Z * R * T / m * Log(P1 / P2) + x_liq /
rho_liq * (P1 - P2))

Asheim_model = A / b * c ^ (0.5)

End Function
```

```
If P2_new < 0 Then
Exit Do
End If

error_P2 = Abs((P2_new - P2) / P2)
P2 = P2_new

Loop

Sachdeva_DP_model = P2

End Function
```

F.1.3: Spreadsheet procedures

Macros for optimizing models

```
Sub bernoulli_H_solve()
        SolverReset
        SolverOK
SetCell:=Worksheets("1.Input_Sheet").Range("I20"),
MaxMinVal:=2,
ByChange:=Worksheets("1.Input_Sheet").Range("E36")
        SolverSolve UserFinish:=False
End Sub
Sub bernoulli_Simpson_solve()
        SolverReset
        SolverOK
SetCell:=Worksheets("1.Input_Sheet").Range("l20"),
MaxMinVal:=2,
ByChange:=Worksheets("1.Input_Sheet").Range("E39")
        SolverSolve UserFinish:=False
End Sub
Sub bernoulli_Chisholm_solve()
        SolverReset
        SolverOK
SetCell:=Worksheets("1.Input_Sheet").Range("o20"),
MaxMinVal:=2,
ByChange:=Worksheets("1.Input_Sheet").Range("E42")
        SolverSolve UserFinish:=False
End Sub
Sub sachdeva_solve()
        SolverReset
        SolverOK
SetCell:=Worksheets("1.Input_Sheet").Range("L6"),
MaxMinVal:=2,
ByChange:=Worksheets("1.Input_Sheet").Range("b48")
        SolverSolve UserFinish:=False
End Sub

Sub statoil_solve()
        SolverReset
        SolverOK
SetCell:=Worksheets("1.Input_Sheet").Range("i6"),
MaxMinVal:=2,
ByChange:=Worksheets("1.Input_Sheet").Range("B34:B44")
        SolverAdd cellRef:=Range("B34:B44"),
relation:=3, formulaText:="0.0001"
        SolverSolve UserFinish:=False
End Sub


Sub asheim_solve()
        SolverReset
        SolverOK SetCell:=Worksheets("Input
sheet").Range("e49"), MaxMinVal:=2,
ByChange:=Worksheets("Input sheet").Range("e48")
        SolverSolve UserFinish:=False
End Sub
```

Expand data from input sheet to model sheets

```
Sub Expand_data()
'USED TO SEND INPUT TEST DATA TO MODELS

'Check if number of sections is okay
    If Worksheets("1.Input_Sheet").Range("E4") < 3 Then
        MsgBox "3 points or more required. Macro will
now exit"
    Exit Sub
    End If
'Clear from dataset 3 and on

endrange = Worksheets("1.Input_Sheet").Range("E4") + 4

Worksheets("3.Data_handling").Range("A6:cc9999").Clear
Worksheets("4.1.Statoil_model_default").Range("A6:cc999
9").Clear
Worksheets("4.2.Bernoulli_model").Range("A6:cc9999").Cl
ear
Worksheets("4.3.Sachdeva_model").Range("A6:cc9999").Cle
ar
Worksheets("4.4_Asheim_model").Range("A6:cc9999").Clear

'Expand sections
Set SourceRange =
Worksheets("4.1.Statoil_model_default").Range("a5:cc5")
Set fillRange =
Worksheets("4.1.Statoil_model_default").Range("A5:cc" &
endrange)
SourceRange.AutoFill Destination:=fillRange

Set SourceRange =
Worksheets("3.Data_handling").Range("a5:cc5")
Set fillRange =
Worksheets("3.Data_handling").Range("A5:cc" & endrange)
SourceRange.AutoFill Destination:=fillRange

Set SourceRange =
Worksheets("4.2.Bernoulli_model").Range("a5:cc5")
Set fillRange =
Worksheets("4.2.Bernoulli_model").Range("A5:cc" &
endrange)
SourceRange.AutoFill Destination:=fillRange

Set SourceRange =
Worksheets("4.3.Sachdeva_model").Range("a5:cc5")
Set fillRange =
Worksheets("4.3.Sachdeva_model").Range("A5:cc" &
endrange)
SourceRange.AutoFill Destination:=fillRange

Set SourceRange =
Worksheets("4.4_Asheim_model").Range("a5:cc5")
Set fillRange =
Worksheets("4.4_Asheim_model").Range("A5:cc" &
endrange)
SourceRange.AutoFill Destination:=fillRange

End Sub
```

F.2: VFP-table generation spreadsheet

Local gas rate – Black Oil Model

```
Function qg_loc(qg, qo, Bg, Rs_GOR, rs_OGR)
qg_loc = qg * (Bg / (1 - Rs_GOR * rs_OGR)) - qo * Bg *
Rs_GOR / (1 - Rs_GOR * rs_OGR)
End Function
```

Local gas density– Black Oil Model

```
Function rho_g_loc(Bg, rs_OGR, rho_g, rho_o)
rho_g_loc = rho_g / Bg + rgo_o * rs_OGR / Bg
End Function
```

Local oil rate – Black Oil Model

```
Function qo_loc(BO, rs_OGR, Rs_GOR, qo, qg)
qo_loc = qg * (-BO * rs_OGR / (1 - Rs_GOR * rs_OGR)) +
qo * BO / (1 - Rs_GOR * rs_OGR)
End Function
```

Local oil density – Black Oil Model

```
Function rho_o_loc(Rs_GOR, BO, rgo_g, rho_o)
rho_o_loc = rho_g * Rs_GOR / BO + rho_o / BO
End Function
```

Interpolating Black Oil Table to find 'Bo' – Part 1/4

```
Function Bo_int_table(GOR, P, Matrix As Range, Matrix2
As Range)

'Identify if producing GOR is above or below
bubblepoint
'=====================================================
=

mm = Matrix2.Rows.Count
NN = Matrix2.Columns.Count

'Finding lower value of GOR/Rs
lower_GOR = Matrix2(1, 1)
For i = 1 To mm
    If Matrix2(i, 1) = GOR Then
        lower_GOR = GOR
        Exit For
    End If
    If Matrix2(i, 1) < GOR Then
        If Matrix2(i, 1) > lower_GOR Then
            lower_GOR = Matrix2(i, 1)
        End If
    End If
Next

'Finding upper value of GOR/Rs
upper_GOR = Matrix2(mm, 1)
For i = 1 To mm
    If Matrix2(i, 1) = GOR Then
        upper_GOR = GOR
        Exit For
    End If
    If Matrix2(i, 1) > GOR Then
        If Matrix2(i, 1) < upper_GOR Then
            upper_GOR = Matrix2(i, 1)
        End If
    End If
Next

'Finding upper and lower pressures
For i = 1 To mm
    If Matrix2(i, 1) = lower_GOR Then
        P1 = Matrix(i, 2)
    End If
    If Matrix2(i, 1) = upper_GOR Then
        P2 = Matrix(i, 2)
    End If
Next

'Interpolating Bobblepoint pressure
If P1 = P2 Then
p_bubble = P1
Else
p_bubble = P1 + (P2 - P1) / (upper_GOR - lower_GOR) *
(GOR - lower_GOR)
End If
```

Interpolating Black Oil Table to find 'Bo' – Part 2/4

```
If P <= p_bubble Then
            'Finding Bo if pressure is below
bubblepoint

'=========================================

            'Finding upper  pressure and bo
            lower_p = Matrix2(1, 2)
            lower_bo = Matrix2(1, 3)
            For i = 1 To mm
                If Matrix2(i, 2) = P Then
                    lower_p = P
                    lower_bo = Matrix2(i, 3)
                    Exit For
                End If
                If Matrix2(i, 2) < P Then
                    If Matrix2(i, 2) > lower_p Then
                        lower_p = Matrix2(i, 2)
                    lower_bo = Matrix2(i, 3)
                    End If
                End If
            Next

            'Finding upper  pressure and bo
            upper_p = Matrix2(mm, 2)
            upper_bo = Matrix2(mm, 3)
            For i = 1 To mm
                If Matrix2(i, 2) = P Then
                    upper_p = P
                    upper_bo = Matrix2(i, 3)
                    Exit For
                End If
                If Matrix2(i, 2) > P Then
                    If Matrix2(i, 2) < upper_p Then
                    upper_p = Matrix2(i, 2)
                    upper_bo = Matrix2(i, 3)
                    End If
                End If
            Next


            'Interpolating Bo
            If upper_p = lower_p Then
            Bo_interpol = lower_bo
            Else
            Bo_interpol = lower_bo + (upper_bo -
lower_bo) / (upper_p - lower_p) * (P - lower_p)
            End If


End If
```

Interpolating Black Oil Table to find 'Bo' – Part 3/4

```
'Finding Bo if pressure is above bubblepoint
'=========================================
If P > p_bubble Then
            'Find upper and lower values in the table
            '=======================================

            m = Matrix.Rows.Count
            N = Matrix.Columns.Count


            lower_GOR = Matrix(1, 1)
            For i = 1 To m
                If Matrix(i, 1) = GOR Then
                    lower_GOR = GOR
                    Exit For
                End If
                If Matrix(i, 1) < GOR Then
                    If Matrix(i, 1) > lower_GOR Then
                        lower_GOR = Matrix(i, 1)
                    End If
                End If
            Next


            upper_GOR = Matrix(m, 1)
            For i = 1 To m
                If Matrix(i, 1) = GOR Then
                    upper_GOR = GOR
                    Exit For
                End If
                If Matrix(i, 1) > GOR Then
                    If Matrix(i, 1) < upper_GOR Then
                        upper_GOR = Matrix(i, 1)
                    End If
                End If
            Next

            lower_p = Matrix(1, 2)
            For i = 1 To m
                If Matrix(i, 2) = P Then
                    lower_p = P
                    Exit For
                End If
                If Matrix(i, 2) < P Then
                    If Matrix(i, 2) > lower_p Then
                        lower_p = Matrix(i, 2)
                    End If
                End If
            Next

            upper_p = Matrix(m, 2)
            For i = 1 To m
                If Matrix(i, 2) = P Then
                    upper_p = P
                    Exit For
                End If
                If Matrix(i, 2) > P Then
                    If Matrix(i, 2) < upper_p Then
                        upper_p = Matrix(i, 2)
                    End If
                End If
            Next
```

Interpolating Black Oil Table to find 'Bo' – Part 4/4

```
            'Locate values
            '=============

            For i = 1 To m
                If Matrix(i, 1) = lower_GOR And
Matrix(i, 2) = lower_p Then
                    g1p1 = Matrix(i, 3)
                End If

                If Matrix(i, 1) = lower_GOR And
Matrix(i, 2) = upper_p Then
                    g1p2 = Matrix(i, 3)
                End If

                If Matrix(i, 1) = upper_GOR And
Matrix(i, 2) = lower_p Then
                    g2p1 = Matrix(i, 3)
                End If

                If Matrix(i, 1) = upper_GOR And
Matrix(i, 2) = upper_p Then
                    g2p2 = Matrix(i, 3)
                    g2p3 = Matrix(i + 1, 3)
                    p3 = Matrix(i + 1, 2)
                End If
            Next

              'interpolate backwards
                    '====================
                    If g2p1 = 0 Then
                    g2p1 = g2p2 + (g2p3 - g2p2) / (p3 -
upper_p) * (P - upper_p)
                    End If



            'Interpolate value
            '=================

            If g1p1 = g1p2 Then
            G1P_int = g1p1
            Else
            G1P_int = g1p1 + (g1p2 - g1p1) / (upper_p -
lower_p) * (P - lower_p)
            End If

            If g2p1 = g2p2 Then
            G2P_int = g2p1
            Else
            G2P_int = g2p1 + (g2p2 - g2p1) / (upper_p -
lower_p) * (P - lower_p)
            End If

            If G2P_int = G1P_int Then
            Bo_interpol = G2P_int
            Else
            Bo_interpol = G1P_int + (G2P_int - G1P_int)
/ (upper_GOR - lower_GOR) * (GOR - lower_GOR)
            End If

End If


Bo_int_table = Bo_interpol

End Function
```

Create VFP table in the spreadsheet – Part 1/2

```
Sub Create_table()

index = 9

Range("A9:e1000000").Clear
Range("f10:ah1000000").Clear

'THP values
THP_lower = Range("B3")
THP_upper = Range("B4")
THP_number = Range("B5")

If THP_number = 1 Then
THP_interval = 0
Else
THP_interval = (THP_upper - THP_lower) / (THP_number -
1)
End If

Dim THP() As Double
ReDim THP(THP_number)

For i = 1 To THP_number
THP(i) = THP_lower + (i - 1) * THP_interval
Next

'WFR values
WFR_lower = Range("C3")
WFR_upper = Range("C4")
WFR_number = Range("C5")

If WFR_number = 1 Then
WFR_interval = 0
Else
WFR_interval = (WFR_upper - WFR_lower) / (WFR_number -
1)
End If

Dim WFR() As Double
ReDim WFR(WFR_number)

For i = 1 To WFR_number
WFR(i) = WFR_lower + (i - 1) * WFR_interval
Next

'GFR values
GFR_lower = Range("D3")
GFR_upper = Range("D4")
GFR_number = Range("D5")

If GFR_number = 1 Then
GFR_interval = 0
Else
GFR_interval = (GFR_upper - GFR_lower) / (GFR_number -
1)
End If
```

Create VFP table in the spreadsheet – Part 2/2

```
Dim GFR() As Double
ReDim GFR(GFR_number)

For i = 1 To GFR_number
GFR(i) = GFR_lower + (i - 1) * GFR_interval
Next

'FLO values
FLO_lower = Range("E3")
FLO_upper = Range("E4")
FLO_number = Range("E5")

If FLO_number = 1 Then
FLO_interval = 0
Else
FLO_interval = (FLO_upper - FLO_lower) / (FLO_number -
1)
End If

Dim FLO() As Double
ReDim FLO(FLO_number)

For i = 1 To FLO_number
FLO(i) = FLO_lower + (i - 1) * FLO_interval
Next

For A = 1 To THP_number
For B = 1 To WFR_number
For C = 1 To GFR_number
For D = 1 To FLO_number

Range("a" & index).Value = index - 8
Range("b" & index).Value = THP(A)
Range("c" & index).Value = WFR(B)
Range("d" & index).Value = GFR(C)
Range("e" & index).Value = FLO(D)

index = index + 1

Next
Next
Next
Next

Total = FLO_number * GFR_number * WFR_number *
THP_number

Set SourceRange =
Worksheets("5.VFP_Table").Range("f9:ah9")
Set fillRange = Worksheets("5.VFP_Table").Range("f9:ah"
& Total + 8)
SourceRange.AutoFill Destination:=fillRange


End Sub
```

Write VFP-file in eclipse format – Part 1/2

```
Sub writeVFPtable()
Application.DecimalSeparator = "."
Dim filepath As String
filepath = Range("g2")
Open filepath For Output As #1

'THP values
THP_lower = Range("B3")
THP_upper = Range("B4")
THP_number = Range("B5")

If THP_number = 1 Then
THP_interval = 0
Else
THP_interval = (THP_upper - THP_lower) / (THP_number -
1)
End If
Dim THP() As Double
ReDim THP(THP_number)

For i = 1 To THP_number
THP(i) = THP_lower + (i - 1) * THP_interval
Next

'WFR values
WFR_lower = Range("C3")
WFR_upper = Range("C4")
WFR_number = Range("C5")

If WFR_number = 1 Then
WFR_interval = 0
Else
WFR_interval = (WFR_upper - WFR_lower) / (WFR_number -
1)
End If

Dim WFR() As Double
ReDim WFR(WFR_number)

For i = 1 To WFR_number
WFR(i) = WFR_lower + (i - 1) * WFR_interval
Next

'GFR values
GFR_lower = Range("D3")
GFR_upper = Range("D4")
GFR_number = Range("D5")

If GFR_number = 1 Then
GFR_interval = 0
Else
GFR_interval = (GFR_upper - GFR_lower) / (GFR_number -
1)
End If

Dim GFR() As Double
ReDim GFR(GFR_number)

For i = 1 To GFR_number
GFR(i) = GFR_lower + (i - 1) * GFR_interval
Next

'FLO values
FLO_lower = Range("E3")
FLO_upper = Range("E4")
FLO_number = Range("E5")

If FLO_number = 1 Then
FLO_interval = 0
Else
FLO_interval = (FLO_upper - FLO_lower) / (FLO_number -
1)
End If

Dim FLO() As Double
ReDim FLO(FLO_number)
For i = 1 To FLO_number
FLO(i) = FLO_lower + (i - 1) * FLO_interval
Next
```

Write VFP-file in eclipse format – Part 2/2

```
'Print headlines and stuff
Print #1, "-- Dummy VFP table for pressure drop over
AICDS - Eclise format --"
Print #1, "VFPPROD"
Print #1, ""
Print #1, "--   Table Datum   RateType    WFRType
GFRType THPType ALQType UNITS   TABType"
Print #1, vbTab & "1" & vbTab & "1036" & vbTab & "LIQ"
& vbTab & "WCT" & vbTab & "GOR" & vbTab & "THP" & vbTab
& "'" & vbTab & "Metric" & vbTab & "BHP /"
Print #1, ""

'Extract parameters
Dim VAL As String
Print #1, "-- LIQUID RATE units (sm3/day): " &
FLO_number & " value(s)"
For i = 1 To FLO_number
        VAL = FLO(i)
        VAL = Replace(VAL, ",", ".")
        Print #1, VAL,
Next
Print #1, "/"
Print #1, ""

Print #1, "-- THP units (bara): " & THP_number & "
value(s)"
For i = 1 To THP_number
        VAL = THP(i)
        VAL = Replace(VAL, ",", ".")
        Print #1, VAL,
Next
Print #1, "/"
Print #1, ""

Print #1, "-- WATER FRACTION units (sm3/sm3): " &
WFR_number & " value(s)"
For i = 1 To WFR_number
        VAL = WFR(i)
        VAL = Replace(VAL, ",", ".")
        Print #1, VAL,
Next
Print #1, "/"
Print #1, ""

Print #1, "-- GOR units(sm3/sm3): " & GFR_number & "
value(s)"
For i = 1 To GFR_number
        VAL = GFR(i)
        VAL = Replace(VAL, ",", ".")
        Print #1, VAL,
Next
Print #1, "/"
Print #1, ""

Print #1, "-- 'ALQ' units: 1 value(s)"
Print #1, "0 /"
Print #1, ""

'Printing tubing table
index = 1

For l = 1 To THP_number
For k = 1 To WFR_number
For i = 1 To GFR_number
    Print #1, l & " " & k & " " & i & " " & 1,
    For j = 1 To FLO_number
        VAL = Worksheets("5.VFP_Table").Range("aa" &
index + 8)
        VAL = Replace(VAL, ",", ".")
        Print #1, VAL,
        index = index + 1
    Next
    Print #1, " /"
Next
Next
Next
Print #1, ""
Print #1, "-- END OF FILE --"
Close #1
End Sub
```

F.3: Network Analysis spreadsheet

GOR-Model

```
Function GOR_M(q_oil, q_crit, exponent, rs, C)

GOR_M = rs
If q_oil > q_crit Then
GOR_M = rs + ((q_oil - q_crit) * C) ^ exponent

End If


End Function
```

Pipeflow pressure drop

```
Function dP_Pipe(Q, F, L, D, rho, h)

D = (D * 2.54 / 100)
A = 3.14 * (D ^ 2) / 4
v = Q / (A * 86400)

dP_Pipe = (0.5 * F * L * rho * v ^ 2 / D / 100000) +
(rho * 9.81 * h / 100000)

End Function
```

Reynolds number

```
Function Re_number(rho, v, ID, visc)

Re_number = rho * v * ID / visc

End Function
```

Laminar flow friction factor

```
Function Friction_laminar(Re)

Friction_laminar = 64 / Re

End Function
```

Turbulent flow friction factor – Haalands equation

```
Function Friction_turbulent(Re, roughness, ID)

Friction_turbulent = ((-1.8 * Log((roughness / (ID *
3.7)) ^ (1.11) + (6.9 / Re))) / (Log(10))) ^ (-2)

End Function
```

Solve producton network by tuning drawdown

```
Sub Network_solve()
        SolverReset
        SolverOK
SetCell:=Worksheets("1.Input_sheet").Range("e40"),
MaxMinVal:=3, ValueOf:=0,
ByChange:=Worksheets("1.Input_sheet").Range("j9:j38")
        SolverSolve UserFinish:=False
End Sub
```

Solving vertical flow by finding THP

```
Sub Verticalflow_solve()
        SolverReset
        SolverOK
SetCell:=Worksheets("1.Input_sheet").Range("e59"),
MaxMinVal:=3, ValueOf:=0,
ByChange:=Worksheets("1.Input_sheet").Range("e51")
        SolverSolve UserFinish:=False
End Sub
```